

Durham E-Theses

Covariant infrared finite amplitudes

Mark Morley-Fletcher

How to cite:

Morley-Fletcher, Mark (2005) Covariant infrared finite amplitudes. Doctoral thesis, Durham University.

Use policy

The full-text may be used and/or reproduced, and given to third parties in any format or medium, without prior permission or charge, for personal research or study, educational, or not-for-profit purposes provided that:

- a full bibliographic reference is made to the original source
- a <https://etheses.durham.ac.uk/id/eprint/2718/> is made to the metadata record in Durham E-Theses
- the full-text is not changed in any way

The full-text must not be sold in any format or medium without the formal permission of the copyright holders.

Please consult the [full Durham E-Theses policy](#) for further details.

Covariant Infrared Finite Amplitudes

A thesis presented for the degree of

Doctor of Philosophy

by

Mark Morley-Fletcher

The copyright of this thesis rests with the author or the university to which it was submitted. No quotation from it, or information derived from it may be published without the prior written consent of the author or university, and any information derived from it should be acknowledged.

Institute for Particle Physics Phenomenology

University of Durham

November 2005



31 MAY 2006

Abstract

The calculation of observables in gauge theories with massless particles - such as QCD - by traditional methods is significantly complicated by the presence of soft and collinear singularities, collectively termed infrared divergences, in the scattering amplitudes. The aim of this thesis is to investigate calculational methods which produce finite results at the amplitude level. We discuss the origin of the infrared divergences and outline some previous approaches to constructing finite amplitudes. After reviewing the traditional method for performing calculations we see how incorrect assumptions result in the presence of infrared divergences and what steps must be taken in order to produce infrared finite results.

We then investigate how these ideas could be applied to the calculation of specific amplitudes. We see that there are problems involved in applying this exact approach, but that it suggests the adoption of a workable, more pragmatic alternative. We use this method in an explicit example calculation of the contributing cross sections for the process $e^+e^- \rightarrow 2 \text{ jets}$ at $\mathcal{O}(\alpha_s)$. We demonstrate that we recover the same result as that obtained with standard field theory techniques. We then briefly discuss how this approach might be adapted to suit more complex calculations and, eventually, a completely numerical approach.

Acknowledgements

Many thanks to my supervisor, Adrian Signer, who has been a constant source of help and advice. Particular mention must be made of his willingness to be approached on any matter at all as “there are no stupid questions” despite my continued efforts to provide evidence to the contrary. Darren and Gareth have also been a pleasure to work with and have made my research easier in a variety of ways. I have also had incredible support from my office mates: Angelique, James, Paul, Rich and Tom. They have been a constant source of friendly help and companionship in work, relaxation and all states in between. Finally, thanks are also due to the many people who have taken part in sport, music and other leisure activities with me while I have been at Durham and helped to provide the breadth of experiences which have made my time here so enjoyable.

This work was supported by a PPARC studentship.

Declaration

I declare that no material presented in this thesis has previously been submitted for a degree at this or any other university.

The research described in this thesis has been carried out in collaboration with Dr. Adrian Signer, Dr Darren Forde and Gareth Brown.

©The copyright of this thesis rests with the author.

Contents

Abstract	i
Acknowledgements	ii
Declaration	iii
1 Introduction	1
1.1 Physical Observables	1
1.2 Amplitude calculations and divergences	5
1.2.1 Infrared divergences	7
1.3 Current calculational methods	9
1.4 Infrared Finite Amplitudes	12
1.4.1 Previous work on infrared finite amplitudes	13
1.5 Overview of the rest of the thesis	15
2 Conventional Methods	17
2.1 Free fields	18
2.2 The Feynman propagator	21
2.3 The LSZ reduction formula	22
2.4 Perturbative expansion	26
2.4.1 The interaction picture	27

2.5	Wick's theorem	33
2.6	Feynman diagrams	35
2.6.1	Disconnected diagrams	37
2.7	Phase Space calculations	39
2.8	Infrared safe example	41
3	A New Approach	46
3.1	The asymptotic condition	48
3.2	The asymptotic fields	49
3.3	The modified LSZ formula	53
3.4	Correlation functions in the AIP	57
3.5	Wick's Theorem	59
3.6	Practical applications	61
3.6.1	Propagators in the AIP	61
3.6.2	Interpretation and application of the asymptotic states	62
3.6.3	An alternative method	65
4	Splitting the Lagrangian	69
4.1	Splitting requirements	72
4.2	Power counting techniques	73
4.2.1	Reduced diagrams	76
4.2.2	Infrared power counting	76
4.3	Infrared finiteness	78
4.3.1	Power counting for the soft subdiagram	80
4.3.2	Power counting including jets	81
4.3.3	Two point vertices in reduced diagrams	85

4.4	Splitting functions	87
4.4.1	Two point vertices in hard reduced diagrams	89
4.5	Calculating propagators	93
4.5.1	The fermion propagator	93
4.5.2	The gluon propagator	95
4.5.3	Checking the limits	99
4.6	Infrared finite amplitudes	102
4.7	Phase space integrals	105
5	Example calculations	107
5.1	$e^+e^- \rightarrow$ two jets at NLO	108
5.1.1	Allocating cross sections to the different asymptotic states	115
5.1.2	The complete result	116
5.2	Extending our approach	120
5.2.1	Categorising external states	126
5.2.2	Towards a numerical approach	133
6	Conclusions and outlook	135
A	The full result for the vertex correction calculation	139
B	Cross sections for a basic jet definition	147

List of Figures

2.1	A general r particle Green's function.	25
2.2	A possible Feynman diagram for Eq.(2.54)	36
2.3	A typical Feynman diagram in ϕ^4 theory including both connected and disconnected pieces.	38
2.4	The set of disconnected diagrams, V_i , in ϕ^4 theory.	38
2.5	The vertex correction diagram	42
2.6	The real emission diagram	43
2.7	The cut diagrams for Eq.(2.62)	44
3.1	Some diagrams which may contribute to a single asymptotic external state.	64
3.2	Some diagrams which may contribute to a two pseudojet external state.	65
3.3	The emission of a hard gluon contributes to a three jet final state; the emission of a soft gluon contributes to a two jet final state.	67
4.1	Correction to the fermion propagator	90
4.2	Fermion loop correction to the gluon propagator	91
4.3	Gluon loop correction to the gluon propagator	91
5.1	Some of the cut diagrams for the vertex correction calculation.	109

5.2	A comparison between the results for cross sections formed using the final states $ q_{p_1}\bar{q}_{p_2}g_{p_3}\rangle$ (solid line) and $ \{q_{p_1}\bar{q}_{p_2}g_{p_3}\}\rangle$ (dashed line) for $\Delta_s = 0.01$	119
5.3	A comparison between the results for cross sections formed using the final states $ q_{p_1}\bar{q}_{p_2}g_{p_3}\rangle$ (solid line) and $ \{q_{p_1}\bar{q}_{p_2}g_{p_3}\}\rangle$ (dashed line) for $\Delta_s = 0.002$	120
5.4	A comparison between the results for the $ \{q_{p_1}\bar{q}_{p_2}\}\rangle$ cross section (long dashed line), the two jet part of the $ \{q_{p_1}\bar{q}_{p_2}g_{p_3}\}\rangle$ cross section (short dashed line), their sum (dotted line) and the two jet result obtained from $ q_{p_1}\bar{q}_{p_2}\rangle$ and $ q_{p_1}\bar{q}_{p_2}g_{p_3}\rangle$ (solid line) for $y_{cut} = 0.05$	121
5.5	Some diagrams which will be zero under the new splitting functions.	125
5.6	Showering from an external leg. Here we have used the notation $p_{a,b} = \sum_{i=a}^b p_i$	125
5.7	Cuts for the N_F contribution at NNLO	127
5.8	Cut diagram with apparently mismatched external states.	131
5.9	The naive external states expected from the cut diagram in Figure 5.8.	132

Chapter 1

Introduction

1.1 Physical Observables

While physical theories contain many elements which are interesting in themselves, the ultimate goal of any theoretical calculation must be to provide predictions for the results of physical processes. The processes with which we will be concerned in this thesis are investigated in collider experiments. These produce huge amounts of data which must be analysed in order to produce useful observations. The relevant quantities which can be calculated from the data are known as *physical observables*. The goal for our theoretical calculations must therefore be to provide predictions for these physical observables.

To achieve this we conventionally start with a *field theory* - QED or QCD for example - which describes the physics relevant to the particular observable which we are interested in calculating. This field theory will be described through the relevant Lagrangian, and it is to this which we must turn in order to perform our calculations. Unfortunately we are currently unable to solve



the equations of motion derived from any of the Lagrangians representing realistic theories such as QED or QCD, and can only solve the free field theories (where there are no interactions between the different fields) in these cases. The traditional method for dealing with such situations is to treat the full theory as a small perturbation of the soluble part of the theory (the free theory in this case), and calculate results to the required order in perturbation theory. This approach is not perfectly applicable in the case of QCD however due to the running of the coupling constant. At high momenta (or small distances) the coupling constant of QCD becomes small and perturbation theory can be used. However, at small momenta (or large distances) the coupling constant becomes large and perturbation theory is no longer a valid approach.

One approach to resolving this situation (and this is the approach which we shall use in this thesis) is to simply go ahead and use perturbation theory anyway. This places several limits on the calculations we are able to perform: firstly, we are unable to carry out calculations for low energy processes. This is not really a problem in our situation as all the collider experiments producing values for the physical observables which we wish to predict will be operating at energies well above the threshold where perturbation theory becomes a viable option; however, if we were interested in calculating the results of low energy processes we would need to find another way of doing it. Secondly, we conventionally formulate our perturbation theories such that our asymptotic states are “free” quarks and gluons. In fact, the physical asymptotic states which are observed in detectors are *hadrons*, and these will usually appear as a *jet* - a shower of particles all travelling quickly in approximately the same direction. When we perform our calculations in per-

turbation theory neither hadrons or jets appear as our final products since it cannot reproduce low energy effects. The full process could be considered to consist of three stages: the underlying interaction takes place at high energy and can be calculated perturbatively. The probability for this interaction to take place is represented by the amplitude, \mathcal{A} which will be the focus for most of this thesis. This underlying interaction results in the production of “free” quarks and gluons; these will then form jets through interactions at lower energies. Finally, at lower energies still, hadronisation will occur as the particles which make up the jets form bound states. We shall concern ourselves with the perturbative regime of QCD. More detailed discussions of the parton showers which make up jets and of hadronisation can be found in [1,2] and the references therein. In order to produce predictions for complete processes we must calculate amplitudes for incoming and outgoing quarks and gluons and then marry these up with some algorithm, a Monte-Carlo simulation for example, which will take account of the low energy processes and turn them into jets and hadrons.

A second possible approach is that of *lattice QCD* which allows us to calculate quantities numerically by discretising Euclidean space-time into hypercubes and evaluating the QCD Lagrangian on each resulting lattice point. The QCD Lagrangian does not make sense without an ultraviolet cut-off because of divergences which occur at high momenta or short distances (we shall see more about this later) and the lattice spacing provides a natural cut off. As long as the lattice spacing is small when compared with the physical extent of the hadrons which are being studied then this discrete version of the theory should be an adequate approximation at that scale. Lattice QCD has been used extensively to study quantities which are unsuitable for perturbative

calculations such as hadronic masses. We shall not consider it any further in this thesis however, but will return to perturbative calculations.

In order to calculate amplitudes which correspond to the processes involved in our chosen observable we will use perturbation theory in conjunction with the relevant field theory. We take the modulus squared of these amplitudes and integrate this over the required region of the parameter space. This is called integrating over the *phase space*. The desired result is usually achieved by performing the integral over the entire region of phase space and weighting it with a particular function which describes the required observable. The weighting function, J , can be as simple as one, which would give the total cross section, or can take more complicated forms for observables such as specific jet definitions. The whole calculation can be represented by

$$O = \int dLips(k_i, \dots) |\mathcal{A}|^2 \times J(k_i, \dots) \quad (1.1)$$

where $dLips$ is the Lorentz invariant phase space, \mathcal{A} is the relevant amplitude and $J(k_i, \dots)$ is the weighting function for the required observable, O .

As our observable will be measured in a physical detector which will inevitably have limits on the accuracy of its measurements, we must also take into account the fact that certain processes, while perfectly distinct at a theoretical level, may actually be physically indistinguishable. Therefore, our definition of the observable may well have to include amplitudes with different numbers of incoming and outgoing states, and therefore with different phase space integrals. Consequently, our final calculation of the observable will-in-general be an incoherent sum of terms of the form of Eq.(1.1).

The amplitude, \mathcal{A} , contains all the details of the specific field theory involved

in the process while the phase space integral deals essentially with kinematic issues. The main area of interest for this thesis will be the investigation of alternate methods for calculating the amplitude.

1.2 Amplitude calculations and divergences

The next step is now to calculate the amplitudes themselves. Each amplitude corresponding to a particular process at a particular order in perturbation theory can be naturally divided into a sum of *Feynman diagrams*. These are pictorial representations of the amplitude which contain all the information necessary to perform the relevant calculation. A Feynman diagram without any internal loops is referred to as a *tree level* diagram, a diagram with one internal loop is a *one-loop* diagram and so on. When we calculate Feynman diagrams beyond tree level we find that the majority of them are divergent. These divergences fall into two categories: ultraviolet (UV) divergences and infrared (IR) divergences. UV divergences appear as a result of high momentum modes running through internal loops in the diagram. For example, the momentum integration for a one-loop Feynman diagram might be¹

$$I(p_1, p_2) = \int \frac{d^4 k}{(2\pi)^4} \frac{\gamma^\nu (\not{p}_1 + \not{k}) \gamma^\mu (\not{p}_2 - \not{k}) \gamma_\nu}{k^2 (p_1 + k)^2 (p_2 - k)^2} \quad (1.2)$$

We can immediately see that we will have a problem since in the limit $k \rightarrow \infty$ we obtain

$$I(p_1, p_2) \sim \int^\infty \frac{d^4 k}{k^6} \sim \int^\infty \frac{dk}{k} \quad (1.3)$$

¹The example here is from the vertex correction shown in Figure 2.5 for massless QCD in Feynman gauge.

where \int^∞ indicates that we are interested in the integral near its upper limit of infinity. This will clearly give an infinite result.

These infinities can be systematically dealt with by regularising the integral in some way; the most common method, which we shall use throughout this thesis, is dimensional regularisation. This requires us to perform the necessary momentum integrals in $D = 4 - 2\epsilon$ dimensions, where D is unspecified but is taken to be such that the integral is finite. Our example loop integral would now become

$$I(p_1, p_2) \sim \int^\infty \frac{d^D k k^2}{k^6} \sim \int^\infty k^{-1-2\epsilon} dk \quad (1.4)$$

which is now finite for $D < 4$.

Once the integrals have been performed, we let ϵ tend to zero in order to recover the result in four dimensions. The UV singularities will then reveal themselves as poles in $1/\epsilon$. These UV singularities can be removed by the procedure of renormalisation. We relate the quantities in the Lagrangian, such as those labelled as the mass and the coupling, to the renormalised mass and coupling of the theory in some chosen renormalisation scheme. The difference between the renormalised quantities of the theory and the quantities in the Lagrangian (the bare quantities) will be found to be infinite and this process will result in the removal of the UV divergences. This is a standard procedure and we will not concern ourselves with it any further in this thesis; instead we shall concentrate on infrared divergences.

1.2.1 Infrared divergences

IR divergences appear as a result of low momentum modes running through internal loops and also in the phase space integrals of Eq.(1.1). If we take the limit $k \rightarrow 0$ of Eq.(1.2) we can again see the problem since we obtain

$$I(p_1, p_2) \sim \int_0 \frac{d^4 k}{k^2 p_1 \cdot k p_2 \cdot k} \sim \int_0 \frac{dk}{k} \quad (1.5)$$

which will again give an infinite result.

Specifically, infrared divergences relate to two different circumstances. Firstly, when a massless particle emitted from an initial or final state particle goes soft (i.e. its energy goes to zero). Secondly, when a massless particle goes collinear to an external massless particle from which it has been emitted². Renormalisation does nothing to remove these singularities since their underlying cause is completely different from that of the UV singularities. We shall investigate the origin of the infrared divergences further in Section 1.4.1.

One result of these infrared divergences is to limit the types of quantities which we can calculate in perturbation theory. We can only calculate physical observables if they can be defined in an infrared safe manner [3]. Closer investigation shows that these infrared safe observables are distinguished by the fact that they do not depend on the long range behaviour of the theory. To highlight the connection with the two cases mentioned in the previous paragraph, we could equally state that IR safe quantities do not depend on whether or not a parton emits a soft gluon and similarly do not depend on whether a parton splits into two collinear partons or not. These conditions are essentially those required for the physically indistinguishable processes

²We shall use the terms “infrared divergences” and “infrared singularities” to refer to both soft and collinear singularities throughout this thesis.

described in Section 1.1.

To handle these IR divergences we need to regulate the momentum integrals in some way as mentioned earlier in the case of the UV divergences. The simplest method is to introduce a mass for any massless fields in the Lagrangian. In this case (adding a mass for the gluon but leaving the quarks massless) our example loop integral in Eq.(1.2) would become

$$I(p_1, p_2, m_\gamma) = \int \frac{d^4 k}{(2\pi)^4} \frac{\gamma^\nu(\not{p}_1 + \not{k})\gamma^\mu(\not{p}_2 - \not{k})\gamma_\nu}{(k^2 - m_\gamma^2)(p_1 + k)^2(p_2 - k)^2} \quad (1.6)$$

and consequently in the limit $k \rightarrow 0$ we now find

$$I(p_1, p_2, m_\gamma) \sim \int_0 \frac{d^4 k}{p_1 \cdot k p_2 \cdot k} \sim \int_0 k dk \quad (1.7)$$

which will no longer give an infinite result. Amplitudes which have been regulated in this manner will now contain logarithms of the mass which diverge as our regulator is taken to zero.

A more common method is that of dimensional regularisation, which we previously mentioned in the case of UV divergences. Considering our example loop integral again, in the limit $k \rightarrow 0$ we now find

$$I(p_1, p_2, \epsilon) \sim \int_0 \frac{d^D k}{k^2 p_1 \cdot k p_2 \cdot k} \sim \int_0 k^{-1-2\epsilon} dk \quad (1.8)$$

which is finite for $D > 4$. The infrared singularities will again reveal themselves as poles in $1/\epsilon$. Despite the seeming contradiction that we appear to simultaneously pick $D > 4$ for the infrared divergences and $D < 4$ for the ultraviolet divergences, this does not cause any problems with the calculations and we arrive at correct results when we finally take the $\epsilon \rightarrow 0$ limit at

the end. This is due to the fact that, more formally, we start by calculating an off-shell Green's function which will contain no infrared divergences. We can therefore regulate this by choosing $D < 4$ and remove the ultraviolet divergences through renormalisation. Our Green's function is now ultraviolet finite and so we can choose $D > 4$ in order to regulate the infrared divergences which appear as we now allow the external legs to go on-shell. The popularity of dimensional regularisation is in part due to this fact that it allows us to use only one regulator to deal with all the divergences in an amplitude. Since both sets of divergences appear as poles in $1/\epsilon$, the poles from the two types of singularities will mix together. This will not, however, cause any problems with UV renormalisation.

Once we have our IR regulated amplitudes we can use them to calculate our infrared safe observables. Since these observables do not depend (among other things) on whether or not a parton emits a soft gluon, it is clear that our observable will be a sum of amplitudes with differing numbers of particles in the final state. For processes with certain specific numbers of particles in the final state, the phase space integrations will also produce infrared divergences. We can deal with these divergences through dimensional regularisation as well. Once we have considered both sets of divergences the final result will be finite.

1.3 Current calculational methods

As we saw in Section 1.1, the different phase space integrals which we have to perform to calculate a specific observable will generally contain different numbers of particles. This means that unless we are calculating fully in-

clusive quantities we must integrate the contributing terms separately over different phase space regions. In this case we are unable to take advantage of the cancellation of soft and collinear divergences at the integrand level. Consequently this does not allow us to use a completely numerical approach for the calculation of these phase space integrals. This is not a problem for simple leading order calculations, but as we calculate at higher and higher orders in perturbation theory the increasing complexity of the amplitudes makes analytic calculations progressively more difficult. In an attempt to overcome this problem much work has been done on methods of splitting up the integration so that the singular regions are removed [4]. These are then integrated analytically, while the remaining finite regions are calculated numerically. Two of these methods are the phase space *slicing* method [5], and the *subtraction* method [6, 7]. A general version of the algorithm for both methods is available for processes at NLO involving any number of lepton and hadron jets.

The general approach of the subtraction method proceeds as follows [8–10]. The total NLO contribution to an observable consists of a real piece $d\sigma^R$ (with $m + 1$ partons in the final state) and a virtual piece $d\sigma^V$ (with m partons in the final state). The integrals can then be rewritten as follows

$$\sigma_{NLO} = \int_{m+1} d\sigma^R + \int_m d\sigma^V \quad (1.9)$$

$$= \int_{m+1} (d\sigma^R - d\sigma^A) + \int_{m+1} d\sigma^A + \int_m d\sigma^V \quad (1.10)$$

$$= \int_{m+1} (d\sigma^R - d\sigma^A) + \int_m \left(d\sigma^V + \int_1 d\sigma^A \right) \quad (1.11)$$

where the subscript on the integrals denotes the number of external particles present in the final state phase space. Here $d\sigma^A$ is chosen to be an approxi-

mation of $d\sigma^R$ such that it has the same pointwise singular behaviour, acting as a local counterterm and allowing the first integral to be performed numerically. The first integral is finite by definition, so providing we are calculating an infrared safe observable the final result of the second integral (over m external particles) must also be finite. This means that if we can calculate the single integral over $d\sigma^A$ analytically, we can once again remove the regulator from the second integral and calculate it numerically.

The crucial part of this process is that we are free to choose the form of $d\sigma^A$ so that we are able to perform the single integral analytically. It is possible to define a method of generating $d\sigma^A$ for NLO processes which is process independent. It is also possible, for a suitable choice of $d\sigma^A$, to numerically integrate the virtual piece over the internal one-loop integral [11]. Following these methods, it should be possible to use a completely numerical approach for any NLO observable.

Once we move on to NNLO calculations however, we are faced once again with yet more complicated amplitudes and phase space integrals. A lot of effort has been focused on these two separate areas of the calculations. In the case of the amplitudes themselves progress has been made both on the development of methods for evaluating specific two-loop integrals which appear in the calculations [12–14] and on their application in explicit amplitude calculations [15–17].

In the area of phase space calculations there have been efforts to produce a general subtraction procedure for NNLO processes. The first step in developing such a procedure is to understand the soft and collinear singularities of the various amplitudes, and hence to be able to generate them. Despite all the work in this area, the difficulties associated with performing the diver-

gent phase space integrals remains a significant stumbling block to further calculation of NNLO observables.

1.4 Infrared Finite Amplitudes

As we have already seen, it is possible to make progress in calculations despite the presence of infrared divergences, and much work is continuing in that area. The increasing difficulties which are encountered with each attempt to produce more accurate calculations, however, suggest that an attempt to avoid the singularities at the amplitude level would provide great rewards if successful. Consequently it seems useful to investigate the origin of these singularities in the hope of eventually avoiding them altogether.

There are several benefits which would arise as a result of defining infrared finite amplitudes. Most obviously there is the conceptual advantage of constructing a well-defined S -matrix without singularities. More practically, in the light of the presently available calculational methods detailed in the previous section, the development of infrared finite amplitudes would have clear advantages. Given that the final integrals over the phase space will be calculated numerically, there is very little real benefit in performing complicated amplitude calculations analytically since the analyticity will be lost in the final result. Consequently, the ability to calculate amplitudes numerically would be of great benefit. The construction of infrared finite amplitudes would allow such a calculation. Another possible benefit of this approach would be to facilitate the combination of fixed order results with parton shower Monte-Carlo programs. We shall see later on in Section 5.2 that elements of our approach suggest a natural connection with a parton

shower approach, and may present the possibility of performing calculations at higher orders in the strong coupling at soft energies rather than at hard energies.

1.4.1 Previous work on infrared finite amplitudes

The traditional method for dealing with infrared divergences was first developed by Bloch and Nordsieck in response to the soft-photon divergence or so-called “infrared catastrophe” [3]. This method, along with the various developments which have followed, is often referred to as the *cross section method*. Although this method swiftly became the standard approach for performing calculations, much work has been done since then in investigating a different approach to the singularities.

The requirement of the cross section method to sum over incoherent but physically indistinguishable cross sections led to the argument that the true asymptotic *in* and *out* states cannot be approximated as noninteracting particles. In quantum mechanics it is well known that the asymptotic states in a Coulomb potential are not simply plane waves, but must be modified by non-vanishing Coulomb phase factors. This is due to the long-range nature of the interaction [18]. In field theory, the addition of particle creation to this scenario will further alter the character of the asymptotic states.

This means that our assumption in setting our *in* and *out* states to be eigenstates of the free Hamiltonian is incorrect, and it is this choice of *in* and *out* states which is the origin of the infrared divergences which appear in the traditional calculations as this incorrect formulation results in a singular, ill-defined scattering operator. In order to avoid infrared divergences in our

calculations altogether we must define a method which correctly maps the full states of the theory to the proper asymptotic states.

Previous work in this area can be divided into two approaches. The first approach defines states called *dressed* states in such a way that infrared finite transition amplitudes could be calculated using the normal S -matrix between these modified states. This approach has been used initially in QED with massive fermions [18] with several attempts to extend it to cover soft singularities in non-abelian theories [19–25]. Dressed states including multiple soft gluon emission can be constructed to all orders in the coupling [26]; it can then be shown that the S -matrix between such states is completely free of singularities [27]. The second approach uses the true *asymptotic* states of the full theory. This will result in a different S -matrix which is then used to calculate transition amplitudes between these asymptotic states [28–31].

Non-abelian gauge theories present several problems not present in QED. Alongside the more complicated structure of the soft singularities due to the self-interaction of the gauge bosons we find the additional problem of collinear singularities. The presence of these singularities means that the asymptotic Hamiltonian is more complicated [31] and the prospect of including these effects to all orders in perturbation theory does not appear to be very promising. However, the idea of constructing an asymptotic Hamiltonian which includes the necessary long range interactions along with the usual free Hamiltonian and then using this either to construct asymptotic states or to dress the usual states [32, 33] is still applicable.

A general method for constructing a soft Moller operator and using this to construct asymptotic states in the style of the second approach above has been presented and applied to a simple example [34]. It allowed the

are not eigenstates of the free Hamiltonian. We identify the difficulties involved in such a method and outline a related method which will be more straightforward to implement.

In Chapter 4 we deal with a specific choice of the split of the Lagrangian into an asymptotic part and a hard interaction part. We show how amplitudes calculated with the hard interactions will be infrared finite, and consider the effect of such a split on the propagators of the theory.

In Chapter 5 we perform an explicit calculation to show how the new approach will work for a simple example and demonstrate that we obtain the same jet cross sections to $\mathcal{O}(\alpha_s)$ as the conventional method. We then examine the limitations of our chosen split of the Lagrangian and discuss how a more appropriate choice can be made when we perform calculations numerically. We consider how this new choice makes the connection between the full method using an altered LSZ formula and the related method which we have used in the previous example clearer.

considering processes which involve transitions between states with different particle number we must therefore deal with field theories. For all our field theory calculations we will start with a Lagrangian which describes the details of the particular theory in which the calculation is to be performed. The Lagrangian will usually be made up of a kinetic (or free) part, which describes the evolution of the fields in the absence of any interactions, and an interaction part, which describes the interactions between the various fields present in the theory. For example, the Lagrangian for QED is given by [35],

$$\begin{aligned}\mathcal{L}_{QED} &= \mathcal{L}_0 + \mathcal{L}_I \\ &= \bar{\psi}(i\cancel{\partial} - m)\psi - \frac{1}{4}(\partial_\mu A_\nu - \partial_\nu A_\mu)^2 - e\bar{\psi}\gamma^\mu\psi A_\mu\end{aligned}\quad (2.1)$$

Here the ψ are the fermionic electron fields and A_μ is the vector photon field. The interaction term is $-e\bar{\psi}\gamma^\mu\psi A_\mu$, the electron kinetic term is $\bar{\psi}(i\cancel{\partial} - m)\psi$ and the photon kinetic term is $-\frac{1}{4}(\partial_\mu A_\nu - \partial_\nu A_\mu)^2$. We want to work with a quantum field theory and so we will need to quantise the theory which is described by our given Lagrangian. Throughout this thesis we will use canonical quantisation. This involves promoting all the fields and their conjugate momenta to operators and imposing suitable commutation relations in the case of integer spin fields and anti-commutation relations in the case of half integer spin fields [35, 36]. We shall begin by developing this process for the kinetic part of the Lagrangian alone - that is for free fields.

2.1 Free fields

To demonstrate the basic form of a free quantum field theory we consider the Klein-Gordon field, governed by the Lagrangian $\mathcal{L} = \frac{1}{2}(\partial_\mu\phi)^2 - \frac{1}{2}m^2\phi^2$.

Chapter 2

Conventional Computational Methods

In this chapter we shall look at the methods traditionally used in amplitude calculations. We present a quick summary, following a similar approach to the more detailed treatments which can be found in books such as [35–37] and focusing on the areas which we shall need to modify in order to produce infrared finite amplitudes. Once we have an understanding of the conventional approach we shall use this to investigate the necessary modifications in Chapter 3. In our calculations we will consider the specific case of scalar fields, but the same general ideas can be extended to fermions and vector fields relatively easily.

Our aim is to calculate the amplitudes, \mathcal{A} , described in Section 1.1. In order to go about this task we shall use quantum field theory. Where basic quantum mechanics is concerned mainly with the quantisation of dynamical systems of particles, quantum field theory deals with dynamical systems of fields. Since we will be dealing with relativistic situations and therefore

We follow the usual procedure of starting with a classical field theory and “quantising” it by promoting the fields, ϕ , and their conjugate momenta, π , to operators. These will then obey the usual commutation relations

$$\begin{aligned} [\phi(t, \vec{x}), \pi(t, \vec{y})] &= i\delta(\vec{x} - \vec{y}) \\ [\phi(t, \vec{x}), \phi(t, \vec{y})] &= 0, \quad [\pi(t, \vec{x}), \pi(t, \vec{y})] = 0 \end{aligned} \quad (2.2)$$

We can expand the fields in terms of annihilation and creation operators in the Schrödinger picture as follows [35]

$$\phi(\vec{x}) = \int \frac{d^3k}{(2\pi)^3} \frac{1}{\sqrt{2\omega_k}} \left(a(\vec{k})e^{i\vec{k}\cdot\vec{x}} + a^\dagger(\vec{k})e^{-i\vec{k}\cdot\vec{x}} \right) \quad (2.3)$$

$$\pi(\vec{x}) = \int \frac{d^3k}{(2\pi)^3} \sqrt{\frac{\omega_k}{2}} \left(a(\vec{k})e^{i\vec{k}\cdot\vec{x}} - a^\dagger(\vec{k})e^{-i\vec{k}\cdot\vec{x}} \right) \quad (2.4)$$

The commutation relation from Eq.(2.2) then gives us the following commutation relations for our annihilation and creation operators

$$\begin{aligned} [a(t, \vec{k}), a^\dagger(t, \vec{k}')] &= (2\pi)^3 \delta(\vec{k} - \vec{k}') \\ [a(t, \vec{k}), a(t, \vec{k}')] &= 0, \quad [a^\dagger(t, \vec{k}), a^\dagger(t, \vec{k}')] = 0 \end{aligned} \quad (2.5)$$

We can then express the Hamiltonian in terms of these operators [35], arriving at the form

$$H = \int \frac{d^3k}{(2\pi)^3} \omega_k \left(a^\dagger(\vec{k})a(\vec{k}) + \frac{1}{2} [a(\vec{k}), a^\dagger(\vec{k})] \right) \quad (2.6)$$

In the Heisenberg picture, we can make the operators time-dependent in the

calculation of $e^+e^- \rightarrow$ hadrons at NLO, but since it used a Hamiltonian approach it resulted in infrared-finite amplitudes which were not covariant. Consequently, the construction and computation of these amplitudes and the resulting cross sections was rather cumbersome.

1.5 Overview of the rest of the thesis

In this thesis we investigate the possibility of constructing scattering amplitudes which are free of infrared divergences. While most previous work has focused on general theoretical considerations of the various possible approaches, our aim is to work towards establishing a method for performing explicit calculations order-by-order in perturbation theory. The ultimate goal (which is beyond the scope of this thesis) will be a completely numerical approach to the calculation of amplitudes. We wish to modify the approach of [34] and make it manifestly covariant. In order to achieve this we shall exchange the Hamiltonian approach for a Lagrangian based formalism.

The structure of the thesis is as follows: in Chapter 2 we provide a basic overview of the basic theoretical method used in performing calculations of observables. The reason we do this is in order to establish the form of the relevant features of the traditional approach; consequently, when we outline our new approach in the following chapters it will be clear where the differences and similarities lie.

In Chapter 3 we explore the asymptotic interaction picture as a means of adapting the conventional method in order to ensure infrared finite amplitudes. We follow the general route outlined in Chapter 2, while adapting the argument in order to take account of the fact that the in and out states

usual manner through the relation

$$\phi(x) = \phi(t, \vec{x}) = e^{iHt} \phi(\vec{x}) e^{-iHt} \quad (2.7)$$

The Heisenberg equation of motion for an operator \mathcal{O} ,

$$i \frac{\partial}{\partial t} \mathcal{O} = [\mathcal{O}, H] \quad (2.8)$$

will then allow us to calculate their time dependence. We find that $i \frac{\partial}{\partial t} \phi(t, \vec{x}) = i\pi(t, \vec{x})$ as required and can also check that

$$\frac{\partial^2 \phi}{\partial t^2} = (\nabla^2 - m^2) \phi \quad (2.9)$$

so that ϕ does indeed satisfy the Klein-Gordon equation.

Finally, we can use the form of H given in Eq.(2.6) to derive the commutation relations

$$[H, a^\dagger(\vec{k})] = \omega_k a^\dagger(\vec{k}) \quad , \quad [H, a(\vec{k})] = -\omega_k a(\vec{k}) \quad (2.10)$$

This then gives us the results

$$e^{iHt} a(\vec{k}) e^{-iHt} = a(\vec{k}) e^{-i\omega_k t} \quad , \quad e^{iHt} a^\dagger(\vec{k}) e^{-iHt} = a^\dagger(\vec{k}) e^{i\omega_k t} \quad (2.11)$$

which allow us to write our expression for the Heisenberg field in its most useful form

$$\phi(x) = \int \frac{d^3 k}{(2\pi)^3} \frac{1}{\sqrt{2\omega_k}} \left(a(\vec{k}) e^{-ik \cdot x} + a^\dagger(\vec{k}) e^{ik \cdot x} \right) \Big|_{k^0 = \omega_k} \quad (2.12)$$

2.2 The Feynman propagator

We now consider the vacuum expectation value of the time-ordered product of two fields, $\langle 0|T\{\phi(x)\phi(y)\}|0\rangle$. This object, called the Feynman propagator, will prove to be useful later on. A simple calculation will show [35]

$$\langle 0|T\{\phi(x)\phi(y)\}|0\rangle \equiv D_F(x-y) = \int \frac{d^4p}{(2\pi)^4} \frac{i}{p^2 - m^2 + i\epsilon} e^{-ip \cdot (x-y)} \quad (2.13)$$

It is easy to verify that $D_F(x-y)$ is a Green's function of the Klein-Gordon operator since we have

$$\begin{aligned} (\partial^2 + m^2)D_F(x-y) &= (\partial^2 + m^2)(\theta(x^0 - y^0)\langle 0|\phi(x)\phi(y)|0\rangle \\ &\quad + \theta(y^0 - x^0)\langle 0|\phi(y)\phi(x)|0\rangle) \end{aligned} \quad (2.14)$$

Considering only the $\theta(x^0 - y^0)$ term we get

$$\begin{aligned} D_{x^0} &= (\partial^2\theta(x^0 - y^0)) \langle 0|\phi(x)\phi(y)|0\rangle + 2(\partial_\mu\theta(x^0 - y^0))(\partial^\mu\langle 0|\phi(x)\phi(y)|0\rangle) \\ &\quad + \theta(x^0 - y^0)(\partial^2 + m^2)\langle 0|\phi(x)\phi(y)|0\rangle \\ &= -\delta(x^0 - y^0)\langle 0|\pi(x)\phi(y)|0\rangle + 2\delta(x^0 - y^0)\langle 0|\pi(x)\phi(y)|0\rangle + 0 \\ &= \delta(x^0 - y^0)\langle 0|\pi(x)\phi(y)|0\rangle \end{aligned} \quad (2.15)$$

We can do a similar calculation for the $\theta(y^0 - x^0)$ term, and adding them together we get

$$\begin{aligned} (\partial^2 + m^2)D_F(x-y) &= \delta(x^0 - y^0)\langle 0|\pi(x)\phi(y)|0\rangle - \delta(x^0 - y^0)\langle 0|\phi(y)\pi(x)|0\rangle \\ &= \delta(x^0 - y^0)\langle 0|[\pi(x), \phi(y)]|0\rangle \\ &= -i\delta^4(x-y) \end{aligned} \quad (2.16)$$

as required.

2.3 The LSZ reduction formula

We now want to use our quantised theory to calculate \mathcal{A} . We represent the amplitude as the overlap of the *in* states (which describe the initial configuration for the process we're investigating) with the *out* states (which describe the final configuration) [37]. The amplitude for a quark and an antiquark (with momenta k_1 and k_2) to scatter into n quark jets (with momenta p_1 to p_n) would then be given by

$$\mathcal{A} \equiv {}_{out}\langle q(p_1) \dots q(p_{n/2}) \bar{q}(p_{n/2+1}) \dots \bar{q}(p_n) | q(k_1) \bar{q}(k_2) \rangle_{in} \quad (2.17)$$

where all the quarks are fields of the full Lagrangian.

Clearly, if we are to make use of the formalism which we have developed in the previous sections we need some way of relating the “full” fields to the “free” fields with which we have been dealing until now. We find this relation in the asymptotic condition, which uses the observation that at asymptotic times the particles in a scattering process behave as free particles and propagate under the influence of their self-interactions only¹ to state [36]

$$\lim_{t \rightarrow \pm\infty} \langle \alpha | \phi(x) | \beta \rangle = Z^{-1/2} \langle \alpha | \psi(x) | \beta \rangle \quad (2.18)$$

where ψ is the field obeying the equations of motion of the full Lagrangian, and ϕ obeys the equations of motion of the free Lagrangian as before; the

¹We have already seen that this observation is incorrect and is the cause of infrared divergences. We shall address this in our approach to calculating infrared finite amplitudes, beginning in the next chapter.

factor of proportionality, Z , will turn out to be one of the elements which is required to cancel the UV divergences in the amplitude and is known as the *field-strength renormalisation*.

As before we will examine the case of scalar fields, but this method can easily be extended to encompass other fields as well [36]. We represent a general case where we have m particles with momenta q_1 to q_m in the initial state, and n particles with momenta p_1 to p_n in the final state as follows

$$\mathcal{A} = \text{}_{out}\langle p_1, \dots, p_n | q_1, \dots, q_m \rangle_{in} \quad (2.19)$$

Our aim is now to manipulate this expression until we arrive at something which will give us a clear picture of how to perform the calculation. Since the *in* and *out* states are defined at asymptotic times where (for the purposes of this chapter at least) we assume that the fields obey the equations of motion given by the free Lagrangian, we can proceed by extracting an asymptotic creation operator from the initial state and then add and subtract terms with an asymptotic final state creation operator with the same momentum

$$\begin{aligned} \mathcal{A} &= \text{}_{out}\langle p_1, \dots, p_n | a_{in}^\dagger(q_1) | q_2, \dots, q_m \rangle_{in} \quad (2.20) \\ &= \text{}_{out}\langle p_1, \dots, p_n, -q_1 | q_2, \dots, q_m \rangle_{in} + \text{}_{out}\langle p_1, \dots, p_n | a_{in}^\dagger(q_1) - a_{out}^\dagger(q_1) | q_2, \dots, q_m \rangle_{in} \end{aligned}$$

where $\text{}_{out}\langle \{p\}, -q_1 |$ represents an out state with a particle of momentum q_1 , if present, removed from the set $\{p\}$; if there is no such particle present then this term will be absent. This represents the case where one of the incident particles does not play any part in the scattering since all of its quantum numbers are conserved. We shall not concern ourselves with such “disconnected” pieces and so will drop them from now on.

Inverting the expressions in equations (2.3) and (2.4), we find the result

$$a_{in/out}^\dagger(k) = \lim_{t \rightarrow \mp\infty} i \int d^3x e^{-ik \cdot x} \overleftrightarrow{\partial}_0 \phi(x) \quad (2.21)$$

where $A \overleftrightarrow{\partial} B$ is defined as $A(\partial B) - (\partial A)B$, and ϕ is the field obeying the equations of motion of the free Lagrangian. A similar expression can be derived for $a_{in/out}(k)$. We can use this together with the identity

$$\left(\lim_{t \rightarrow \infty} - \lim_{t \rightarrow -\infty} \right) \int d^3x F(\vec{x}, t) = \lim_{t_f \rightarrow \infty, t_i \rightarrow -\infty} \int_{t_i}^{t_f} dt \frac{\partial}{\partial t} \int d^3x F(\vec{x}, t) \quad (2.22)$$

and the asymptotic condition defined in Eq.(2.18) to rewrite our expression as follows:

$$\begin{aligned} \mathcal{A} &= iZ^{-1/2} \int d^4x \partial_0 \left(e^{-iq_1 \cdot x} \overleftrightarrow{\partial}_0 \langle p_1, \dots, p_n | \psi(x) | q_2, \dots, q_m \rangle \right) \\ &= iZ^{-1/2} \int d^4x \langle p_1, \dots, p_n | e^{-iq_1 \cdot x} (\partial_0^2 \psi(x)) - (\partial_0^2 e^{-iq_1 \cdot x}) \psi(x) | q_2, \dots, q_m \rangle \end{aligned} \quad (2.23)$$

Now since $e^{-iq_1 \cdot x}$ satisfies the Klein-Gordon equation

$$(\square_x + m^2)e^{-iq_1 \cdot x} = (\partial_0^2 - \nabla^2 + m^2)e^{-iq_1 \cdot x} = K_x e^{-iq_1 \cdot x} = 0 \quad (2.24)$$

we can substitute for $\partial_0^2 e^{-iq_1 \cdot x}$ in Eq.(2.23) and integrate ∇^2 by parts² onto $\psi(x)$ to arrive at

$$iZ^{-1/2} \int d^4x e^{-iq_1 \cdot x} \langle p_1, \dots, p_n | K_x \psi(x) | q_2, \dots, q_m \rangle \quad (2.25)$$

We can extract all the *in* and *out* states through the same procedure to find

²We discard surface terms as usual.

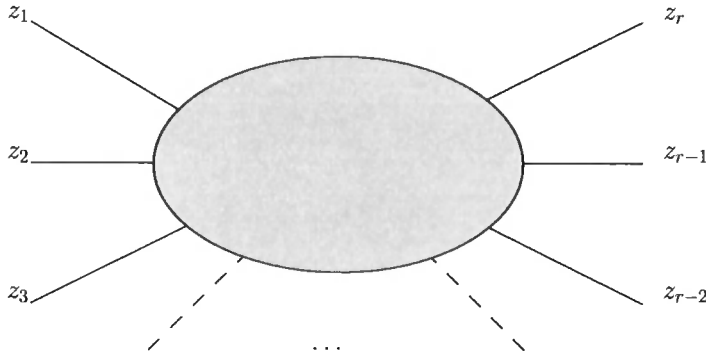


Figure 2.1: A general r particle Green's function.

that

$${}_{out}\langle p_1, \dots, p_n | q_1, \dots, q_m \rangle_{in} \equiv (iZ)^{-\frac{n+m}{2}} \int d^4x_1 \dots d^4x_m d^4y_1 \dots d^4y_n \quad (2.26)$$

$$e^{i\sum p_i \cdot y_i} e^{-i\sum q_i \cdot x_i} K_{y_1} \dots K_{y_n} K_{x_1} \dots K_{x_m} \langle 0 | T \{ \psi(y_1) \dots \psi(y_n) \psi(x_1) \dots \psi(x_m) \} | 0 \rangle$$

where $|0\rangle$ is the vacuum of the free theory. This is the final form of the LSZ reduction formula.

Eq.(2.26) is the starting point for all calculations of scattering amplitudes in modern quantum field theory. We shall see that $\langle 0 | T \{ \psi(z_1) \dots \psi(z_r) \} | 0 \rangle$ represents the sum of all Feynman diagrams with r particles created or destroyed at $(z_1 \dots z_r)$; this is illustrated in Figure 2.1. It is the complete r -particle Green's function. The Klein-Gordon operators, K_i , remove the propagators for the external legs, and so the reduction formula states that the S -matrix element is given by the Green's function for the $r = m + n$ particles with the external legs removed and the external momenta set on-shell.

2.4 Perturbative expansion of the correlation functions

Now that we have derived the LSZ reduction formula we have a recipe for calculating S -matrix elements. In order to proceed with the calculation we must now develop methods of working with the full field correlation functions. In order to do this we shall use perturbation theory.

The idea behind perturbation theory is that we apply it to a calculation which we are unable to perform, but which we are able to model in terms of a simpler theory which we can solve, and a small “correction” to that theory. The solution we are looking for will then take the form of the solution to the simple theory plus a series in powers of the small correction. In our case, we take the simpler theory to be the free theory (i.e. $\mathcal{L}_I = 0$) and we require the interaction part of the theory to be a small correction (i.e. the coupling constant present in \mathcal{L}_I must be small). In order to exploit this division in the most convenient way we shall transform the full fields into what is known as the *interaction picture*. We will then be able to relate the correlation function of the full fields, ψ , to the free fields, ϕ , which come from our free theory. We will see later that this relation will take the form

$$\langle 0|T\{\psi(x_1)\dots\psi(x_n)\}|0\rangle = \frac{\langle 0|T\{\phi(x_1)\dots\phi(x_n)\exp\left(-i\int_{-\infty}^{\infty}d^4x\mathcal{L}_I\right)\}|0\rangle}{\langle 0|T\{\exp\left(-i\int_{-\infty}^{\infty}d^4x\mathcal{L}_I\right)\}|0\rangle} \quad (2.27)$$

This expression now consists of correlation functions containing only fields which evolve in time in the same way as free fields. To perform the perturbative calculation we can expand $\exp\left(-i\int_{-\infty}^{\infty}d^4x\mathcal{L}_I\right)$ as a series. The problem of calculating the overlap of states is then reduced to that of calculating

various correlation functions of time ordered products of free fields. Higher terms in the expansion of $\exp\left(-i \int_{-\infty}^{\infty} d^4x \mathcal{L}_I\right)$ will correspond to higher orders in perturbation theory and will be suppressed due to the small size of the coupling constant³. We describe a contribution as *leading order* (LO) if the power of the coupling constant in the amplitude is the lowest possible value for that process. The next order in the perturbation series is known as *next-to-leading order* (NLO). This will have one more power in the coupling constant than the LO contribution. The next order in the series is known as *next-to-next-to-leading order*, and so on.

2.4.1 The interaction picture

We start from the Heisenberg picture where we have

$$\psi(x) = e^{iHt} \psi(\vec{x}) e^{-iHt} \quad (2.28)$$

At any fixed time t_0 , we can write ψ in terms of creation and annihilation operators:

$$\psi(t_0, \vec{x}) = \int \frac{d^3k}{(2\pi)^3 \sqrt{2\omega_k}} \left(a(t_0, \vec{k}) e^{i\vec{k}\cdot\vec{x}} + a^\dagger(t_0, \vec{k}) e^{-i\vec{k}\cdot\vec{x}} \right) \quad (2.29)$$

We define the field in the interaction picture through

$$\psi_I(t, \vec{x}) = e^{iH_0(t-t_0)} \psi(t_0, \vec{x}) e^{-iH_0(t-t_0)} \quad (2.30)$$

and immediately see from inspecting the expression in terms of the creation and annihilation operators that this is just the usual expression for the free

³Providing, of course, that we are at a suitable energy scale such that α_s is small.

field

$$\psi_I(t, \vec{x}) = \phi(t, \vec{x}) = \int \frac{d^3k}{(2\pi)^3 \sqrt{2\omega_k}} \left(a(t_0, \vec{k}) e^{-ik \cdot x} + a^\dagger(t_0, \vec{k}) e^{ik \cdot x} \right) \Big|_{x_0=t-t_0} \quad (2.31)$$

We now want to express the full Heisenberg field in terms of the interaction picture field. Formally we have

$$\begin{aligned} \psi(t, \vec{x}) &= e^{iH(t-t_0)} e^{-iH_0(t-t_0)} \psi_I(t, \vec{x}) e^{iH_0(t-t_0)} e^{-iH(t-t_0)} \\ &\equiv U^\dagger(t, t_0) \psi_I(t, \vec{x}) U(t, t_0) \end{aligned} \quad (2.32)$$

where we have defined the unitary operator

$$U(t, t_0) = e^{iH_0(t-t_0)} e^{-iH(t-t_0)} \quad (2.33)$$

which is known as the time-evolution operator. We now want to express this operator in terms of the interaction picture fields. We start by noting that $U(t, t_0)$ satisfies the following differential equation (with initial condition $U(t_0, t_0) = 1$)

$$\begin{aligned} i \frac{\partial}{\partial t} U(t, t_0) &= e^{iH_0(t-t_0)} (H - H_0) e^{-iH(t-t_0)} \\ &= e^{iH_0(t-t_0)} (H_{int}) e^{-iH(t-t_0)} \\ &= e^{iH_0(t-t_0)} (H_{int}) e^{-iH_0(t-t_0)} e^{iH_0(t-t_0)} e^{-iH(t-t_0)} \\ &= H_I(t) U(t, t_0) \end{aligned} \quad (2.34)$$

where

$$H_I(t) = e^{iH_0(t-t_0)} (H_{int}) e^{-iH_0(t-t_0)} \quad (2.35)$$

is the interaction Hamiltonian in the interaction picture. Since the inter-

action Hamiltonian in the Heisenberg picture contains a product of fields (also in the Heisenberg picture) and we are free to insert a factor of $1 = e^{-iH_0(t-t_0)}e^{iH_0(t-t_0)}$ in between the fields, we can see that $H_I(t)$ is just H_{int} with all the fields placed in the interaction picture.

We now solve Eq.(2.34) for $U(t, t_0)$ (see e.g. [35] for details), arriving at the form

$$U(t, t_0) = T \left\{ \exp \left[-i \int_{t_0}^t dt' H_I(t') \right] \right\} \quad (2.36)$$

where the time ordering of the exponential is defined as the Taylor series with each term time ordered.

We can easily generalise our definition of U so that its second argument can assume values other than the reference time t_0 . The correct definition is simply

$$U(t, t') = T \left\{ \exp \left[-i \int_{t'}^t dt'' H_I(t'') \right] \right\} \quad (t \geq t') \quad (2.37)$$

$U(t, t')$ satisfies the same differential equation as $U(t, t_0)$, (2.34), but now with the initial condition that $U=1$ for $t = t'$. This equation shows that U is unitary since we can see that

$$U(t, t') = e^{iH_0(t-t_0)} e^{-iH(t-t')} e^{-iH_0(t'-t_0)} \quad (2.38)$$

We also find the following useful identities for $t_1 \geq t_2 \geq t_3$:

$$U(t_1, t_2)U(t_2, t_3) = U(t_1, t_3) \quad (2.39)$$

$$U(t_1, t_3)U^\dagger(t_2, t_3) = U(t_1, t_2) \quad (2.40)$$

We are now in a position to manipulate our correlation function. For the

moment we shall assume that $z_1^0 > z_2^0 > \dots > z_n^0$. We then find

$$\begin{aligned}
& \langle 0 | \psi(z_1) \dots \psi(z_n) | 0 \rangle = \\
& \langle 0 | U^\dagger(z_1^0, t_0) \psi_I(z_1) U(z_1^0, t_0) U^\dagger(z_2^0, t_0) \dots U^\dagger(z_n^0, t_0) \psi_I(z_1) U(z_n^0, t_0) | 0 \rangle \\
& = \langle 0 | U^\dagger(T, t_0) U(T, z_1^0) \psi_I(z_1) U(z_1^0, z_2^0) \psi_I(z_2) \dots \psi_I(z_n) U(z_n^0, -T) U(-T, t_0) | 0 \rangle
\end{aligned} \tag{2.41}$$

where we have introduced a new reference time T which we will now allow to approach ∞ ; in this limit we will now have T later than z_1^0 and $-T$ earlier than z_n^0 , allowing us to place the majority of the expression in a time-ordered product as follows

$$\begin{aligned}
& \langle 0 | T \{ \psi(z_1) \dots \psi(z_n) \} | 0 \rangle = \\
& \langle 0 | U^\dagger(T, t_0) T \left\{ \psi_I(z_1) \dots \psi_I(z_n) \exp \left[-i \int_{-T}^T dt H_I(t) \right] \right\} U(-T, t_0) | 0 \rangle
\end{aligned} \tag{2.42}$$

where we have rewritten $U(T, -T)$ using the form given by Eq.(2.37)

We now have our expression completely in terms of the free fields except for the operators $U(-T, t_0)$ and $U^\dagger(T, t_0)$. We shall remove them by showing that the vacuum $|0\rangle$ is the eigenstate of these operators in the limit $T \rightarrow \infty$.

We consider an arbitrary in-state $|\alpha, p\rangle_{in}$ containing a particle, p , along with any other number of particles which we denote collectively by the symbol α .

We can then write

$$\begin{aligned}
{}_{in}\langle\alpha, p|U(-T, t_0)|0\rangle &= {}_{in}\langle\alpha|a_{in}(p)U(-T, t_0)|0\rangle \\
&= -i \int d^3x e^{-i(p^0 t' - \vec{p}\cdot\vec{x})} \vec{\partial}_{t'} \quad {}_{in}\langle\alpha|\phi(-t', \vec{x})U(-T, t_0)|0\rangle \\
&= -i \int d^3x e^{-i(p^0 t' - \vec{p}\cdot\vec{x})} \vec{\partial}_{t'} \quad {}_{in}\langle\alpha|U(-t', t_0)\psi(-t', \vec{x})[U(-t', t_0)]^\dagger U(-T, t_0)|0\rangle
\end{aligned} \tag{2.43}$$

Using the asymptotic condition from Eq.(2.18) as we send $T = t' \rightarrow \infty$ this approaches

$$\begin{aligned}
&Z^{-1/2} \quad {}_{in}\langle\alpha|U(-T, t_0)a_{in}(p)|0\rangle + i \int d^3x e^{-i(p^0 t' - \vec{p}\cdot\vec{x})} \\
&\times \quad {}_{in}\langle\alpha|\dot{U}(-T, t_0)\psi(-T, \vec{x}) + U(-T, t_0)\psi(-T, \vec{x})\dot{U}^\dagger(-T, t_0)U(-T, t_0)|0\rangle
\end{aligned} \tag{2.44}$$

The first term will clearly vanish since $a_{in}(p)|0\rangle = 0$. A closer look will reveal that the second term vanishes as well

$$\dot{U}\psi + U\psi\dot{U}^\dagger U = \dot{U}U^\dagger\phi U + \phi U\dot{U}^\dagger U = [\dot{U}U^\dagger, \phi]U = -i[H_I, \phi]U = 0 \tag{2.45}$$

where we have used Eq.(2.34) in the second last step and assumed no derivative couplings in H_I .

We are therefore able to conclude that

$${}_{in}\langle\alpha, p|U(-T, t_0)|0\rangle \rightarrow 0 \text{ as } T \rightarrow \infty \tag{2.46}$$

for all in-states $\{\alpha, p\}$ containing at least one particle. It then follows that

$$U(-T, t_0)|0\rangle = \lambda_-|0\rangle \text{ when } T \rightarrow \infty \quad (2.47)$$

and we can similarly show that

$$U(T, t_0)|0\rangle = \lambda_+|0\rangle \text{ when } T \rightarrow \infty \quad (2.48)$$

Now these constants λ_+ and λ_- appear in Eq.(3.32) in the form

$$\begin{aligned} \lambda_- \lambda_+^* &= \langle 0|U^\dagger(T, t_0)|0\rangle \langle 0|U(-T, t_0)|0\rangle \\ &= \langle 0|U(-T, t_0)U^\dagger(T, t_0)|0\rangle = \langle 0|U(-T, T)|0\rangle \\ &= \langle 0|T \left\{ \exp \left[i \int_{-T}^T dt H_I(t) \right] \right\} |0\rangle \\ &= \langle 0|T \left\{ \exp \left[-i \int_{-T}^T dt H_I(t) \right] \right\} |0\rangle^{-1} \end{aligned}$$

We can now rewrite Eq.(3.32) as

$$\langle 0|\psi(z_1) \dots \psi(z_n)|0\rangle = \lim_{T \rightarrow \infty} \frac{\langle 0|T \left\{ \psi_I(z_1) \dots \psi_I(z_n) \exp \left[-i \int_{-T}^T dt H_I(t) \right] \right\} |0\rangle}{\langle 0|T \left\{ \exp \left[-i \int_{-T}^T dt H_I(t) \right] \right\} |0\rangle} \quad (2.49)$$

where we have assumed the time-order $z_1^0 > z_2^0 > \dots > z_n^0$.

To arrive at the general case for any time ordering of the z 's we note that the right hand side of the expression is in time order, and would be so regardless of whatever time ordering we were to choose at the start of our manipulation.

We can therefore write the general case as:

$$\langle 0|T \{ \psi(z_1) \dots \psi(z_n) \} |0\rangle = \lim_{T \rightarrow \infty} \frac{\langle 0|T \left\{ \psi_I(z_1) \dots \psi_I(z_n) \exp \left[-i \int_{-T}^T dt H_I(t) \right] \right\} |0\rangle}{\langle 0|T \left\{ \exp \left[-i \int_{-T}^T dt H_I(t) \right] \right\} |0\rangle} \quad (2.50)$$

This expression will be our starting point for performing perturbative calculations. We simply need to expand the exponential as a power series to whatever order is necessary for our calculation. Once we have identified the order to which we want to calculate our amplitude, we are left with various correlation functions of free fields. Next we shall look at how we reduce these (potentially) large correlation functions into separate propagators and how we can eventually represent them as sums of Feynman diagrams.

2.5 Wick's theorem

Our immediate aim is to break down our time ordered correlation functions containing an arbitrary number of fields into products of propagators containing only two fields each. In order to achieve this we shall consider only two time ordered fields, and gradually extend the number upwards. If we start by placing the time ordered fields $T \{ \phi(x)\phi(y) \}$ in normal order (denoted by $:\phi(x)\phi(y):$ and meaning that all the creation operators have been placed to the right of all the annihilation operators) we can see that

$$T \{ \phi(x)\phi(y) \} = : \phi(x)\phi(y) : + \text{complex number} \quad (2.51)$$

since time order and normal order differ only in commutators of the annihilation and creation operators. We can easily identify the complex number by taking the vacuum expectation value of the expression since we note that the vacuum expectation value of any normal ordered product of operators must vanish. We find

$$T\{\phi(x)\phi(y)\} = : \phi(x)\phi(y) : + \langle 0|T\{\phi(x)\phi(y)\}|0\rangle \quad (2.52)$$

Our ultimate goal is to prove the general case for an arbitrary number of fields⁴

$$\begin{aligned} T\{\phi(x_1)\dots\phi(x_n)\} &= : \phi(x_1)\dots\phi(x_n) : \\ &+ [\langle 0|T\{\phi(x_1)\phi(x_2)\}|0\rangle : \phi(x_3)\dots\phi(x_n) : + \text{permutations}] + \dots \\ &+ [\langle 0|T\{\phi(x_1)\phi(x_2)\}|0\rangle \dots \langle 0|T\{\phi(x_{n-1})\phi(x_n)\}|0\rangle + \text{permutations}] \end{aligned} \quad (2.53)$$

which can be done by induction [36]. The advantage of writing our time ordered fields in this form is clear, since when we take the vacuum expectation value all the terms containing normal ordered pieces vanish, leaving us with nothing in the case of an odd number of fields, or a sum of all possible time ordered pairs in the case of an even number

$$\begin{aligned} &\langle 0|T\{\psi(x_1)\dots\psi(x_n)\}|0\rangle \\ &= \begin{cases} 0 & : \text{odd } n \\ \sum_P \langle 0|T\{\psi(x_1)\psi(x_2)\}|0\rangle \dots \langle 0|T\{\psi(x_{n-1})\psi(x_n)\}|0\rangle & : \text{even } n \end{cases} \end{aligned}$$

⁴The example here is for an even number of fields n . In the case of n odd, the final line would include one single field as well as the vacuum expectation values of time ordered pairs.

where P is a sum over all permutations of the x_i such that we only count $\langle 0|T\{\psi(x_1)\psi(x_2)\}|0\rangle$ and $\langle 0|T\{\psi(x_2)\psi(x_1)\}|0\rangle$ as a single term. These time ordered correlation functions of two free fields are the propagators of our theory which we have already met in Section 2.2.

2.6 Feynman diagrams

From this point it is simple to place the general time ordered correlation function in the form of a sum of Feynman diagrams. We work from a Lagrangian standpoint so that $\int dt H_I(t)$ becomes $-\int d^4x \mathcal{L}_I(x)$. Once we have expanded the exponential of Eq.(2.50) to the required order for our calculation, we will then have a time ordered correlation function comprising our external fields - located at distinct points in space-time - and a series of groups of fields corresponding to the possible interactions of the theory - all fields in the group will be located at the same space-time point which is integrated over all space-time. The number of these groups will correspond to the order of our expansion. For example, in the case of ϕ^4 theory, where $\mathcal{L}_I = \frac{\lambda}{4!}\phi^4$, with two external particles an expansion to first order in the coupling constant, λ , would give

$$\begin{aligned} \langle 0|T\left\{\phi(x)\phi(y)\exp\left(-i\int d^4z\frac{\lambda}{4!}\phi^4\right)\right\}|0\rangle_{\mathcal{O}(\lambda)} \\ = \langle 0|T\left\{\phi(x)\phi(y)\left(\frac{-i\lambda}{4!}\right)\int d^4z\phi(z)\phi(z)\phi(z)\phi(z)\right\}|0\rangle \quad (2.54) \end{aligned}$$

We can now apply Wick's theorem to this correlation function. We get one term for each way of contracting pairs of the ϕ operators. Many of these contractions will be equivalent (for example, if we contract $\phi(x)$ with $\phi(y)$)

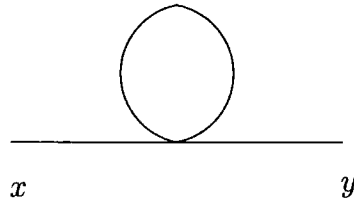


Figure 2.2: A possible Feynman diagram for Eq.(2.54)

in the example above then there are three ways to contract the $\phi(z)$'s with each other). Each distinct way of performing these contractions will make up one of our Feynman diagrams.

We now consider one possible configuration of these propagators. To create our diagram we represent each propagator $\langle 0|T\{\phi(x)\phi(y)\}|0\rangle$ as a line connecting the points x and y . Vertices will appear as a result of the interaction terms since these will contain three or more fields at the same space-time point. Consequently, when we use these diagrams as a resource for calculation, any factors other than the fields present in the interaction Lagrangian will be associated with the relevant vertex. For example, a Feynman diagram from the expression in Eq.(2.54) is shown in Figure 2.2. It is relatively straightforward to come up with a set of *Feynman rules* which allow us to write down the amplitude to be calculated directly from the Feynman diagram (see e.g. [35]). Conventionally we will use Feynman rules which are formulated in momentum space. Since momentum is conserved at each vertex we will be left with one four-dimensional momentum integral for every closed loop in the diagram.

The topological structure of Feynman diagrams at LO is usually that of a tree diagram (i.e. there are no closed loops in the diagram). The NLO contribution will have one more power in the coupling constant than the LO

contribution and will consequently have an extra vertex but no new external legs. NLO diagrams must therefore have an extra loop when compared to leading order diagrams. This means that NLO contributions usually have the topology of a single loop, in other words a one-loop Feynman diagram. We can see that as we increase the order of the calculation the same thing will keep happening. For example, NNLO processes will have one loop more than NLO processes and so usually result in two-loop Feynman diagrams.

2.6.1 Disconnected diagrams

When we consider the perturbative expansion of the correlation function that appears in the LSZ reduction formula, we see in Eq.(2.50) that along with the Green's function for however many external particles we are considering we also need to calculate the Green's function with no external particles, $\langle 0|T \left\{ \exp \left[-i \int_{-T}^T dt H_I(t) \right] \right\} |0\rangle$. Following our prescription for drawing Feynman diagrams, we can see that this will correspond to *disconnected diagrams* where none of the legs are connected to external points⁵. If we now consider the Green's function with external legs we can see that a typical Feynman diagram derived from this starting point will contain several disconnected pieces as well as a diagram with the external legs connected (see Figure 2.3).

We label the set of possible disconnected pieces V_i ; these are connected internally, but disconnected from external points, as illustrated in Figure 2.4.

We then consider an arbitrary diagram which has n_i pieces of the form V_i for

⁵These are not to be confused with the disconnected pieces which appeared briefly in Section 2.3 when we described the LSZ reduction formula. Disconnected pieces contain no parts which aren't connected to external legs, but consist of two or more parts with no connection between them.

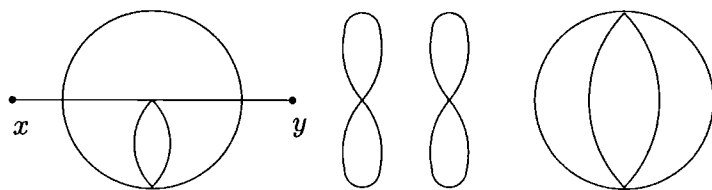


Figure 2.3: A typical Feynman diagram in ϕ^4 theory including both connected and disconnected pieces.

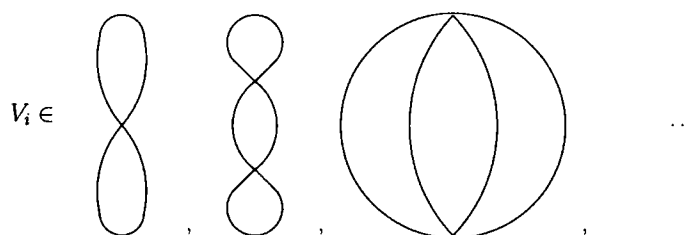


Figure 2.4: The set of disconnected diagrams, V_i , in ϕ^4 theory.

each i , along with one piece which is connected to the external legs. If we also let V_i denote the *value* of the piece V_i , then the value of this diagram will be given by

$$(\text{value of connected piece}) \times \prod_i \frac{1}{n_i!} (V_i)^{n_i} \tag{2.55}$$

where $1/n!$ is a symmetry factor which arises from interchanging the n_i copies of V_i . The numerator of Eq.(2.50) will be given by the sum of all possible diagrams which we can write as follows

$$\sum_{\text{all connected pieces}} \sum_{\text{all } \{n_i\}} (\text{value of connected piece}) \times \prod_i \frac{1}{n_i!} (V_i)^{n_i} \tag{2.56}$$

where “all n_i ” refers to ordered sets of nonnegative integers only. We can

factor out the sum of connected pieces from this expression, arriving at

$$= \sum(\text{connected}) \times \sum_{\text{all } \{n_i\}} \prod_i \frac{1}{n_i!} (V_i)^{n_i} \quad (2.57)$$

In a similar fashion we can factor the rest of expression as well

$$\begin{aligned} &= \sum(\text{connected}) \times \left(\sum_{n_1} \frac{1}{n_1!} (V_1)^{n_1} \right) \left(\sum_{n_2} \frac{1}{n_2!} (V_2)^{n_2} \right) \dots \\ &= \sum(\text{connected}) \times \prod_i \sum_{n_i} \frac{1}{n_i!} (V_i)^{n_i} \\ &= \sum(\text{connected}) \times \prod_i \exp(V_i) \\ &= \sum(\text{connected}) \times \exp\left(\sum_i V_i\right) \end{aligned} \quad (2.58)$$

This shows that the sum of *all* diagrams is equal to the sum of all *connected* pieces multiplied by the exponential of the sum of all *disconnected* pieces.

By a similar argument we can show that $\langle 0|T \left\{ \exp \left[-i \int_{-T}^T dt H_I(t) \right] \right\} |0\rangle$ is simply the exponential of the sum of all disconnected pieces alone. Consequently, when we calculate $\langle 0|T \{ \psi(z_1) \dots \psi(z_n) \} |0\rangle$ using Eq.(2.50) we see that the exponential factor in the numerator will cancel the denominator and so our final prescription for calculating our correlation functions will simply be the sum of all possible connected Feynman diagrams.

2.7 Phase Space calculations

Since we are forced to perform our calculation through a perturbative expansion, this means that we will be calculating amplitudes to a particular order in that expansion. It follows that we will also calculate the physical

observables of Eq.(1.1) to a particular order. Since physical observables contain the modulus squared of the amplitude, the contribution to a particular order will involve the multiplication of amplitudes at different orders. For a general physical observable σ_J at order n we will have

$$\begin{aligned} \sigma_J|_n = & \int dLips(p_1, \dots, p_k) \mathcal{A}_1^* \times \mathcal{A}_{n-1} J(p_1, \dots, p_k) \\ & + \int dLips(p_1, \dots, p_l) \mathcal{A}_2^* \times \mathcal{A}_{n-2} J(p_1, \dots, p_l) \\ & + \dots + \int dLips(p_1, \dots, p_m) \mathcal{A}_{n-1}^* \times \mathcal{A}_1 J(p_1, \dots, p_m) \quad (2.59) \end{aligned}$$

where $Lips(p_1, \dots, p_j)$ is the phase space associated with integrating over the momenta of the external particles in the amplitudes given by \mathcal{A}_i , and i denotes the order in the coupling to which we have calculated the amplitude. $J(p_1, \dots, p_j)$ is the weighting function for the physical observable and will also depend on the momenta of the external particles. This means that if we want to calculate a process up to a certain order in perturbation theory we would need all the amplitudes from leading order up to that order to get the complete result. Since we must include all physically indistinguishable contributions in our calculation of the process the amplitudes at different orders may contain different numbers of incoming and outgoing particles. This means that each piece will in general have a different phase space integral and the sum of the amplitudes will, in general, be an incoherent sum.

We could now use IR regulated amplitudes to calculate an infrared safe quantity. When we combine all the pieces of Eq.(2.59) this will then give us a completely finite result with the exception of one significant case [3, 38, 39]. We find that all the divergent parts of an amplitude which contributes to Eq.(2.59) will cancel with similar divergent parts associated with the other

amplitudes. We are then free to remove the regulator leaving us with our desired result. The only exception to this occurs when we have initial state collinear singularities. In this situation the initial state singularities do not all cancel and instead we absorb them into the definition of what are known as parton distribution functions (PDFs) which describe the probability of finding a certain type of parton within an incoming particle [1]. The factorisation theorem [1] then allows us to separate out the long range behaviour, including the collinear singularities and non-perturbative effects, into these PDFs. The short distance behaviour then has no initial state infrared divergences and can be calculated perturbatively.

2.8 An example infrared safe calculation

We now give a brief illustration of the cancellation of infrared divergences when calculating IR safe observables. We take as an example the total cross section for $e^+e^- \rightarrow 2$ jets at NLO. As described in Section 2.4 we need to consider amplitudes which give physically indistinguishable contributions and so we will have to calculate the amplitude for an incoming photon and an outgoing quark and anti-quark (known as the virtual contribution since it involves a virtual gluon) and the amplitude for an incoming photon and an outgoing quark, anti-quark and gluon (known as the real contribution since we have a real gluon in this case). The first process is shown in Figure 2.5 and its amplitude is given by

$$\begin{aligned} \mathcal{A}(q_{p_1}, \bar{q}_{p_2}; \gamma(P)) = \\ e\mathcal{A}_{0,1}(q_{p_1}, \bar{q}_{p_2}; \gamma(P)) + eg^2\mathcal{A}_{2,1}(q_{p_1}, \bar{q}_{p_2}; \gamma(P)) + \mathcal{O}(g^4) \end{aligned} \quad (2.60)$$

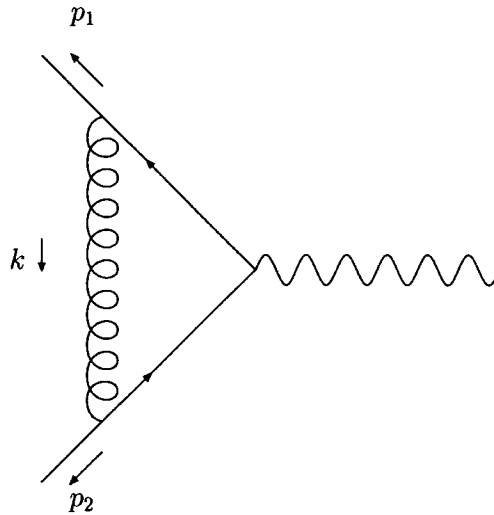


Figure 2.5: The vertex correction diagram

where e is the electromagnetic coupling constant and g is the strong coupling constant, $\mathcal{A}_{0,1}$ contains a single quark-antiquark-photon vertex and $\mathcal{A}_{2,1}$ contains a quark-antiquark-photon vertex and two quark-antiquark-gluon vertices.

The second process is shown in Figure 2.6 and its amplitude is given by

$$\mathcal{A}(q_{p_1}, \bar{q}_{p_2}, g_{p_3}; \gamma(P)) = eg\mathcal{A}_{1,1}(q_{p_1}, \bar{q}_{p_2}, g_{p_3}; \gamma(P)) + \mathcal{O}(g^3) \quad (2.61)$$

where $\mathcal{A}_{1,1}$ represents the amplitude containing a single quark-antiquark-photon vertex and a single quark-antiquark-gluon vertex. We can rewrite the general form of Eq.(2.59) for this specific process at order e^2g^2 as

$$\begin{aligned} \sigma_J|_{e^2g^2} = \lim_{\epsilon \rightarrow 0} & \left(\int dLips(p_1, p_2) \mathcal{A}_{2,1}^* \times \mathcal{A}_{0,1} J(p_1, p_2) \right. \\ & + \int dLips(p_1, p_2, p_3) |\mathcal{A}_{1,1}|^2 J(p_1, p_2, p_3) \\ & \left. + \int dLips(p_1, p_2) \mathcal{A}_{0,1}^* \times \mathcal{A}_{2,1} J(p_1, p_2) \right) \quad (2.62) \end{aligned}$$

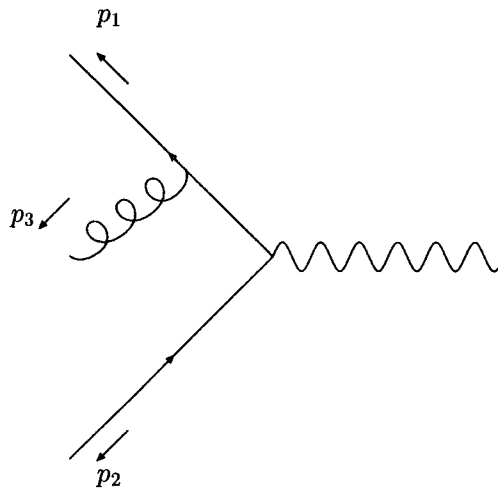


Figure 2.6: The real emission diagram

where ϵ is our regulator in dimensional regularisation as before. We can, in fact, represent Eq.(2.59) in the form of a diagram as well. We notice that if we interpret the \mathcal{A}^* s which appear in the equation as mirror image Feynman diagrams and fuse the final states with those of their respective \mathcal{A} s then each separate term will give rise to the same composite diagram. Each possible way of cutting this composite diagram in two generates a *cut diagram* which corresponds to one term in our original equation. This can now be thought of as the sum over the cuts of the composite diagram. The cut diagrams in our particular example are shown in Figure 2.7 where cuts 1, 2 and 3 refer to the first, second and third terms in Eq.(2.62) respectively.

To ensure that σ_J is an infrared safe observable the weighting function $J(p_1, \dots)$ must satisfy certain conditions in the soft and collinear limits. Notably it must not change between processes which differ only by the emission

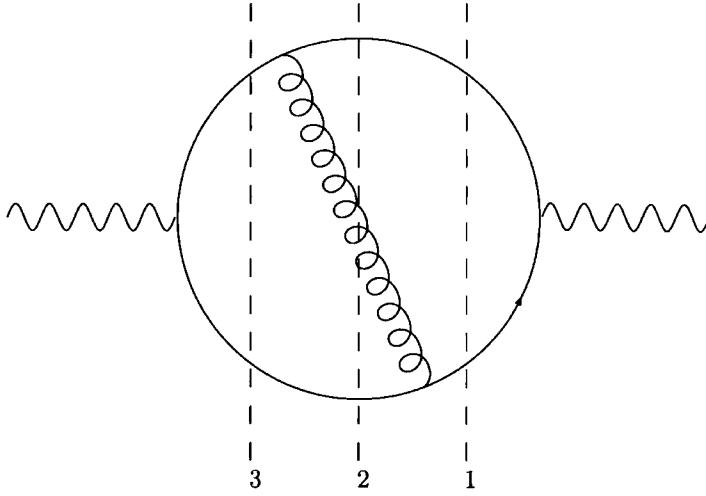


Figure 2.7: The cut diagrams for Eq.(2.62)

of a soft or collinear particle so that we have

$$\begin{aligned}
 J(p_1, \dots, p_m, 0, p_{m+2}, \dots, p_n) &= J(p_1, \dots, p_m, p_{m+2}, \dots, p_n) \\
 J(p_1, \dots, (1 - \lambda)p_m, \lambda p_m, p_{m+2}, \dots, p_n) &= J(p_1, \dots, p_m, p_{m+2}, \dots, p_n)
 \end{aligned}
 \tag{2.63}$$

For this example however we will just choose the simplest example of the total cross section and set $J = 1$. We can now perform the phase space integration and obtain

$$\sigma \equiv \sigma_{J=1} = \int d\sigma_0 + \lim_{\epsilon \rightarrow 0} \int (e^2 g^2 d\sigma_{q\bar{q}} + e^2 g^2 d\sigma_{q\bar{q}g}) + \mathcal{O}(g^4)
 \tag{2.64}$$

where

$$d\sigma_0 \sim |\mathcal{A}_{0,1}(q_{p_1}, \bar{q}_{p_2}; \gamma(P))|^2
 \tag{2.65}$$

$$d\sigma_{q\bar{q}} \sim 2\text{Re} [\mathcal{A}_{0,1}(q_{p_1}, \bar{q}_{p_2}; \gamma(P)) \mathcal{A}_{2,1}^*(q_{p_1}, \bar{q}_{p_2}; \gamma(P))]
 \tag{2.66}$$

$$d\sigma_{q\bar{q}g} \sim |\mathcal{A}_{1,1}(q_{p_1}, \bar{q}_{p_2}, g_{p_3}; \gamma(P))|^2
 \tag{2.67}$$

As expected, both the virtual cross section, $d\sigma_{q\bar{q}}$, and the real cross section, $d\sigma_{q\bar{q}g}$ contain infrared singularities which only cancel when we combine them to form an infrared safe observable. We obtain the following results for the various cross sections

$$\sigma_0 = \frac{4\pi\alpha_{em}^2 e_q^2 N_c}{3s} \quad (2.68)$$

$$\sigma_{q\bar{q}} = \sigma_0 C_F \frac{\alpha_s}{\pi} c_\Gamma \left(\frac{1}{\epsilon^2} + \frac{3}{2\epsilon} + \frac{19}{4} - \frac{\pi^2}{2} \right) + \mathcal{O}(\epsilon) \quad (2.69)$$

$$\sigma_{q\bar{q}g} = \sigma_0 C_F \frac{\alpha_s}{\pi} c_\Gamma \left(-\frac{1}{\epsilon^2} - \frac{3}{2\epsilon} - 4 + \frac{\pi^2}{2} \right) + \mathcal{O}(\epsilon) \quad (2.70)$$

where $c_\Gamma = 1 + \mathcal{O}(\epsilon)$ and $C_F = (N_c^2 - 1)/(2N_c) = 4/3$. Our final result for the cross section at next to leading order will be obtained by summing these results and then setting ϵ to zero

$$\sigma = \sigma_0 + \sigma_{q\bar{q}} + \sigma_{q\bar{q}g} = \sigma_0 \left(1 + \frac{\alpha_s}{4\pi} 3C_F \right) \quad (2.71)$$

where since all negative powers of ϵ have cancelled it is safe to remove the regulator by taking the limit $\epsilon \rightarrow 0$.

Chapter 3

A New Approach

The goal of our approach to performing calculations in perturbation theory is to remove the problems of infrared divergences. In the standard approach to computing transition amplitudes within a Hamiltonian framework we split the Hamiltonian, H , into two parts so that $H = H_0 + H_I$ where H_I contains all the interactions of the theory. The external states, $|\phi_i\rangle$ are characterised by a complete set of quantum numbers, i , of the free Hamiltonian, H_0 . The matrix element for this state to evolve into a given final state, $\langle\phi_f|$ is then given by $\langle\phi_f|S|\phi_i\rangle$, where $S = \Omega_-^\dagger \Omega_+$ can be expressed in terms of Möller operators

$$\Omega_\mp \equiv \lim_{\tau \rightarrow \pm\infty} e^{i\tau H} e^{-i\tau H_0} \quad (3.1)$$

However, as we saw earlier, in the presence of long-range interactions free states are not true asymptotic states and this incorrect formulation leads to infrared singularities.

In order to overcome this problem we choose to work in the asymptotic interaction picture (AIP) [31]. We split our interaction Hamiltonian into hard and soft parts, $H_I = H_H + H_S$, such that all the long range interactions

Chapter 3: A New Approach

are contained in H_S . We then define our asymptotic Hamiltonian as $H_A = H_0 + H_S$ and now propose an approach where our external states, $|\Xi_i\rangle$ are characterised by a complete set of quantum numbers, i , of the asymptotic Hamiltonian, H_A . We can then construct modified Möller operators

$$\Omega_{A\mp} \equiv \lim_{\tau \rightarrow \pm\infty} e^{i\tau H} e^{-i\tau H_A} \quad (3.2)$$

and compute modified matrix elements of the asymptotic S -matrix

$$\langle \Xi_f | S_A | \Xi_i \rangle \equiv \langle \Xi_f | \Omega_{A-}^\dagger \Omega_{A+} | \Xi_i \rangle \quad (3.3)$$

which will be infrared finite.

This is the approach which was followed in [34], and while it proved possible to perform a simple calculation in this fashion, the amplitudes produced by this method are not covariant. This results in various complications which make the construction of cross sections for more complicated examples impractical. Consequently, we wish to create a similar approach based on a Lagrangian formalism in order to arrive at covariant amplitudes.

We achieve this by splitting the QCD Lagrangian into “free” and “interaction” parts in a similar manner to the Hamiltonian AIP approach so that

$$\mathcal{L} = \mathcal{L}_A + \mathcal{L}_H = \mathcal{L}_0 + \mathcal{L}_S + \mathcal{L}_H \quad (3.4)$$

Here, \mathcal{L}_0 is the usual free Lagrangian which is used to define the traditional free states; the usual interaction Lagrangian has been split into a soft or infrared part, \mathcal{L}_S , which contains all the soft and collinear parts of the interactions, and a hard part, \mathcal{L}_H , containing the rest of the interaction Lagrangian

such that $\mathcal{L}_I = \mathcal{L}_S + \mathcal{L}_H$. We will define our asymptotic states through our asymptotic Lagrangian $\mathcal{L}_A = \mathcal{L}_0 + \mathcal{L}_S$, thus including the necessary infrared parts of the Lagrangian in our definition. We can then create our asymptotic interaction picture using \mathcal{L}_A in exactly the same way that the standard interaction picture is created with \mathcal{L}_0 .

As in the standard interaction picture we will find that we are interested in the calculation of time ordered correlation functions such as

$$\langle 0 | T \{ \psi(x_1) \dots \psi(x_n) \} | 0 \rangle \quad (3.5)$$

although in our case these will be related to S_A -matrix elements calculated using asymptotic fields derived from \mathcal{L}_A rather than \mathcal{L}_0 . This will require us to modify the usual LSZ derivation. We will examine this later; we start by looking a little more closely at the asymptotic states themselves.

3.1 The asymptotic condition

The adiabatic assumption asserts that as $t \rightarrow \pm\infty$ we find the following weak operator limit result¹

$$\langle \alpha | \psi(x) | \beta \rangle = Z_A^{1/2} \langle \alpha | \phi_A(x) | \beta \rangle \quad (3.6)$$

where $Z_A^{1/2}$ relates the fields of the full theory ψ to the asymptotic fields ϕ_A which obey the equations of motion generated by \mathcal{L}_A . It is usual to take the asymptotic field ϕ_A to be the free field ϕ ; however, as we have seen, it is

¹This condition is often written as $\psi(x) \rightarrow Z_A^{1/2} \phi_A(x)$ with the understanding that it does not hold in general but only for quantities calculated between two states as detailed here.

this assumption which leads to the appearance of infrared divergences in our amplitude calculations. Consequently, in our new approach, we shall adopt the asymptotic condition

$$\psi(x) \rightarrow Z_{\Xi}^{1/2} \Xi(x) \quad (3.7)$$

where we use Ξ to represent our asymptotic fields. Amplitudes calculated in the asymptotic interaction picture on these asymptotic states should be free of infrared divergences and should also be equivalent to amplitudes calculated in the interaction picture on the free states once the infrared divergences have been regularised.

3.2 The asymptotic fields

We want to find a suitable representation for the asymptotic states of a full theory satisfying

$$(\square_x + m^2)\psi(x) = \frac{\partial \mathcal{L}_I}{\partial \psi(x)} \quad (3.8)$$

and the equal-time commutation relations

$$[\psi(t, \vec{x}), \psi(t, \vec{y})] = [\pi(t, \vec{x}), \pi(t, \vec{y})] = 0 \quad (3.9)$$

$$[\psi(t, \vec{x}), \pi(t, \vec{y})] = i\delta(\vec{x} - \vec{y}) \quad (3.10)$$

Assuming no derivative coupling terms are present in \mathcal{L}_{int} then we also have

$$\pi(x) = \partial_0 \psi(x) \quad (3.11)$$

We now require that our asymptotic field $\Xi(x)$ fulfils the following properties:

- In order to preserve the covariance of the states, $\Xi(x)$ must transform in the same way as the corresponding $\psi(x)$ under coordinate displacements and Lorentz transformations. In particular, for displacements, this will give

$$[P^\mu, \Xi(x)] = -i \frac{\partial \Xi(x)}{\partial x_\mu} \quad (3.12)$$

- $\Xi(x)$ will obey the equations of motion deriving from \mathcal{L}_A and will therefore satisfy the following equation

$$(\square_x + m^2)\Xi(x) = \frac{\partial \mathcal{L}_S}{\partial \Xi(x)} \quad (3.13)$$

We are unable to solve this equation for Ξ exactly, and so we will not have the same ability to calculate with the asymptotic fields that we have with the free fields, but will have to find ways of relating the two perturbatively. We shall discuss this in more depth later but for the moment we notice that the fact that the expression for our asymptotic fields contains part of the interaction Lagrangian suggests that parton number will no longer be a good quantum number for our external states. We can use the conditions in Eqs.(3.12) and (3.13) to illustrate this by investigating the states which $\Xi(x)$ creates from the vacuum.

Consider an arbitrary eigenstate

$$P^\mu |n\rangle = p^\mu |n\rangle \quad (3.14)$$

and form the following matrix element with the vacuum $|0\rangle$

$$-i \frac{\partial}{\partial x_\mu} \langle n | \Xi(x) | 0 \rangle = \langle n | [P^\mu, \Xi(x)] | 0 \rangle = p_n^\mu \langle n | \Xi(x) | 0 \rangle \quad (3.15)$$

Repeating the operation and using Eq.(3.13) we find

$$(\square_x + m^2)\langle n|\Xi(x)|0\rangle = (m^2 - p_n^2)\langle n|\Xi(x)|0\rangle = \langle n|\frac{\partial\mathcal{L}_S}{\partial\Xi(x)}|0\rangle \quad (3.16)$$

In other words, the states we are producing are not those with $p_n^2 = m^2$ as in the usual free case, but their invariant mass will differ from this in a way which depends on our asymptotic Lagrangian. This can be identified with the interpretation that these states no longer consist solely of the original parton, but include a cloud of soft and collinear partons as well.

We now assume that we can write the asymptotic fields in terms of creation and annihilation operators as in the free case, arriving at the form

$$\Xi(t, \vec{x}) = \int \frac{d^3k}{(2\pi)^3\sqrt{2E_k}} \left(a_a(t, \vec{k})e^{i\vec{k}\cdot\vec{x}} + a_a^\dagger(t, \vec{k})e^{-i\vec{k}\cdot\vec{x}} \right) \quad (3.17)$$

with the conjugate momentum now given by

$$\begin{aligned} \Pi_\Xi(t, \vec{x}) &= \int \frac{d^3k}{(2\pi)^3\sqrt{2E_k}} \left(\partial_0 a_a(t, \vec{k})e^{i\vec{k}\cdot\vec{x}} + \partial_0 a_a^\dagger(t, \vec{k})e^{-i\vec{k}\cdot\vec{x}} \right) \\ &= i \int \frac{d^3k}{(2\pi)^3\sqrt{2E_k}} \left([H_A, a_a(t, \vec{k})] e^{i\vec{k}\cdot\vec{x}} + [H_A, a_a^\dagger(t, \vec{k})] e^{-i\vec{k}\cdot\vec{x}} \right) \end{aligned} \quad (3.18)$$

where we will no longer have the relation $k_0 = \sqrt{\vec{k}^2 + m^2}$ since, as we saw earlier, our asymptotic states will have a different invariant mass from the usual free states.

Our annihilation operators are defined so that they give zero when they act on the vacuum at asymptotic times

$$\lim_{t \rightarrow \infty} \langle 0|a_a^\dagger(t, \vec{k}) = 0 \text{ and } \lim_{t \rightarrow -\infty} a_a(t, \vec{k})|0\rangle = 0 \quad (3.19)$$

while the creation operators create an asymptotic state

$$\lim_{t \rightarrow -\infty} a_a^\dagger(t, \vec{k})|0\rangle = \lim_{t \rightarrow -\infty} |\Xi(t, \vec{k})\rangle = |\Xi_{in}(\vec{k})\rangle \quad (3.20)$$

and they satisfy the usual equal time commutation relations

$$\begin{aligned} [a_a(t, \vec{k}), a_a^\dagger(t, \vec{k}')] &= (2\pi)^3 \delta(\vec{k} - \vec{k}') \\ [a_a(t, \vec{k}), a_a(t, \vec{k}')] &= 0, \quad [a_a^\dagger(t, \vec{k}), a_a^\dagger(t, \vec{k}')] = 0 \end{aligned} \quad (3.21)$$

We now use the commutation relation for the asymptotic fields, $[\Xi(t, \vec{x}), \Pi_\Xi(t, \vec{y})] = i\delta(\vec{x} - \vec{y})$, to investigate the structure of the commutators which appear in our expression for $\Pi_\Xi(x)$. Applying this relation we require

$$\begin{aligned} i \int \frac{d^3 k}{(2\pi)^3 \sqrt{2E_k}} \frac{d^3 k'}{(2\pi)^3 \sqrt{2E_{k'}}} & \left([a_a(t, \vec{k}), [H_A, a_a(t, \vec{k}')]] e^{i\vec{k}\cdot\vec{x}} e^{i\vec{k}'\cdot\vec{y}} \right. \\ & + [a_a(t, \vec{k}), [H_A, a_a^\dagger(t, \vec{k}')]] e^{i\vec{k}\cdot\vec{x}} e^{-i\vec{k}'\cdot\vec{y}} + [a_a^\dagger(t, \vec{k}), [H_A, a_a(t, \vec{k}')]] e^{-i\vec{k}\cdot\vec{x}} e^{i\vec{k}'\cdot\vec{y}} \\ & \left. + [a_a^\dagger(t, \vec{k}), [H_A, a_a^\dagger(t, \vec{k}')]] e^{-i\vec{k}\cdot\vec{x}} e^{-i\vec{k}'\cdot\vec{y}} \right) = i\delta(\vec{x} - \vec{y}) \quad (3.22) \end{aligned}$$

and we see that the expected relation

$$[H_A, a_a(t, \vec{k})] = -E_k a_a(t, \vec{k}), \quad [H_A, a_a^\dagger(t, \vec{k})] = E_k a_a(t, \vec{k}) \quad (3.23)$$

is indeed suggested. This allows us to write the creation and annihilation

operators in terms of the fields as follows

$$\begin{aligned} a_a(t, \vec{k}) &= \int d^3x e^{-i\vec{k}\cdot\vec{x}} (E_k \Xi(t, \vec{x}) + i\Pi_\Xi(t, \vec{x})) \\ a_a^\dagger(t, \vec{k}) &= \int d^3x e^{i\vec{k}\cdot\vec{x}} (E_k \Xi(t, \vec{x}) - i\Pi_\Xi(t, \vec{x})) \end{aligned} \quad (3.24)$$

or, putting them in the Heisenberg picture via $a_a(t, \vec{k}) = e^{iH_A t} a_a(\vec{k}) e^{-iH_A t}$ and applying the commutation relation from Eq.(3.23), we find

$$\begin{aligned} a_a(\vec{k}) &= \int d^3x e^{-ik\cdot x} (E_k \Xi(t, \vec{x}) + i\Pi_\Xi(t, \vec{x})) \Big|_{k^0=E_k} \\ a_a^\dagger(\vec{k}) &= \int d^3x e^{ik\cdot x} (E_k \Xi(t, \vec{x}) - i\Pi_\Xi(t, \vec{x})) \Big|_{k^0=E_k} \end{aligned} \quad (3.25)$$

3.3 The modified LSZ reduction formula

Now that we have some understanding of the asymptotic states we shall look at how the definition of the LSZ reduction formula will proceed in the asymptotic interaction picture. Here we will do this for a scalar theory but the extension to fermions and vector fields should proceed easily as in the usual derivation. This will then allow us to relate the time ordered correlation functions of Eq.(3.5) to S_A -matrix elements calculated on the asymptotic states. As in the usual case we start by extracting an asymptotic creation operator from the initial state

$$\begin{aligned} \mathcal{A} &= \text{out} \langle p_1, \dots, p_n | q_1, \dots, q_m \rangle_{in} \\ &= \lim_{q_1^0 \rightarrow -\infty} \text{out} \langle p_1, \dots, p_n | a_{in}^\dagger(q_1) | q_2, \dots, q_m \rangle_{in} \end{aligned} \quad (3.26)$$

where $a_{in}^\dagger(q_1)$ is an asymptotic creation operator a_a^\dagger . We now write the creation operator as an asymptotic *in* field using equation Eq.(3.24)

$$\begin{aligned} & \lim_{q_1^0 \rightarrow -\infty} \text{out} \langle p_1, \dots, p_n | a_{in}^\dagger(q_1) | q_2, \dots, q_m \rangle_{in} \\ &= \lim_{t \rightarrow -\infty} \int d^3x e^{i\vec{q}_1 \cdot \vec{x}} \langle p_1, \dots, p_n | E_{q_1} \Xi_{in}(t, \vec{x}) - i\Pi_\Xi(t, \vec{x}) | q_2, \dots, q_m \rangle \end{aligned} \quad (3.27)$$

where we have dropped the *in* and *out* labels from the *in* and *out* states. In the asymptotic limit we can then write

$$\begin{aligned} iE_k \Xi(t, \vec{x}) + \Pi_\Xi(t, \vec{x}) &= i(e^{-iE_k t} \overleftrightarrow{\partial}_0 \Xi(t, \vec{x})) \\ &= iZ_\Xi^{-1/2} (e^{-iE_k t} \overleftrightarrow{\partial}_0 \psi(t, \vec{x})) \end{aligned} \quad (3.28)$$

Eq.(3.27) then becomes

$$\lim_{t \rightarrow -\infty} (-i) Z_\Xi^{-1/2} \int d^3x e^{-iq_1 \cdot x} \overleftrightarrow{\partial}_0 \langle p_1, \dots, p_n | \psi(t, \vec{x}) | q_2, \dots, q_m \rangle \quad (3.29)$$

where the invariant mass is different from its value in the traditional interaction picture since it now depends on \mathcal{L}_S and we write it as $q_1^2 = M_A^2$. We then add and subtract the following term

$$\lim_{q_1^0 \rightarrow \infty} \text{out} \langle p_1, \dots, p_n | a_{out}^\dagger(q_1) | q_2, \dots, q_m \rangle_{in} \quad (3.30)$$

and use the result

$$\left(\lim_{t \rightarrow \infty} - \lim_{t \rightarrow -\infty} \right) \int d^3x F(x, t) = \lim_{t_f \rightarrow \infty, t_i \rightarrow -\infty} \int_{t_i}^{t_f} dt \frac{\partial}{\partial t} \int d^3x F(x, t) \quad (3.31)$$

to write Eq.(3.29) as

$$iZ_{\Xi}^{-1/2} \int d^4x \partial_0 \left(e^{-iq_1 \cdot x} \overleftrightarrow{\partial}_0 \langle p_1, \dots, p_n | \psi(t, \vec{x}) | q_2, \dots, q_m \rangle \right) \\ + \lim_{q_1^0 \rightarrow -\infty} \text{out} \langle p_1, \dots, p_n | a_{\text{out}}^\dagger(q_1) | q_2, \dots, q_m \rangle_{\text{in}} \quad (3.32)$$

We can represent the second term in the following way

$$\lim_{q_1^0 \rightarrow -\infty} \text{out} \langle p_1, \dots, p_n | a_{\text{out}}^\dagger(q_1) | q_2, \dots, q_m \rangle_{\text{in}} = \lim_{q_1^0 \rightarrow -\infty} \text{out} \langle p_1, \dots, p_n, -q_1 | q_2, \dots, q_m \rangle_{\text{in}} \quad (3.33)$$

where $\text{out} \langle \{p\}, -q_1 |$ represents an out state with a particle of momentum q_1 , if present, removed from the set $\{p\}$ ². In other words, the second term in Eq.(3.32) represents a disconnected piece. In the usual LSZ formalism we would drop any terms such as this since they wouldn't contribute to the scattering; however, in our case, since our asymptotic states are able to interact weakly we will not necessarily be able to discard these terms. We shall not investigate them further at this stage and will proceed along the traditional reasoning for the LSZ reduction, but we will keep in mind that they will have to be investigated later.

Once we have dropped any terms which correspond to disconnected pieces this can be rewritten as

$$iZ_{\Xi}^{-1/2} \int d^4x \langle p_1, \dots, p_n | e^{-iq_1 \cdot x} (\partial_0^2 \psi(t, \vec{x})) - (\partial_0^2 e^{-iq_1 \cdot x}) \psi(t, \vec{x}) | q_2, \dots, q_m \rangle \quad (3.34)$$

Now we know that

$$\partial_0^2 e^{-iq_1 \cdot x} = (\nabla^2 - M_A^2) e^{-iq_1 \cdot x} \quad (3.35)$$

²As before, if there is no such particle present then this term will be absent

so this leads to

$$iZ_{\Xi}^{-1/2} \int d^4x \langle p_1, \dots, p_n | e^{-iq_1 \cdot x} (\partial_0^2 \psi(t, \vec{x})) - ((\nabla - M_A^2) e^{-iq_1 \cdot x}) \psi(t, \vec{x}) | q_2, \dots, q_m \rangle \quad (3.36)$$

After we have used integration by parts to swap the space integrals in the first term this becomes

$$iZ_{\Xi}^{-1/2} \int d^4x e^{-iq_1 \cdot x} \langle p_1, \dots, p_n | A_x \psi(t, \vec{x}) | q_2, \dots, q_m \rangle \quad (3.37)$$

with $q_1 = (E_{q_1}, \vec{q}_1)$ and where we have defined A_x by rewriting Eq.(3.13) in the form $A_x \Xi(x) = (\square_x + m^2) \Xi(x) - \frac{\partial \mathcal{L}_S}{\partial \Xi(x)}$. We can extract all the *in* and *out* states in a similar way to find that

$$\begin{aligned} \text{out} \langle p_1, \dots, p_n | q_1, \dots, q_m \rangle_{\text{in}} &\equiv (iZ_{\Xi})^{-\frac{n+m}{2}} \int d^4x_1 \dots d^4x_m d^4y_1 \dots d^4y_n \\ &e^{i \sum p_i \cdot y_i} e^{-i \sum q_i \cdot x_i} A_{y_1} \dots A_{y_n} A_{x_1} \dots A_{x_m} \langle 0 | T \{ \psi(y_1) \dots \psi(y_n) \psi(x_1) \dots \psi(x_m) \} | 0 \rangle \end{aligned} \quad (3.38)$$

remembering that we will have to consider all combinations of disconnected pieces as well.

This takes a very similar form to the usual LSZ reduction formula, Eq.(2.26). As in the familiar case we have the following time ordered correlation function $\langle 0 | T \{ \psi(y_1) \dots \psi(y_n) \psi(x_1) \dots \psi(x_m) \} | 0 \rangle$ and once again the external legs are removed. In this case, however, it is the A_x and A_y operators which are responsible for removing the external legs. This means that our external states are no longer the free states which we understand, but the asymptotic states which we cannot calculate. This will require us to reach some understanding of how we actually represent these external states; we shall

discuss this later. Once again we find that we set these external states on-shell but, as mentioned earlier, in this case on-shell no longer means $p^2 = m^2$, but the invariant mass will now depend on \mathcal{L}_S as found in Eq.(3.16). This is understandable as a consequence of the fact that the external states will now incorporate soft interactions and so will no longer be interpretable as a single particle (such as a quark), but rather as a collection of particles close in form to a single particle (such as a quark with a cloud of soft gluons). Similarly, we note that the propagators of these fields will no longer have a single particle pole, but a branch point, reflecting the fact that an arbitrary number of soft partons must be included in this as well.

3.4 Correlation functions in the AIP

Now that we have our modified LSZ reduction formula we need to see how we will go about extracting results from it. Once again, our main area of interest will be the time ordered correlation functions. Unlike in the conventional LSZ formula, however, our correlation functions are related to asymptotic states through the operators A_x rather than to free states through the Klein-Gordon operators K_x . Consequently we must place our correlation functions in the asymptotic interaction picture rather than in the interaction picture as we did before.

We construct the asymptotic interaction picture in precisely the same way that we constructed the interaction picture, but now we substitute \mathcal{L}_A for \mathcal{L}_0 and \mathcal{L}_H for \mathcal{L}_I . We start by defining asymptotic evolution operators following Eq.(2.33) where we are now using the asymptotic Hamiltonian, H_A , which has been derived from the Lagrangian, \mathcal{L}_A . We can write these evolution

operators as

$$U_A(t, t_0) = T \left\{ \exp \left(-i \int_{t_0}^t dt_1 H_H(t_1) \right) \right\} \quad (3.39)$$

where $H_H = H - H_A$.

In order to place the correlation functions in the asymptotic interaction picture we relate the full fields ψ to the asymptotic fields Ξ via

$$\psi(t, \vec{x}) = U_A^\dagger(t, t_0) \Xi(t, \vec{x}) U_A(t, t_0) \quad (3.40)$$

The correlation functions can then be written

$$\begin{aligned} & \langle 0 | T \{ \psi(x_1) \dots \psi(x_n) \} | 0 \rangle \\ &= \langle 0 | T \left\{ U_A^\dagger(x_1, t_0) \Xi(x_1) U_A(x_1, t_0) \dots U_A^\dagger(x_n, t_0) \Xi(x_n) U_A(x_n, t_0) \right\} | 0 \rangle \\ &= \langle 0 | U_A^\dagger(T, t_0) T \{ U_A(T, x_1) \Xi(x_1) U_A(x_1, x_2) \dots \\ & \times U_A(x_{n-1}, x_n) \Xi(x_n) U_A(x_n, -T) \} U_A(-T, t_0) | 0 \rangle \end{aligned} \quad (3.41)$$

in the limit $T \rightarrow \infty$. We can then see that the vacuum, $|0\rangle$ will be an eigenstate of $U_A(-T, t_0)$ and $U_A^\dagger(T, t_0)$ in the same way that we saw this for the conventional interaction picture in Section 2.4.1, and so we eventually arrive at

$$\langle 0 | T \{ \psi(x_1) \dots \psi(x_n) \} | 0 \rangle = \frac{\langle 0 | T \{ \Xi(x_1) \dots \Xi(x_n) \exp \left(-i \int_{-\infty}^{\infty} d^4x \mathcal{L}_H \right) \} | 0 \rangle}{\langle 0 | T \{ \left(-i \int_{-\infty}^{\infty} d^4x \mathcal{L}_H \right) \} | 0 \rangle} \quad (3.42)$$

The fields in \mathcal{L}_H are now all asymptotic fields Ξ . The amplitudes generated in this way will consist entirely of “hard” vertices generated by our new interaction part of the Lagrangian which has had the soft and collinear parts removed; these pieces of \mathcal{L} are now entirely contained in the propagators of

the Ξ fields. The denominator of Eq.(3.42) will remove any disconnected pieces in exactly the same way that the equivalent expression did in the interaction picture, as we saw in Section 2.6.1.

3.5 Wick's Theorem

We want to calculate the time ordered correlation functions which appear in Eq.(3.42) (removing disconnected pieces as usual and hence only considering the numerator). We now choose to split our interaction Lagrangian $\mathcal{L}_I = \mathcal{L}_S + \mathcal{L}_H$ by defining soft and hard vertex functions f_s and f_h so that

$$\mathcal{L}_S = f_s(\{p\})\mathcal{L}_I \quad (3.43)$$

$$\mathcal{L}_H = f_h(\{p\})\mathcal{L}_I \quad (3.44)$$

$$f_s(\{p\}) + f_h(\{p\}) = 1 \quad (3.45)$$

where the set $\{p\}$ represents the momenta of all lines attached to that particular interaction vertex. Once we expand the term $\exp\left(-i \int_{-\infty}^{\infty} d^4x \mathcal{L}_H\right)$ which appears in the time ordered correlation function we can see that the resulting terms will be made up of time ordered products of asymptotic fields multiplied by hard vertex factors (along with the usual constant vertex factors such as the coupling)

$$\langle 0 | \Xi(x_1) \dots \Xi(x_n) | 0 \rangle f_h(q_1, q_2, q_3) \dots f_h(q_{m-2}, q_{m-1}, q_m) \times \text{other vertex factors} \quad (3.46)$$

We want to use Wick's theorem as in the usual case to reduce the time ordered correlation function to a series of propagators. Since our asymptotic fields are made up of annihilation and creation operators with the same commutation

relations as in the free case we can proceed with exactly the same method. It can easily be shown that [36]

$$T \{ \Xi(x) \Xi(y) \} = : \Xi(x) \Xi(y) : + \langle 0 | T \{ \Xi(x) \Xi(y) \} | 0 \rangle \quad (3.47)$$

We can then use induction to prove the relations for the time ordered product of larger numbers of fields as the sum of all possible normal orders and contractions [36]. From this result we can easily infer

$$\langle 0 | T \{ \Xi(x_1) \dots \Xi(x_n) \} | 0 \rangle = \begin{cases} 0 & : \text{odd } n \\ \sum_P \langle 0 | T \{ \Xi(x_1) \Xi(x_2) \} | 0 \rangle \dots \langle 0 | T \{ \Xi(x_{n-1}) \Xi(x_n) \} | 0 \rangle & : \text{even } n \end{cases}$$

where P is a sum over all permutations of the x_i such that we only count $\langle 0 | T \{ \Xi(x_1) \Xi(x_2) \} | 0 \rangle$ and $\langle 0 | T \{ \Xi(x_2) \Xi(x_1) \} | 0 \rangle$ as a single term. This is exactly the same decomposition into propagators as in the free field case. We now have a prescription for calculating amplitudes in our theory: we proceed in exactly the same way as in the usual free field case, but we add hard vertex factors to each interaction point, use the propagator for the asymptotic fields, and associate our external states with asymptotic states rather than free states. As we saw earlier, however, we are unable to solve the equations of motion for the asymptotic states and so will also be unable to calculate the propagator for the asymptotic fields exactly.

3.6 Practical applications

We have now reproduced the main features of traditional amplitude calculations with the modifications which are required in order to address the incorrect assumption that the in and out states of the theory are free states. However, as we have seen, there are certain aspects of our modified approach which we are unable to deal with in the same way as before, specifically the asymptotic propagators and the asymptotic external states. We will now explore the practical aspects of performing calculations using our new approach.

3.6.1 Propagators in the AIP

In Section 3.5 we saw how the correlation functions, $\langle 0|T\{\psi(x_1)\dots\psi(x_n)\}|0\rangle$, which appear in our reduction formula, Eq.(3.38), can be rewritten in terms of the asymptotic propagators $\langle 0|T\{\Xi(x_1)\Xi(x_2)\}|0\rangle$. In contrast to the standard field theory approach we cannot solve for these propagators exactly. We can, however, calculate them perturbatively by relating the asymptotic fields to the free fields. This takes exactly the same form as the relation between the full fields of the theory and the free fields, but where we now substitute \mathcal{L}_S for the usual full interaction Lagrangian, \mathcal{L}_I . In order to do this we take the full Heisenberg representation of the asymptotic fields, Ξ , and make the usual transformation into the interaction picture using the following evolution operator

$$U_S(t, t') = T \left\{ \exp \left(-i \int_{t'}^t dt'' H_S(t'') \right) \right\} \quad (3.48)$$

where the fields in H_S are now in the interaction picture. The propagator is given by the two point correlation function of the asymptotic fields. We now

follow exactly the same procedure as in Eq.(3.41) and Eq.(3.42) to write our correlation function in terms of the free fields. We end up with

$$\langle 0|T\{\Xi(x_1)\Xi(x_2)\}|0\rangle = \frac{\langle 0|T\left\{\phi(x_1)\phi(x_2)\exp\left(-i\int_{-\infty}^{\infty}d^4x\mathcal{L}_S(x)\right)\right\}|0\rangle}{\langle 0|T\left\{\exp\left(-i\int_{-\infty}^{\infty}d^4x\mathcal{L}_S(x)\right)\right\}|0\rangle} \quad (3.49)$$

This means that we can calculate the propagators perturbatively by considering the Feynman diagrams for the two point correlation function for that particular propagator, but adding a soft splitting function f_s to each vertex. Once again, the denominator of the above formula will remove any disconnected diagrams for us and so we only need to consider fully connected diagrams.

To proceed further with this approach we must next decide on a particular form for our split of \mathcal{L}_I into \mathcal{L}_H and \mathcal{L}_S . We shall do this in the next chapter.

3.6.2 Interpretation and application of the asymptotic states

The other area of our new approach which we are unable to treat in the conventional manner is that of the external states which appear in our modified LSZ formula. If we were able to calculate the asymptotic states in our new picture then we could apply our modified LSZ formula in a very similar way to the conventional method. Unfortunately we are forced to relate the asymptotic picture to the free picture and calculate propagators perturbatively as we saw earlier. It is clear that a similar approach will have to be applied to the expressions which represent the amputation of the external propagators, $A_x\langle 0|T\{\Xi(x)\Xi(y)\}|0\rangle$, but it is rather less clear how to proceed

with this. In order to investigate this further we shall start to consider a perturbative approach, but we shall see that questions remain which will have to be addressed pragmatically rather than theoretically for the time being at least.

We can rewrite this expression as follows:

$$A_x \langle 0 | T \{ \Xi(x) \Xi(y) \} | 0 \rangle = \left(K_x - \frac{\partial \mathcal{L}_S}{\partial \Xi(x)} \Xi^{-1}(x) \right) \langle 0 | T \{ \phi(x) \phi(y) \exp \left(-i \int_{-\infty}^{\infty} d^4 z \mathcal{L}_S(z) \right) \} | 0 \rangle \quad (3.50)$$

where we have dropped the denominator which corresponds to disconnected diagrams; from now on we shall assume that these have been factored out.

Two things make this different from the usual expression encountered in the conventional case. Firstly where we would usually have $\langle 0 | T \{ \phi(x) \phi(y) \} | 0 \rangle$ corresponding to a simple propagator we now have a perturbative series including soft interactions. Secondly, there is a whole new term involved which again depends on \mathcal{L}_S . We first consider the effect of the perturbative series replacing the simple propagator.

We can treat this part of the expression in exactly the same way that we would treat the conventional LSZ formula: expand as a perturbation series and then remove the relevant external propagator. The upshot of this is that where we might have expected a simple external line, we now have an external line attached to a soft self energy diagram. This corresponds to taking the residue of the pole caused by the external leg as usual, but using the perturbatively calculated asymptotic propagators rather than the free propagators.

The second part of the expression is altogether more complex. It is not

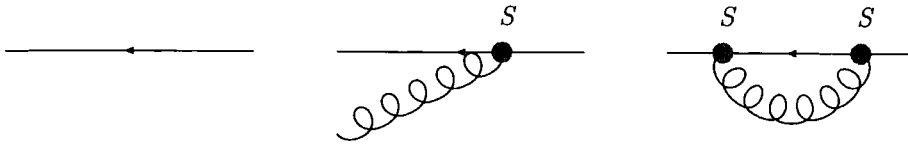


Figure 3.1: Some diagrams which may contribute to a single asymptotic external state.

immediately clear how to treat an operator such as $\frac{\partial \mathcal{L}_S}{\partial \Xi(x)} \Xi^{-1}(x)$ so we shall start by making some general observations. First of all, the presence of $\frac{\partial \mathcal{L}_S}{\partial \Xi(x)}$ suggests the presence of various fields located at the same point in space-time as our external particle. This would seem to indicate that, as expected, parton number will not be a good quantum number for our external states and that they will contain both quarks and gluons. Secondly, this part will contain powers of the coupling constant even at the lowest order in perturbation theory and so will be suppressed relative to the leading order part of the first term. Consequently, the leading part of our external states will be the same as the conventional external states, but as we consider higher orders in perturbation theory we add soft self-interactions and other soft particles to this state in ways which we are unable to determine exactly; some examples of these two observations are shown in Figure 3.1. Thirdly, the presence of some form of soft interaction terms suggests the possibility of some connection between the conventional external states as shown in Figure 3.2. It is reasonable to presume, however, that these external states will be those which mimic the conventional external state when we are unable to resolve energies small enough to distinguish them.

When we derived the modified version of the LSZ formula in Section 3.3 we also disregarded the effect of the altered asymptotic states when we discarded any disconnected pieces. These will not remain disconnected as in

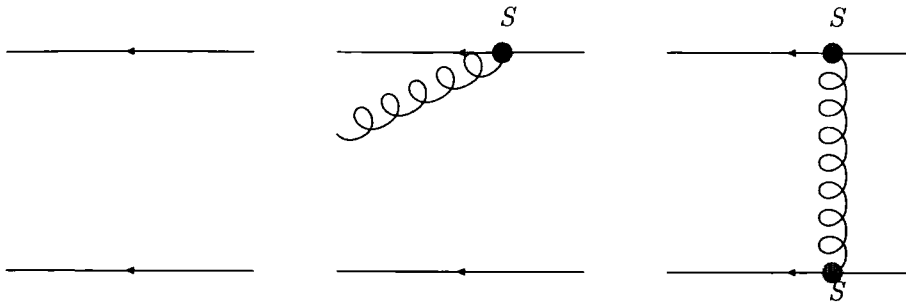


Figure 3.2: Some diagrams which may contribute to a two pseudojet external state.

the conventional method, but can potentially interact softly with the rest of the in and out states and consequently need to be taken into account in a similar way. Once again, although the basic idea behind this effect is straightforward, it is not clear exactly how to approach this theoretically.

3.6.3 An alternative method

The ideal approach to our method of calculating amplitudes would be to work perturbatively only with the coupling appearing in \mathcal{L}_H . Since we would be applying this to QCD, the natural scale for this coupling would be a hard scale, justifying a perturbative expansion. Soft effects, related to a coupling with a soft scale, would then be taken into account to all orders and even non-perturbative effects would be included. This corresponds to solving for our asymptotic states exactly which we are unable to do. This leads us to apply a perturbative approach to the soft area of the theory as well. As we have seen, we are able to apply this approach to calculating the propagators of the theory, but we run into problems when attempting to calculate the external states themselves.

We can use the fact that we have a qualitative understanding of these ex-

ternal states to approach the whole problem from a more technical point of view. We have seen above that although we have defined a theory with hard interactions only, if we are forced to treat the soft part of the theory perturbatively we will in actuality be calculating diagrams which contain soft vertices as well as hard. We have split the original interaction Lagrangian into hard and soft parts, and so calculating amplitudes in the conventional manner would correspond to summing diagrams with all possible combinations of soft and hard vertices. It seems natural to hypothesise that the application of these two different formulations of the amplitude calculation will result in the same answers. In the absence of a clear theoretical prescription for performing calculations based on our altered LSZ formula we shall use the approach of calculating all possible combinations of soft and hard vertices when we consider specific examples. In this case though, we find that the consideration of asymptotic rather than free external states will cause us to group these amplitudes in different ways to the usual method.

In the conventional treatment, we group the amplitudes by the number of final state particles and then perform the phase space integrals accordingly. In our case we are led to group our amplitudes by the asymptotic external states, and so while the case of $\gamma \rightarrow q\bar{q}$ with one of the quarks then emitting a hard gluon would be considered a “three jet” event, the similar process of $\gamma \rightarrow q\bar{q}$ with one of the quarks then emitting a soft gluon would fall into the category of a “two jet” event since soft gluon emission from a quark line will clearly appear in the asymptotic quark state as shown in Figure 3.3.

The infrared finite nature of this viewpoint comes from this new division of amplitudes. Essentially, rather than attempting to correct the assumption that the in and out states are free by including long range interactions in

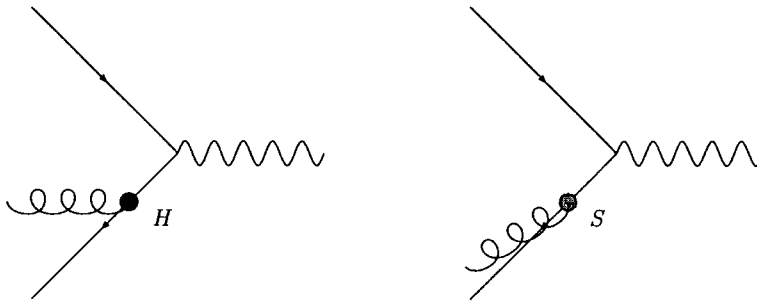


Figure 3.3: The emission of a hard gluon contributes to a three jet final state; the emission of a soft gluon contributes to a two jet final state.

the asymptotic Lagrangian, we are simply changing our definition of which amplitudes belong in which external states to reflect the fact that they are not in fact free. If, for example, we were considering an order in perturbation theory which would give us four jet diagrams at most, then we would find that the infrared divergences arising from the phase space integration of the four jet diagrams would all be contained in the pseudo two and three jet configurations; in other words those four jet diagrams where the soft and hard vertices were distributed such that they belonged to the sets with either two or three external asymptotic “particles”. These divergences would then cancel with those introduced by soft vertices into the two and three jet diagrams. Thus, by splitting our amplitudes up based on the number of external *asymptotic* “particles” rather than the number of external free particles we would now find that the sum of the amplitudes squared for each process would be separately finite.

In order to apply this approach we need a system of determining which diagrams are to be placed in which groups. Ultimately we should hope to define a basic algorithm for categorising the various diagrams. As we shall see in Section 5.2, such an approach does not seem very far off; for the time being though, we shall have to deal with each diagram individually. The

simplest way of doing this is to consider the soft vertices and identify which diagrams should have various jets collapsed into pseudo jets, although the locations of the various hard vertices will have a part to play as well. There are, of course, more aspects of this to consider; we shall examine these when we consider different examples in Chapter 5.

Chapter 4

Splitting the interaction

Lagrangian

Our next task is to perform the split of \mathcal{L}_I into \mathcal{L}_S and \mathcal{L}_H . This corresponds to defining the forms of the splitting functions $f_s(\{p\})$ and $f_h(\{p\})$ which we introduced in Section 3.5. Strictly speaking, we should choose \mathcal{L}_S such that \mathcal{L}_A is precisely the asymptotic limit of \mathcal{L} . However, we are unable to calculate this limit and so we must be a little less precise in our definition. It is enough for us to choose \mathcal{L}_A such that its asymptotic limit is equivalent to the asymptotic limit of \mathcal{L} . This will ensure that we do not neglect any long-range interactions in our definition of our asymptotic states; the fact that we are likely to include some short-range interactions as well is unnecessary, but does not cause any problems. Consequently our asymptotic Lagrangian will differ from the “true” asymptotic Lagrangian by a finite amount.

Since we shall not be using the exact \mathcal{L}_A we will clearly have a choice in our definition of \mathcal{L}_S . We introduce a parameter Δ which describes how much of \mathcal{L}_I will be put into \mathcal{L}_S . Consequently we see that our splitting functions

from Eq.(3.45) must depend on Δ and therefore take the form $f_s(\{p\}; \Delta)$ and $f_h(\{p\}; \Delta)$. The asymptotic states which we considered in Section 3.6.2 are derived from our \mathcal{L}_A and consequently the parameter Δ contained in \mathcal{L}_A will be present in their definition. We must now ask ourselves how these states are related to the states that we would measure in an experimental situation.

We suspect that the amplitudes themselves may be independent of Δ . If we examine the matrix elements in the asymptotic interaction picture we have

$$\langle \Xi_\beta(\Delta) | S_A(\Delta) | \Xi_\alpha(\Delta) \rangle \quad (4.1)$$

where we have written the Δ dependence of each of the quantities explicitly. Of course we are free to choose any Δ and could equally well have written

$$\begin{aligned} \langle \Xi_\beta(2\Delta) | S_A(2\Delta) | \Xi_\alpha(2\Delta) \rangle &= \langle \Xi_\beta(\Delta) | \Omega_d^{(-)\dagger} \Omega_d^{(-)} S_A(\Delta) \Omega_d^{(-)\dagger} \Omega_d^{(-)} | \Xi_\alpha(\Delta) \rangle \\ &= \langle \Xi_\beta(\Delta) | S_A(\Delta) | \Xi_\alpha(\Delta) \rangle \end{aligned} \quad (4.2)$$

where $\Omega_d^{(-)}$ is a unitary operator which relates the two pictures. We know that $\Omega_d^{(-)}$ is unitary since the two different pictures should only differ by a finite amount. The fact that both pictures will give the same result suggests that the amplitudes should be independent of our choice of Δ . In practice, however, this is unlikely to hold since we were unable to calculate the asymptotic propagators exactly and so were forced to define them perturbatively. This may introduce a dependence on Δ in our amplitudes which is related to the order in the perturbation series at which we are working.

It is clear from the dependence on Δ of our external states that they are not fundamental in any sense¹. However, despite the dependence on Δ we can see

¹The fact that we do not attempt to obtain fundamental external states is a significant

that our external states and their corresponding amplitudes will be extremely useful for perturbative calculations. As in the traditional approach, a physical cross section will receive contributions from several squared amplitudes integrated over the phase space. If we make sure that we don't choose our external states to be too inclusive and consequently that the physical quantity to be calculated does not resolve the pseudojets related to our external states, then the cross section which we calculate should be independent of Δ . It is, in effect, a resolution parameter which determines to what extent we want to be able to resolve any jets which appear in our calculations; different observables which we wish to calculate will place different restrictions on suitable values of Δ . A similar interpretation was placed on the parameter used to split the Hamiltonian in [34].

The use of states other than the true asymptotic states suggests that our definitions of physical observables may have to be altered in order to match the behaviour of these states; however, since our usual choice of asymptotic states based on H_0 also falls into this category this is hardly a new problem.

We now need to investigate the properties which our splitting functions must exhibit in order to split the Lagrangian in a covariant manner. For the moment, we shall consider three-point vertices only as these are all that will be needed at lower orders. Four-point vertices should not introduce any new problems.

difference between our approach and the majority of the previous work mentioned in Section 1.4.1.

4.1 Soft-Hard splitting requirements

There are several possible choices for our splitting functions, but all of them must fulfil several criteria. Firstly, we require that none of the legs of the vertices are special. We must have

$$f_i(p_1, p_2, p_3; \Delta) = f_i(p_2, p_1, p_3; \Delta) = f_i(p_3, p_2, p_1; \Delta) \quad (4.3)$$

where $i = s$ or h . Secondly, we want the UV regions to be excluded from the soft regions² which imposes the constraint

$$f_s(\pm\infty, p_2, p_3; \Delta) = 0 \quad (4.4)$$

Thirdly, we require that our vertex functions separate the soft and collinear regions from the hard regions. Taking a three point vertex as an example again, this suggests

$$\begin{aligned} f_s(0, p_2, p_3; \Delta) &= 1 \\ f_s(p_1, \lambda p_1, p_3; \Delta) &= 1 \end{aligned} \quad (4.5)$$

However, it is generally accepted (see e.g. [40,41]) that it is enough to exclude the emission of soft and collinear partons from external lines in order to achieve finite amplitudes. Since this condition would allow us to specify a simpler form of the vertex functions, this is the approach that we shall adopt. Once we accept this form of the conditions, we can alter Eq.(4.5) to

$$f_s(p_1, p_2, p_3; \Delta) = 1, \text{ all momenta on-shell} \quad (4.6)$$

²This is not strictly necessary for our approach to work, but it is highly desirable as it will greatly simplify the process of renormalisation.

This fits the new requirement since momentum conservation will ensure that all three momenta are on-shell for the emission of a soft or collinear parton from an external line. Let us now investigate the infrared behaviour of amplitudes restricted by these hard vertex functions.

4.2 Power counting techniques

We have seen in Section 3.6.3 that our approach will result in infrared finite amplitudes by effectively redistributing the existing infrared singularities present in the amplitudes which will contribute to an observable so that they now cancel within each amplitude. Since the various parts of any conventional amplitude can only be reassigned to an asymptotic amplitude with the same or fewer “particles” in the final state it follows that, for our approach to work successfully, any amplitude containing hard vertices only must be infrared finite. We shall now consider the infrared behaviour of such amplitudes; to do this we shall use a slightly extended version of the straightforward method of powercounting [42].

We want to examine the general structure of infrared singularities in massless scattering amplitudes. In order to do this we consider the general form of the massless Green’s function $G(\{p_e\})$ with external momenta $\{p_e\}$ once it has been put in Feynman parameterised form

$$G(\{p_e\}) = \left(\prod_i \int_0^1 d\alpha_i \right) \delta \left(\sum_i \alpha_i - 1 \right) \left(\prod_r \int d^d k_r \right) \frac{F(\alpha_i, k_r, p_e)}{\sum_j \alpha_j l_j^2(p, k) + i\epsilon} \quad (4.7)$$

where there are i lines in the diagram and r loops. The function $F(\alpha_i, k_r, p_e)$

represents the numerator factors present in the diagram and

$$l_j^\mu(p_e, k_r) = \sum_n (b_{j,n} k_n^\mu + c_{j,n} p_n^\mu) \quad (4.8)$$

with b and c being complex numbers and k_n^μ being the internal loop momenta such that l_j^μ is the momentum of the j th line.

Singularities in the amplitude will arise from zeros of the denominator. In the absence of any such zeros, the integrand in Eq.(4.7) is bounded and analytic everywhere in the integration region, and $G(\{p_e\})$ is an analytic function of the $\{p_e\}$. However, a much stronger condition than the simple presence of a zero of the denominator is necessary to produce a singularity in $G(\{p_e\})$. This is because the integrals of Eq.(4.7) are contour integrals in complex (k, α) space. This means that the k_r^μ and α_i integrals can be deformed from one path to another. In the case of isolated poles this means that we can choose a new contour where the denominator does not vanish, and the integrand is an analytic function of the external momenta everywhere. Thus, isolated poles in the integrand do not produce singularities in the amplitude.

There are two classes of unavoidable singularity which we shall have to consider. The first case is the *end-point* singularity; these occur when the integrand contains a pole at one of the fixed end points of the integration contour. The contour cannot then be deformed around the singularity and this corresponds to a real singularity of the amplitude. The second case is the *pinch* singularity. This type of singularity occurs when the contour is trapped between two poles and the singularity cannot be avoided. In our multi-variable case, these pinch points become surfaces in the space of the complex variables $\{k_j, \alpha_j\}$ if at each possible pinch point one variable is trapped while we keep

the remaining variables fixed. These are known as *pinch surfaces*.

We will not need to consider end point singularities since the momentum integrals were unbounded before Feynman parameterisation and so these will not occur. Consequently, we will only concern ourselves with pinch singularities. To find all the possible pinch surfaces, and hence all the possible regions of infrared singularities, we would have to use the Landau equations [37, 42]. These can be derived as follows: singularities appear when

$$\sum_j \alpha_j l_j^2(p, k) + i\epsilon = 0 \quad (4.9)$$

We expect to find two solutions to this equation since it is quadratic in k^μ . These will only give a pinch singularity when the derivative of this equation is zero at these solutions. This means that

$$\frac{\partial}{\partial k_j^\mu} \left(\sum_j \alpha_j l_j^2(p, k) + i\epsilon \right) = 2 \sum_j b_{ij}(\alpha_i l_i^\mu) = 0 \quad (4.10)$$

The values of $\{k_i, \alpha_j\}$ which satisfy Eq.(4.9) and Eq.(4.10) will then be our pinch surfaces. We now have possible solutions given either by

$$l_i^2 = 0 \text{ and } \sum_i b_{ij} \alpha_i l_i^\mu = 0 \quad (4.11)$$

for every loop j which includes the line i , or by

$$l_i^2 \neq 0 \text{ and } \alpha_i = 0 \quad (4.12)$$

A pinch surface solution to the Landau equations is a necessary, but not sufficient condition for an infrared singularity to exist. To determine whether such singularities exist on any of these surfaces we must look more closely at

the behaviour of the amplitude at these points.

4.2.1 Reduced diagrams

In order to make a closer investigation of the singularity structure we will use diagrams to visualise the pinch surface solutions to the Landau equations. These are known as *reduced diagrams* [40–42] and we construct them in the following way. We start with the normal Feynman diagram for the amplitude which we wish to calculate. Next, we reduce any off-shell lines to a point, connecting the vertices on either end to produce a composite vertex. We do this since the only way for off-shell lines to satisfy the Landau equations is if $\alpha = 0$ which corresponds to a vanishing contribution to the denominator of Eq.(4.7). Since any on-shell lines can satisfy the Landau equations for $\alpha \neq 0$, they are kept unchanged.

4.2.2 Infrared power counting

Not all pinch surfaces will give rise to infrared singularities. In order to investigate whether a particular pinch surface is potentially infrared divergent we need to use powercounting techniques³. In order to do this we must first consider how the momenta $\{k_i, \alpha_j\}$ internal to a diagram $G(\{p_e\})$ given by Eq.(4.7) affect the behaviour of the pinch surfaces of that diagram. The pinch surfaces of G arise when a line goes on-shell and is therefore either soft or collinear to an external particle. This set of requirements upon the momenta of G which lead to pinch surfaces therefore forms a surface σ in

³Even when we have identified the dangerous diagrams through powercounting, they may not be infrared divergent since we will not take the momentum structure of the numerator of the diagram into account just yet. This could set a potentially troublesome diagram to zero.

the space of all the momenta variables. The momenta on this surface can then be divided into two distinct groups. The first group contains momenta which keep G on the pinch surface when they are altered arbitrarily. These are called internal variables to the momentum surface σ . The second group consists of those momenta which will take G away from the pinch surface if they are altered by even a small amount. These variables are called normal to the momentum surface σ . We want to observe the behaviour of G as we alter the normal variables of σ close to the pinch surface. We achieve this by calculating the superficial degree of infrared divergence of the *homogeneous integral* [37, 42].

To define the homogeneous integral we start with the general form of an amplitude as given in Eq.(4.7). We rewrite this as

$$G(\{p_e\}) = \int \prod_j dl_j \int_0 \prod_i dk_i I_\sigma(k_i, l_j, p_e) \quad (4.13)$$

where the l_j are the internal variables and the k_i are the normal variables of σ . The 0 on the k_i integral indicates that we are investigating these variables close to their mass-shell limit which corresponds to operating close to the pinch surface of G . The homogeneous integral \bar{I}_σ is defined as the limit of I_σ as the k_i go on-shell. In the case of a soft limit, for example, we would take the internal loop momenta k_i as our normal variables. We would then construct the homogeneous integral by keeping only the lowest order terms in k_i . In this way a numerator factor such as $(p+k)^\mu$ would become p^μ , and a denominator factor such as $(p+k)^2$ would become $p^2 + 2p.k$.

If we now observe how the homogeneous integral behaves when we scale k_i , this will provide us with an insight into how G approaches its pinch surfaces.

To do this we rewrite the homogeneous integral as [42]

$$\begin{aligned}
\bar{G}(\{p_e\}) &= \int \prod_j dl_j \int_0^\infty \prod_i dk_i \bar{I}_\sigma(k_i, l_j, p_e) \\
&= \int \prod_j dl_j \int_0^\infty d\lambda^2 \int_0^\infty \prod_i dk_i \delta\left(\lambda^2 - \sum_i |k_i|^2\right) \bar{I}_\sigma(k_i, l_j, p_e) \\
&= 2 \int \prod_j dl_j \int_0^\infty d\lambda \lambda^{\mu(\sigma)-1} \int_0^\infty \prod_i dk'_i \delta\left(1 - \sum_i |k'_i|^2\right) \bar{I}_\sigma(k_i, l_j, p_e) \quad (4.14)
\end{aligned}$$

where $\mu(\sigma)$ is known as the superficial degree of infrared divergence and $k'_i = k_i/\lambda$. If $\mu(\sigma) > 0$ then we expect the amplitude to be infrared finite. This may not always be the case though since there could be further *sub-divergences* from the k'_i integrals⁴. We then use powercounting techniques similar to those frequently used for ultraviolet divergences to determine the form of $\mu(\sigma)$. In order for a diagram to be infrared finite we then assume that we need only show that at each possible pinch surface the superficial degree of divergence is greater than zero.

4.3 Infrared finiteness of completely hard amplitudes

From our arguments above we see that we can disregard the exact form of f_s and f_h for the moment and simply define a soft vertex as one where all the attached legs are on-shell and a hard vertex as one where at least one of the attached legs is off-shell. This will allow us to look into the infrared

⁴We shall not consider such divergences here as we are interested in discovering whether the entire theory is infrared finite. Since any sub-divergence is also a diagram which must be investigated in its own right this problem will not arise as long as we find $\mu(\sigma) > 0$ for all diagrams.

behaviour for the most general case to start with; we can then adopt a particular form for f_s and f_h if and when it becomes necessary. Since our modified interaction Lagrangian will be \mathcal{L}_H rather than the usual \mathcal{L}_I , when we calculate Feynman diagrams each vertex will be a hard vertex. We will now investigate whether amplitudes consisting entirely of hard vertices have any potential infrared singularities.

As mentioned earlier we will be considering a field theory with three point vertices only. This could be ϕ^3 scalar theory, QED, or QCD with the four point vertices removed. We start by considering an arbitrary diagram with n vertices and all internal lines on-shell. We now take internal lines off-shell one by one until we are left with a reduced diagram which corresponds to an original diagram where no vertex is connected to three on-shell lines. This reduced diagram corresponds to a particular point in loop momentum space. Consequently we can produce many different possible reduced diagrams by choosing different values for the loop momenta such that different combinations of internal lines are on and off shell. We can see that in order to investigate any infrared divergences associated with the diagram we must consider all the possible reduced diagrams produced in this manner.

From now on we are now going to deal with reduced diagrams, and hence any lines present in the diagrams we consider will be on-shell. All internal lines in the reduced diagram can be divided into two categories: jets and a soft subdiagram. The internal lines with momenta $k_i^\mu = 0$ form the soft subdiagram while a connected set of lines k_i^μ which all have momenta proportional to some lightlike momentum p^μ such that

$$k_i^\mu = \beta_i p^\mu, \beta_i > 0, p^2 = 0, \quad (4.15)$$

make up a jet. One option for our reduced diagram is that all the internal lines form a soft subdiagram; in the cases where we also have some jets we can place some restrictions on the form that the diagram must take. First we consider diagrams without any jets.

4.3.1 Power counting for the soft subdiagram

We will now investigate the infrared behaviour of the reduced diagrams without jets (i.e. all internal lines are soft). When all the internal lines are soft we can see that, unless we have any external particles with zero momentum, all the external lines must be connected to a single vertex. Since all the internal lines in the reduced diagram will be soft we can see that each eventual internal line must be connected to two off-shell lines in the original diagram. We will use powercounting techniques to see if such a diagram contains any infrared divergences.

Since we're only dealing with soft rather than collinear singularities in this case we can choose the loop momenta as the normal momenta in the homogeneous integral. Consequently in a diagram with L loops we will have $4L$ normal variables. We will also have I_B internal boson lines which contribute -2 and I_F internal fermion lines which contribute -1 to the superficial degree of divergence. Our powercounting gives us,

$$\mu(S) = 4L - 2I_B - I_F = 4 + 3I_F + 2I_B - 4V \quad (4.16)$$

where the number of vertices, V , obeys the relation $L = I_B + I_F - (V - 1)$. We now write the total number of lines in the diagram in terms of the number

of lines attached to a particular vertex using,

$$I_F = \frac{1}{2} \sum_v f_v \text{ and } I_B = \frac{1}{2} \sum_v b_v \quad (4.17)$$

where the sum is over all vertices v and f_v and b_v represent the number of internal fermion and boson lines attached to a particular vertex respectively.

We can then rewrite Eq.(4.16) as,

$$\mu(S) = \sum_{v-1} \left(b_v + \frac{3}{2} f_v - 4 \right) + e_b + \frac{3}{2} e_f \quad (4.18)$$

We sum over all the vertices in the diagram except the one connected to the external momenta so e_f and e_b are the number of internal fermion and boson lines connected to that vertex. We can now see that if $b_v + \frac{3}{2} f_v \geq 4$ at every vertex then we will have $\mu(S) > 0$. The fact that we have taken two propagators off-shell at each original vertex attached to a soft line means that the only vertices permissible in the reduced diagram apart from the vertex with the external momenta must be those made from off-shell loops. This allows us to have two and three point vertices in the reduced diagram which could potentially give rise to diagrams where $\mu(S) \leq 0$. In order to investigate this further we will need to consider these diagrams in more detail. First, though, we will consider the case where there are jets present in the reduced diagram.

4.3.2 Power counting including jets

We now investigate the case where we allow our reduced diagram to contain jets as well as a soft subdiagram. For the moment, we will conduct our

investigation using ϕ^3 scalar theory. Since we no longer include fermions with their extra factor in the numerator of the propagator this will represent a worst case scenario. The contributions to the superficial degree of divergence will now consist of +4 from each of the L_i soft loops, +2 from each of the L_j collinear loops, -2 from each of the I_i internal soft lines and -1 from each of the I_j collinear lines in each jet loop. Soft loops contribute +4 to the powercounting since all four components of each loop momentum are normal coordinates to the pinch surface. Each loop momentum in a collinear loop only has two components which are normal coordinates and so only contributes +2 to the superficial degree of divergence [42]. We will consider general reduced diagrams where all the vertices are hard. These are not necessarily pinch surfaces.

We go about the powercounting by splitting the superficial degree of divergence, μ , up in to a soft part, $\mu(S)$, and a collinear part, $\mu(C)$. We can then write

$$\mu = \mu(S) + \mu(C) = 4L_i - 2I_i + 2L_j - N_i - N_j \quad (4.19)$$

where N_i is the number of collinear lines also in soft loops such that $N_i + N_j = I_j$.

First, we will calculate $\mu(S)$. We write $L_i = I_i + N_i - (V_1 + V_2 - 1)$ where V_1 is the number of vertices with only soft lines attached and V_2 is the number with both soft and collinear lines. We now have

$$\mu(S) = 4L_i - 2I_i = 4 + 4N_i + 2I_i - 4(V_1 + V_2) \quad (4.20)$$

If we now consider the fact that once we remove the soft lines, the collinear lines which were also part of soft loops must form a system without any loops

we can write $N_i - (V_2 - (1 + \lambda)) = 0$ where $\lambda \geq 0$ and $(1 + \lambda)$ is the number of disconnected parts that the system of collinear lines has been divided into by the removal of the soft lines⁵. This leaves us with

$$\mu(S) = 2I_i - 4V_1 - 4\lambda \quad (4.21)$$

Now we consider $\mu(C)$. We can write $L_j = I_j + N - (V - (1 + \lambda))$ where N is the number of internal lines which are not part of any loops and V is the number of vertices attached to collinear lines (i.e. the total number of vertices is $V + V_1$). This gives us

$$\mu(C) = 2L_j - N_i - N_j = 2 + I_j + 2N - 2V + 2\lambda \quad (4.22)$$

and so combining the two parts we get

$$\mu = 2 + 2I_i + I_j + 2N - 4V_1 - 2V - 2\lambda \quad (4.23)$$

In order to investigate the worst potential case we will first set $N = 0$. To start with we consider the $\lambda = 0$ case. Once again we write the total number of lines in the diagram in terms of the number of lines attached to each vertex using,

$$I_i = \frac{1}{2} \sum_v i_v \text{ and } I_j = \frac{1}{2} \sum_v j_v \quad (4.24)$$

this then gives the result

$$\mu = \sum_v \left(i_v + \frac{1}{2} j_v - 2v_v - 4v_1 \right) + 2 \quad (4.25)$$

⁵The case with soft lines only has been dealt with already and would correspond to $\lambda = -1$.

where v_1 is 1 if the vertex has soft lines only attached to it and 0 otherwise and v_V is 1 if the vertex has any collinear lines attached and is 0 otherwise. We can immediately see again that a reduced diagram consisting of four point and higher vertices would give $\mu > 0$. This is because a vertex where $v_1 = 1$ must have all lines attached soft. Also worth noting is the fact that any mixed vertex cannot have a negative contribution to the powercounting since it must have at least one soft and two collinear lines attached.

Next we need to consider cases with $\lambda \neq 0$. We will examine the case where we have a reduced diagram consisting of four point vertices and higher and see whether increasing the value of λ can create a negative powercounting. In the case where $\lambda = 1$ we must add at least two mixed vertices in order to provide the soft link between two disconnected systems of jets. Now since the power counting for each vertex v is given by $i_v + \frac{1}{2}j_v - 2v_V - 4v_1$ we can see that the minimum contribution to μ for each mixed vertex will come when $i_v = 1$ and $j_v = 3$. This gives a contribution to μ of $+\frac{1}{2}$ for each vertex which when combined with the contribution of -1 from the λ term produces no overall effect. This means that setting $\lambda = 1$ cannot reduce the value of μ . Now we imagine increasing the value of λ further. In order to do this we must add at least one more mixed vertex and then either add another mixed vertex or modify an existing mixed vertex so that it has two soft lines attached. The first case gives no change in μ in precisely the same manner as the $\lambda = 1$ case, and in the second case the reduction in μ due to the increase in λ is matched by the contribution of $+\frac{1}{2}$ due to adding a new mixed vertex and the increased contribution from $+\frac{1}{2}$ to $+1$ due to the modified mixed vertex. It is easy to see that in the general case any possible increase in λ will be matched by corresponding increases in the number of mixed vertices

and the number of soft lines attached to mixed vertices. Thus, in the case of four point interactions and higher, diagrams including jets will be infrared finite.

As with the earlier case where we considered a completely soft reduced diagram this powercounting approach suggests that we could potentially run into infrared singularities if we have effective vertices which correspond to two or three point interactions. We will now investigate these interactions more closely to see whether they will in fact cause problems.

4.3.3 Two point vertices in reduced diagrams

We start by considering an effective two point fermion vertex. If we look at two fermion lines with momentum p connected by such a vertex we will have a composite object given by

$$\frac{i\not{p}}{p^2} [\not{p} \mathcal{S}_h(p^2, \Delta)] \frac{i\not{p}}{p^2} = -\mathcal{S}_h(p^2, \Delta) \frac{\not{p}}{p^2} \quad (4.26)$$

where \mathcal{S}_h corresponds to the system of off-shell lines which have been condensed to a point in the reduced diagram. Now \mathcal{S}_h must not have any mass dimensions, and since it depends only on p^2 and Δ we can see that if we were to expand it in p^2/Δ (since we are interested in the behaviour as p goes on-shell) it must take the following form:

$$\mathcal{S}_h = A + \left(B_1 \frac{p^2}{\Delta} + B_2 \left(\frac{p^2}{\Delta} \right)^2 + \dots \right) + \left(C_1 \frac{\Delta}{p^2} + C_2 \left(\frac{\Delta}{p^2} \right)^2 + \dots \right) \quad (4.27)$$

where A , B_n and C_n are all constants. It is immediately obvious that providing the C 's are all zero, our composite propagator made up of two on-shell

fermion propagators will actually be the powercounting equivalent of one propagator rather than two. As a result, two point fermion vertices would not affect the powercounting in reduced diagrams. If we were to calculate \mathcal{S}_h using the standard Feynman rules it is clear that we would find $B_n = C_n = 0$ since the absence of any dependence on Δ means that p^2 is the only possible mass scale. In this scenario, this composite two-point vertex would clearly not increase the negative powercounting. In order to investigate this in our case however, we will need to pick a form for f_s and f_h in order to perform the calculations explicitly. Before we do this we will make a similar examination of the effective two-point gluon vertex.

If we now examine gluon lines with two point interactions we find that we have a composite object given by

$$\frac{-i}{p^2} \left(g^{\mu\rho} - \xi_X \frac{p^\mu p^\rho}{p^2} \right) \mathcal{P}_h^{\rho\sigma}(p, \Delta) \frac{-i}{p^2} \left(g^{\sigma\nu} - \xi_X \frac{p^\sigma p^\nu}{p^2} \right) \quad (4.28)$$

(where $\xi_X = 1 - \xi$, and we have $\xi = 0$ in Landau gauge and $\xi = 1$ in Feynman gauge) where $\mathcal{P}_h^{\rho\sigma}$ corresponds to the system of off-shell lines which have been condensed to a point in the reduced diagram and we have ignored any colour factors for the moment. Now we decompose $\mathcal{P}_h^{\rho\sigma}$ into two parts with separate tensor structures so that we write

$$\mathcal{P}_h^{\rho\sigma}(p, \Delta) = g^{\rho\sigma} p^2 \mathcal{A}(p^2, \Delta) + p^\rho p^\sigma \mathcal{B}(p^2, \Delta) \quad (4.29)$$

which then gives us the form of our composite object as

$$-\frac{1}{p^2} \left[\mathcal{A} \left(g^{\mu\nu} + \xi_X (\xi_X - 2) \frac{p^\mu p^\nu}{p^2} \right) + \mathcal{B} (1 - \xi_X)^2 \frac{p^\mu p^\nu}{p^2} \right] \quad (4.30)$$

Again, we can expand \mathcal{A} and \mathcal{B} in the same manner as in Eq.(4.27), and again we find that as long as the $\left(\frac{\Delta}{p^2}\right)^n$ coefficients (the C_n coefficients) are zero, the powercounting of a chain made up of these two point interactions will be the same as for a simple propagator. The fact that the usual Feynman rules have p^2 as the only possible mass scale again means that in the standard case we would find that this sort of subdiagram would not increase the negative powercounting. In order to investigate the effects on our theory we must now pick a form for f_s and f_h and perform the necessary calculations explicitly.

Before we perform these calculations though, we notice that the tensor structure of our composite gluon line is different to the structure of the bare gluon propagator. This is because our split of the Lagrangian will break gauge invariance. Since it is gauge invariance which protects the gluon mass in the conventional approach and this is now missing from our approach we therefore expect that we shall find that the gluon will generate a mass.

4.4 Choosing the splitting functions

We now make a specific choice for our vertex functions $f_s(p_1, p_2, p_3; \Delta)$ and $f_h(p_1, p_2, p_3; \Delta)$. We will first choose the form of f_s and then infer f_h from the relation $f_h = 1 - f_s$. Our main consideration in our choice of f_s after fulfilling the necessary conditions in Eqs.(4.3),(4.4) and (4.6) will be to choose a form which makes it as simple as possible for us to perform analytic calculations. Since the eventual aim of this project is to perform calculations numerically this does not immediately seem to be the best criterion upon which to base our choice. However, at the present stage it is important that we are able to perform the calculations analytically in order to gain as much insight as

possible into the workings of our new approach. It is this necessity which leads to our choice of splitting function.

In order to perform the necessary momentum integrals as comfortably as possible, the best case scenario would clearly be to make as much use as possible of the existing methods for performing similar integrals. It follows that the obvious approach is to try and find a way of casting our splitting functions in a similar form to the usual Feynman propagators. We make the following choice for our soft splitting function:

$$f_s(p_1, p_2, p_3; \Delta) = \frac{\Delta}{p_1^2 + p_2^2 + p_3^2 + \Delta} \quad (4.31)$$

This would give the following corresponding form for our hard splitting function:

$$f_h(p_1, p_2, p_3; \Delta) = 1 - f_s(p_1, p_2, p_3; \Delta) = \frac{p_1^2 + p_2^2 + p_3^2}{p_1^2 + p_2^2 + p_3^2 + \Delta} \quad (4.32)$$

We can check that these fill the requirements as follows: firstly, the functions are symmetrical in the momenta $\{p_i\}$ and thus trivially fulfil the requirement of Eq.(4.3); this allows us to only consider p_1^μ in the remaining conditions. Secondly, for $p_1^\mu \rightarrow \pm\infty$ we have

$$f_s(p_1, p_2, p_3; \Delta) \rightarrow \frac{\Delta}{\pm\infty + p_2^2 + p_3^2 + \Delta} \rightarrow 0 \quad (4.33)$$

which fits the requirement in Eq.(4.4). Finally we consider the conditions in Eq.(4.5) in order to check that our decision to replace these conditions with that of Eq.(4.6) is justified. Taking into account momentum conservation at

the vertex we have for $p_1^\mu \rightarrow 0$

$$f_s(p_1, p_2, p_3; \Delta) \rightarrow \frac{\Delta}{2p_2^2 + \Delta} \quad (4.34)$$

and in the case where p_1 is a soft parton emitted from an external line we will have $p_2^2 = 0$ and we will recover $f_s = 1$ as required. Likewise, for $p_1^\mu \rightarrow \lambda p_2^\mu$ we have

$$f_s(p_1, p_2, p_3; \Delta) \rightarrow \frac{\Delta}{(1 + \lambda^2 + (1 + \lambda)^2)p_2^2 + \Delta} \quad (4.35)$$

and in the case where p_1 is a collinear parton emitted from an external line we will have $p_2^2 = 0$ and we will recover $f_s = 1$ as required.

We can see that if we were to take the limit $\Delta \rightarrow 0$ we would find $f_h \rightarrow 1$ and $f_s \rightarrow 0$. As a result we expect the remainder of a soft singularity to manifest itself as $\ln(\Delta)$. This split appears to satisfy all the necessary criteria, however we shall see that although f_s does satisfy (4.4) in the form that it was stated earlier, it does not dampen the ultraviolet behaviour quickly enough in the presence of quadratic singularities. This will require an additional subtraction in the case of the gluon self energy.

4.4.1 Two point vertices in hard reduced diagrams

We now calculate the one-loop corrections to the fermion and gluon propagators with hard vertices. We start with the fermion propagator (shown in Figure 4.1) where we are interested in $\mathcal{S}_h(p^2, \Delta)|_2$. We can see from the definition in Eq.(4.26) that this will be the coefficient of \not{p} in the one-loop

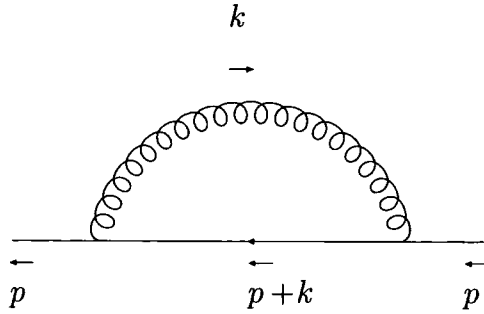


Figure 4.1: Correction to the fermion propagator

correction. We need to calculate the integral

$$-g_s^2 t^A t^A \int \frac{d^D k}{(2\pi)^D} \frac{\gamma_\mu (\not{p} + \not{k}) \gamma_\nu (g^{\mu\nu} - \xi_X \frac{k^\mu k^\nu}{k^2})}{(p+k)^2} \left(\frac{p^2 + k^2 + (p+k)^2}{p^2 + k^2 + (p+k)^2 + \Delta} \right)^2 \quad (4.36)$$

It is reasonably straightforward to perform this integration, and after performing an expansion in p^2 and taking the coefficient of \not{p} we get the result

$$\mathcal{S}_h(p^2, \Delta)|_2 = \frac{iC_F c_\epsilon g_s^2}{64\pi^2} \left[4(1 - \xi_X) \left(\frac{1}{\epsilon} - \ln \left(-\frac{\Delta}{2} \right) \right) - 4 + \xi_X + \mathcal{O} \left(\frac{p^2}{\Delta} \right) \right] \quad (4.37)$$

where $c_\epsilon = (4\pi)^\epsilon \epsilon^{-\epsilon\gamma_E}$.

It is immediately obvious that all the coefficients C_n are zero for this one-loop case (at least up to $\mathcal{O}(\epsilon)^6$). This means that composite two point fermion vertices will not increase the negative powercounting of diagrams and so can be disregarded as a possible source of infrared divergences.

We must now perform a similar calculation for the gluon propagator. In this case we want to calculate $\mathcal{A}(p^2, \Delta)|_2$ and $\mathcal{B}(p^2, \Delta)|_2$. We can see from the definition in Eq.(4.29) that we must consider the coefficient of $g^{\mu\nu} p^2$ for \mathcal{A} and the coefficient of $p^\mu p^\nu$ for \mathcal{B} . This time we will have to calculate two

⁶Any discrepancies at $\mathcal{O}(\epsilon)$ or higher will not alter the argument since they will cancel the potential singularities introduced by any increased negative powercounting.

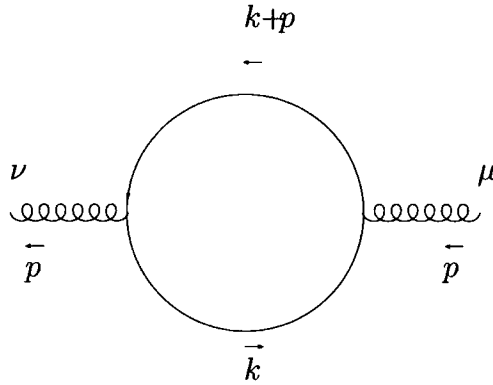


Figure 4.2: Fermion loop correction to the gluon propagator

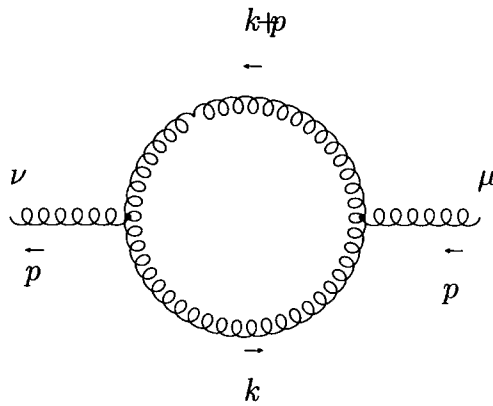


Figure 4.3: Gluon loop correction to the gluon propagator

separate integrals; one for the contribution from the fermion loop and one for the contribution from the gluon loop. The fermion loop contribution is shown in Figure 4.2, and takes the form

$$-g_s^2 \text{tr}(t^A t^B) \int \frac{d^D k}{(2\pi)^D} \frac{1}{(p+k)^2} \frac{1}{k^2} \text{tr}(\gamma^\mu (\not{p} + \not{k}) \gamma^\nu \not{k}) \left(\frac{p^2 + k^2 + (p+k)^2}{p^2 + k^2 + (p+k)^2 + \Delta} \right)^2 \quad (4.38)$$

The gluon loop contribution is shown in Figure 4.3, and takes the form

$$\begin{aligned}
& -g_s^2 f_{ADC} f_{BCD} \int \frac{d^D k}{(2\pi)^D} \frac{\left(g^{\alpha\sigma} - \xi_X \frac{(p+k)^\alpha (p+k)^\sigma}{(p+k)^2}\right) \left(g^{\beta\rho} - \xi_X \frac{k^\beta k^\rho}{k^2}\right)}{(p+k)^2 k^2} \\
& \quad \times \left(-g^{\mu\alpha} k^\beta + g^{\alpha\beta} (p+2k)^\mu - g^{\mu\beta} (p+k)^\alpha\right) \\
& \quad \times \left(-g^{\nu\rho} (p+k)^\sigma + g^{\rho\sigma} (p+2k)^\nu - g^{\nu\sigma} k^\rho\right) \left(\frac{p^2 + k^2 + (p+k)^2}{p^2 + k^2 + (p+k)^2 + \Delta}\right)^2
\end{aligned} \tag{4.39}$$

Again, it is relatively straightforward to perform these calculations, and after performing an expansion in p^2 we get the following results for the fermion loop contribution ($\mathcal{A}_{N_F}(p^2, \Delta)|_2$ and $\mathcal{B}_{N_F}(p^2, \Delta)|_2$)

$$\begin{aligned}
\mathcal{A}_{N_F}(p^2, \Delta)|_2 &= \\
& -\frac{iN_F c_\epsilon g_s^2}{72\pi^2} \left(\left(\frac{9}{\epsilon} - 9 \ln\left(-\frac{\Delta}{2}\right) \right) \frac{\Delta}{p^2} + \frac{6}{\epsilon} - 6 \ln\left(-\frac{\Delta}{2}\right) - 10 \right) + \mathcal{O}\left(\frac{p^2}{\Delta}\right)
\end{aligned} \tag{4.40}$$

$$\mathcal{B}_{N_F}(p^2, \Delta)|_2 = \frac{iN_F c_\epsilon g_s^2}{144\pi^2} \left(\frac{12}{\epsilon} - 12 \ln\left(-\frac{\Delta}{2}\right) - 5 \right) + \mathcal{O}\left(\frac{p^2}{\Delta}\right) \tag{4.41}$$

and also for the gluon loop contribution ($\mathcal{A}_{N_C}(p^2, \Delta)|_2$ and $\mathcal{B}_{N_C}(p^2, \Delta)|_2$)

$$\begin{aligned}
\mathcal{A}_{N_C}(p^2, \Delta)|_2 &= \\
& -\frac{iN_C c_\epsilon (\xi_X - 1) g_s^2}{64\pi^2} \left(\left(\frac{8}{\epsilon} - 8 \ln\left(-\frac{\Delta}{2}\right) + 4 \right) \frac{\Delta}{p^2} - 7 \right) + \mathcal{O}\left(\frac{p^2}{\Delta}\right)
\end{aligned} \tag{4.42}$$

$$\begin{aligned}
\mathcal{B}_{N_C}(p^2, \Delta)|_2 &= \frac{iN_C c_\epsilon g_s^2}{384\pi^2} \left(12(\xi_X + 5) \left(\frac{1}{\epsilon} - \ln\left(-\frac{\Delta}{2}\right) + 1 \right) \frac{\Delta}{p^2} \right. \\
& \quad \left. + \frac{12}{\epsilon} - 12 \ln\left(-\frac{\Delta}{2}\right) - 9\xi_X - 55 \right) + \mathcal{O}\left(\frac{p^2}{\Delta}\right)
\end{aligned} \tag{4.43}$$

This time, however, we do indeed find a contribution like $\frac{\Delta}{p^2}$. This means

that a chain of these two point gluon interactions will indeed contain terms with higher negative powers of p^2 than a single propagator, and so can result in diagrams with infrared divergences. In order to see how our scheme copes with these it is now necessary to look more closely at the propagators themselves.

4.5 Calculation of the propagators

In Section 3.6.1 we saw that although we are unable to calculate the propagators for the asymptotic fields exactly, we can expand them as a perturbative series in the free fields. Now that we have chosen a form for our splitting functions f_s and f_h we can investigate how our asymptotic propagators will behave by calculating the corrections to the free propagators. We will start by calculating the lowest order correction to the fermion propagator.

4.5.1 The fermion propagator

For the case of a fermionic propagator we have

$$\begin{aligned}
 S_{\Xi}(x_1 - x_2) &= \langle 0 | T \{ \Xi(x_1) \bar{\Xi}(x_2) \} | 0 \rangle \\
 &= \frac{\langle 0 | T \left\{ \phi(x_1) \bar{\phi}(x_2) \exp \left(-i \int_{-\infty}^{\infty} d^4x \mathcal{L}_S(x) \right) \right\} | 0 \rangle}{\langle 0 | T \left\{ \exp \left(-i \int_{-\infty}^{\infty} d^4x \mathcal{L}_S(x) \right) \right\} | 0 \rangle} \quad (4.44)
 \end{aligned}$$

If we examine Eq.(4.44) at zero order in the coupling we find

$$S_{\Xi,0} = i \int \frac{d^4p}{(2\pi)^4} \frac{\not{p}}{p^2 + iO_+} e^{-ip \cdot (x_1 - x_2)} \quad (4.45)$$

which is the usual free field propagator. Higher order terms will result in corrections to this. We split up all the higher order terms into 1PI diagrams Σ_{Ξ} . To get the “complete” solution we would then sum the perturbation series to all orders:

$$S_{\Xi} = S_{\Xi,0} + S_{\Xi,0} \Sigma_{\Xi} S_{\Xi,0} + S_{\Xi,0} \Sigma_{\Xi} S_{\Xi,0} \Sigma_{\Xi} S_{\Xi,0} + \dots \quad (4.46)$$

which gives

$$\begin{aligned} S_{\Xi} &= S_{\Xi,0} (1 + \Sigma_{\Xi} (S_{\Xi,0} + S_{\Xi,0} \Sigma_{\Xi} S_{\Xi,0} + \dots)) \\ S_{\Xi} &= S_{\Xi,0} (1 + \Sigma_{\Xi} S_{\Xi}) \end{aligned} \quad (4.47)$$

We can rewrite this as

$$S_{\Xi} = \frac{S_{\Xi,0}}{1 - S_{\Xi,0} \Sigma_{\Xi}} \quad (4.48)$$

In order to derive a form for this we need to calculate Σ_{Ξ} . We will do this perturbatively, order by order in the coupling. If we define the following relation

$$\Sigma_{\Xi}|_2 = i\not{p} F_{\Xi}(p^2/\Delta) \quad (4.49)$$

and use the standard form $S_{\Xi,0}(p) = \frac{i\not{p}}{p^2 + i0_+}$ then we can write S_{Ξ} in the following way which shows the correction to the standard form more clearly

$$S_{\Xi}(p) = \frac{i\not{p}}{p^2 + i0_+} \frac{1}{1 + F_{\Xi}(p^2/\Delta)} \quad (4.50)$$

We will now consider the lowest order correction to the fermion propagator in QCD. From Eq.(4.44) we see that there is no first order term, and so the

first contribution to Σ_{Ξ} will be at second order⁷:

$$\begin{aligned}\Sigma_{\Xi}|_2 &= \int_{-\infty}^{\infty} d^4x d^4y \langle 0|T \{ \phi(x_1) \bar{\phi}(x_2) \mathcal{L}_S(x) \mathcal{L}_S(y) \} |0\rangle \\ &= -g_s^2 C_F \int \frac{d^D k}{(2\pi)^D} \frac{\gamma_{\mu}(\not{p} + \not{k}) \gamma_{\nu}}{(p+k)^2} \frac{(g^{\mu\nu} - \xi_X \frac{k^{\mu} k^{\nu}}{k^2})}{k^2} \left(\frac{\Delta}{p^2 + k^2 + (p+k)^2 + \Delta} \right)^2\end{aligned}\quad (4.51)$$

where p^{μ} is off-shell. Infrared divergences will only appear when p goes on-shell, and our f_s functions will cut off the ultraviolet regions of the integrals. Consequently we can perform the integral in $D = 4$ dimensions without any further UV or IR regulators, arriving at the result

$$\begin{aligned}F_{\Xi}(p^2/\Delta) &= -\frac{C_F g_s^2}{32\pi^2(1+p^2/\Delta)^3} \left(4\xi_X \ln \left(1 + \frac{p^2}{3p^2 + 2\Delta} \right) \left(\frac{\Delta}{p^2} \right)^2 \right. \\ &\quad \left. + 2\xi_X \left(6 \ln \left(1 + \frac{p^2}{3p^2 + 2\Delta} \right) - 1 \right) \left(\frac{\Delta}{p^2} \right) + 2(1 - \xi_X) \ln \left(\frac{p^2}{2p^2 + \Delta} \right) \right. \\ &\quad \left. - 2(1 - 7\xi_X) \ln \left(1 - \frac{p^2}{3p^2 + 2\Delta} \right) + 4\xi_X (3 \ln(2) - 1) + \left(2(1 - 2\xi_X) \ln \left(\frac{p^2}{2p^2 + \Delta} \right) \right. \right. \\ &\quad \left. \left. - 2(1 - 4\xi_X) \ln \left(1 - \frac{p^2}{3p^2 + 2\Delta} \right) + 2\xi_X (2 \ln(2) - 1) \right) \left(\frac{p^2}{\Delta} \right) \right)\end{aligned}\quad (4.52)$$

Later on we will see that the possible IR divergence when p goes on-shell will not be a problem.

4.5.2 The gluon propagator

We now perform a similar calculation for the gluon propagator. We write the full two point correlation function as $P_{\Xi}^{\mu\nu}(p)$, the free field propagator as

⁷We have now dropped the denominator of Eq.(4.44) and so will be discarding any disconnected diagrams.

$P_{\Xi,0}^{\mu\nu}(p)$ and the 1PI higher order terms as $\Pi_{\Xi}^{\mu\nu}(p)$ so we have the relation

$$P_{\Xi}^{\mu\nu}(p) = P_{\Xi,0}^{\mu\nu}(p) + P_{\Xi,0}^{\mu\alpha}(p)\Pi_{\Xi\alpha\beta}(p)P_{\Xi,0}^{\beta\nu}(p) + \dots \quad (4.53)$$

We now write

$$\Pi_{\Xi}^{\mu\nu}(p) = A(p^2)g^{\mu\nu} + B(p^2)\frac{p^\mu p^\nu}{p^2} \quad (4.54)$$

and

$$P_{\Xi}^{\mu\nu}(p) = P_1(p^2)\left(\frac{p^\mu p^\nu}{p^2} - g^{\mu\nu}\right) + P_2(p^2)\frac{p^\mu p^\nu}{p^2} \quad (4.55)$$

and using the fact that $P_{\Xi,0}^{\mu\nu}(p) = \frac{i}{p^2+i0_+}((1-\xi)\frac{p^\mu p^\nu}{p^2} - g^{\mu\nu})$ we find that

$$\begin{aligned} P_{\Xi,0}^{\mu\alpha}(p)\Pi_{\Xi\alpha\beta}(p)P_{\Xi,0}^{\beta\nu}(p) &= P_0(p^2)^2\left(-A(p^2)\left(\frac{p^\mu p^\nu}{p^2} - g^{\mu\nu}\right)\right. \\ &\quad \left.+ \xi^2(A(p^2) + B(p^2))\frac{p^\mu p^\nu}{p^2}\right) \end{aligned} \quad (4.56)$$

(where $P_0(p^2) = \frac{i}{p^2+i\epsilon}$) and in general an n^{th} order term in $P_{\Xi,0}^{\mu\nu}(p)$ will become

$$P_0(p^2)^n\left((-A(p^2))^{n-1}\left(\frac{p^\mu p^\nu}{p^2} - g^{\mu\nu}\right) + (-\xi)^n(A(p^2) + B(p^2))^{n-1}\frac{p^\mu p^\nu}{p^2}\right) \quad (4.57)$$

Equating the $\frac{p^\mu p^\nu}{p^2} - g^{\mu\nu}$ terms we find

$$\begin{aligned} P_1(p^2) &= P_0(p^2) + P_0(p^2)^2(-A(p^2)) + P_0(p^2)^3(-A(p^2))^2 + \dots \\ &= P_0(p^2) - P_0(p^2)A(p^2)P_1(p^2) \\ &\Rightarrow P_1(p^2) = \frac{P_0(p^2)}{1 + P_0(p^2)A(p^2)} \end{aligned} \quad (4.58)$$

Equating the remaining $\frac{p^\mu p^\nu}{p^2}$ terms we find

$$\begin{aligned}
 P_2(p^2) &= -\xi P_0(p^2) + (-\xi P_0(p^2))^2 (A(p^2) + B(p^2)) \\
 &\quad + (-\xi P_0(p^2))^3 (A(p^2) + B(p^2))^2 + \dots \\
 &= -\xi P_0(p^2) - \xi P_0(p^2) (A(p^2) + B(p^2)) P_2(p^2) \\
 &\Rightarrow P_2(p^2) = \frac{-\xi P_0(p^2)}{1 + \xi P_0(p^2) (A(p^2) + B(p^2))} \quad (4.59)
 \end{aligned}$$

Proceeding in a similar manner to the fermion propagator we define

$$\Pi_{\Xi}^{\mu\nu}(p)|_2 = -ip^2 \left(G_{\Xi}(p^2/\Delta) g^{\mu\nu} + H_{\Xi}(p^2/\Delta) \frac{p^\mu p^\nu}{p^2} \right) \quad (4.60)$$

and then we see that

$$\begin{aligned}
 P_{\Xi}^{\mu\nu}(p) &= \frac{i}{p^2 + i\epsilon} \left(\frac{1}{1 + G_{\Xi}(p^2)} \left(\frac{p^\mu p^\nu}{p^2} - g^{\mu\nu} \right) \right. \\
 &\quad \left. - \frac{\xi}{1 + \xi(G_{\Xi}(p^2) + H_{\Xi}(p^2))} \frac{p^\mu p^\nu}{p^2} \right) \quad (4.61)
 \end{aligned}$$

We will now consider the lowest order correction to the gluon propagator in QCD; once again, there's no first order term and so we will work at second order in α_s . The fermion loop contribution is given by

$$\Pi_{\Xi, N_F}^{\mu\nu}|_2 = -g_s^2 \text{tr}(t^A t^B) \int \frac{d^D k}{(2\pi)^D} \frac{\text{tr}(\gamma^\mu (\not{p} + \not{k}) \gamma^\nu \not{k})}{(p+k)^2} \frac{1}{k^2} \left(\frac{\Delta}{p^2 + k^2 + (p+k)^2 + \Delta} \right)^2 \quad (4.62)$$

while the gluon loop contribution is given by

$$\begin{aligned}
\Pi_{\Xi, N_C}^{\mu\nu}|_2 &= -g_s^2 f_{ADC} f_{BCD} \int \frac{d^D k}{(2\pi)^D} \frac{\left(g^{\alpha\sigma} - \xi_X \frac{(p+k)^\alpha (p+k)^\sigma}{(p+k)^2}\right) \left(g^{\beta\rho} - \xi_X \frac{k^\beta k^\rho}{k^2}\right)}{(p+k)^2} \\
&\quad \times \left(-g^{\mu\alpha} k^\beta + g^{\alpha\beta} (p+2k)^\mu - g^{\mu\beta} (p+k)^\alpha\right) \\
&\quad \times \left(-g^{\nu\rho} (p+k)^\sigma + g^{\rho\sigma} (p+2k)^\nu - g^{\nu\sigma} k^\rho\right) \left(\frac{\Delta}{p^2 + k^2 + (p+k)^2 + \Delta}\right)^2
\end{aligned} \tag{4.63}$$

Again, the inclusion of soft vertices will remove the ultraviolet regions of the integrals, and infrared divergences will only appear as p^2 goes on-shell allowing us to perform the integral in $D = 4$ dimensions again. Writing $\text{tr}(t^A t^B) = N_F \delta^{AB}$, we find the following results for the fermion loop:

$$\begin{aligned}
G_{\Xi, N_F}(p^2/\Delta)|_2 &= \frac{N_F g_s^2}{24\pi^2 (1 + p^2/\Delta)^2} \left(4 \ln \left(\frac{3p^2 + 2\Delta}{4p^2 + 2\Delta}\right) \left(\frac{\Delta}{p^2}\right)^3\right. \\
&\quad + \left(12 \ln \left(\frac{3p^2 + 2\Delta}{4p^2 + 2\Delta}\right) + 2\right) \left(\frac{\Delta}{p^2}\right)^2 + 2 \left(6 \ln \left(\frac{3p^2 + 2\Delta}{4p^2 + 2\Delta}\right) + 2\right) \left(\frac{\Delta}{p^2}\right) \\
&\quad \left. + 6 \ln \left(\frac{3p^2 + 2\Delta}{4p^2 + 2\Delta}\right) + 2 \ln \left(\frac{2p^2}{2p^2 + \Delta}\right) + 2\right) \tag{4.64}
\end{aligned}$$

$$\begin{aligned}
H_{\Xi, N_F}(p^2/\Delta)|_2 &= -\frac{N_F g_s^2}{12\pi^2 (1 + p^2/\Delta)^2} \left(8 \ln \left(\frac{3p^2 + 2\Delta}{4p^2 + 2\Delta}\right) \left(\frac{\Delta}{p^2}\right)^3\right. \\
&\quad + 2 \left(15 \ln \left(\frac{3p^2 + 2\Delta}{4p^2 + 2\Delta}\right) + 2\right) \left(\frac{\Delta}{p^2}\right)^2 + 4 \left(9 \ln \left(\frac{3p^2 + 2\Delta}{4p^2 + 2\Delta}\right) + 2\right) \left(\frac{\Delta}{p^2}\right) \\
&\quad \left. + 15 \ln \left(\frac{3p^2 + 2\Delta}{4p^2 + 2\Delta}\right) + \ln \left(\frac{2p^2}{2p^2 + \Delta}\right) + 4\right) \tag{4.65}
\end{aligned}$$

and in the gluon loop case, writing $f^{ADC}f^{BCD} = N_C\delta^{AB}$ we get:

$$G_{\Xi, N_C}(p^2/\Delta)|_2 = -\frac{N_C(\xi_X - 1)g_s^2}{8\pi^2} \ln\left(\frac{3p^2 + 2\Delta}{4p^2 + 2\Delta}\right) \left(\frac{\Delta}{p^2}\right)^2 \quad (4.66)$$

$$\begin{aligned} H_{\Xi, N_C}(p^2/\Delta)|_2 &= \frac{N_C g_s^2}{32\pi^2(1 + p^2/\Delta)^2} \left(4(5 - 3\xi_X) \ln\left(\frac{3p^2 + 2\Delta}{4p^2 + 2\Delta}\right) \left(\frac{\Delta}{p^2}\right)^3 \right. \\ &\quad + 2 \left((35 - 23\xi_X) \ln\left(\frac{3p^2 + 2\Delta}{4p^2 + 2\Delta}\right) + 5 - 3\xi_X \right) \left(\frac{\Delta}{p^2}\right)^2 \\ &\quad + 4 \left((20 - 14\xi_X) \ln\left(\frac{3p^2 + 2\Delta}{4p^2 + 2\Delta}\right) + 5 - 3\xi_X \right) \left(\frac{\Delta}{p^2}\right) \\ &\quad \left. + (31 - 22\xi_X) \ln\left(\frac{3p^2 + 2\Delta}{4p^2 + 2\Delta}\right) + \ln\left(\frac{2p^2}{2p^2 + \Delta}\right) + 10 - 6\xi_X \right) \quad (4.67) \end{aligned}$$

4.5.3 Checking the limits

We now investigate these results by checking that they reproduce the expected behaviour when we take the limits $\Delta \rightarrow 0$ and $p^2 \rightarrow 0$. First, we take p^2 to be finite and non-zero; then, in the $\Delta \rightarrow 0$ limit we find that the fermion propagator correction is given by

$$F_{\Xi}(p^2/\Delta) = \frac{C_F g_s^2}{16\pi^2} \left(\xi_X + \ln\left(\frac{4}{3}\right) (1 - 4\xi_X) \right) \left(\frac{\Delta}{p^2}\right)^2 + \mathcal{O}\left(\left(\frac{\Delta}{p^2}\right)^3\right) \quad (4.68)$$

which tends to zero as expected since we should recover the free propagator as we shrink the soft region down to zero.

We now take the limit $p^2 \rightarrow 0$ assuming Δ to be finite and non-zero and find

$$F_{\Xi}(p^2/\Delta) = -\frac{C_F g_s^2}{64\pi^2} \left(4(1 - \xi_X) \ln\left(\frac{2p^2}{\Delta}\right) + 3\xi_X \right) + \mathcal{O}\left(\frac{p^2}{\Delta}\right) \quad (4.69)$$

This is divergent, which gives us the expected return of the infrared diver-

gences when the propagator goes on-shell.

However, when we consider the resummed propagator given in Eq.(4.50), we see that the full propagator will behave like $\not{p} / (p^2 \ln(p^2))$ as p goes on-shell and so while the infrared behaviour of the propagator is indeed altered we still have a singularity at $p^2 = 0$, indicating that the fermions remain massless.

We now take the same limits for the case of the gluon propagator correction.

Taking the $\Delta \rightarrow 0$ limit we see

$$G_{\Xi, N_F}(p^2/\Delta)|_2 = \frac{N_F g_s^2 (2 - 6 \ln(\frac{4}{3}))}{24\pi^2} \left(\frac{\Delta}{p^2}\right)^2 + \mathcal{O}\left(\frac{\Delta}{p^2}\right)^3 \quad (4.70)$$

$$H_{\Xi, N_F}(p^2/\Delta)|_2 = -\frac{N_F g_s^2 (4 - 15 \ln(\frac{4}{3}))}{12\pi^2} \left(\frac{\Delta}{p^2}\right)^2 + \mathcal{O}\left(\frac{\Delta}{p^2}\right)^3 \quad (4.71)$$

$$G_{\Xi, N_C}(p^2/\Delta)|_2 = -\frac{N_C g_s^2 (1 - \xi_X) \ln(\frac{4}{3})}{8\pi^2} \left(\frac{\Delta}{p^2}\right)^2 + \mathcal{O}\left(\frac{\Delta}{p^2}\right)^3 \quad (4.72)$$

$$H_{\Xi, N_C}(p^2/\Delta)|_2 = \frac{N_C g_s^2 (10 - 6\xi_X - (31 - 22\xi_X) \ln(\frac{4}{3}))}{32\pi^2} \left(\frac{\Delta}{p^2}\right)^2 + \mathcal{O}\left(\frac{\Delta}{p^2}\right)^3 \quad (4.73)$$

Again, all of these tend to zero, and so we recover the free propagator in this limit as expected.

We now take the limit $p^2 \rightarrow 0$ and we find the following results for the fermion loop contribution

$$G_{\Xi, N_F}(p^2/\Delta)|_2 = \frac{N_F g_s^2}{144\pi^2} \left(9\frac{\Delta}{p^2} + 12 \ln\left(\frac{2p^2}{\Delta}\right) - 16\right) + \mathcal{O}\left(\frac{p^2}{\Delta}\right) \quad (4.74)$$

$$H_{\Xi, N_F}(p^2/\Delta)|_2 = \frac{N_F g_s^2}{144\pi^2} \left(1 - 12 \ln\left(\frac{2p^2}{\Delta}\right)\right) + \mathcal{O}\left(\frac{p^2}{\Delta}\right) \quad (4.75)$$

and similarly for the gluon loop contribution

$$G_{\Xi, N_C}(p^2/\Delta)|_2 = \frac{N_C(\xi_X - 1)g_s^2}{64\pi^2} \left(4\frac{\Delta}{p^2} - 7 \right) + \mathcal{O}\left(\frac{p^2}{\Delta}\right) \quad (4.76)$$

$$H_{\Xi, N_C}(p^2/\Delta)|_2 = \frac{N_C g_s^2}{384\pi^2} \left(6(\xi_X + 5)\frac{\Delta}{p^2} + 12 \ln\left(\frac{2p^2}{\Delta}\right) - 9\xi_X - 55 \right) + \mathcal{O}\left(\frac{p^2}{\Delta}\right) \quad (4.77)$$

The full result, incorporating both diagrams and taking $N_F = \frac{1}{2}$, $N_C = 3$, will be as follows

$$G_{\Xi}(p^2/\Delta)|_2 = -\frac{g_s^2}{576\pi^2} \left(18(5 - 6\xi_X)\frac{\Delta}{p^2} - 24 \ln\left(\frac{2p^2}{\Delta}\right) - 157 + 189\xi_X \right) + \mathcal{O}\left(\frac{p^2}{\Delta}\right) \quad (4.78)$$

$$H_{\Xi}(p^2/\Delta)|_2 = \frac{g_s^2}{1152\pi^2} \left(54(5 + \xi_X)\frac{\Delta}{p^2} + 60 \ln\left(\frac{2p^2}{\Delta}\right) - 491 - 81\xi_X \right) + \mathcal{O}\left(\frac{p^2}{\Delta}\right) \quad (4.79)$$

This is divergent, as in the case of the fermion propagator. However, unlike the case of the fermion propagator, these corrections contain a $\frac{\Delta}{p^2}$ divergence as well as the weaker $\ln(\frac{\Delta}{p^2})$ part. This will shift the location of the pole of the gluon propagator and will therefore generate a gluon mass as we predicted in Section 4.3.3. If we look at Eq.(4.61) - taking the case where $\xi_X = 0$ for simplicity - since we now have $p^2 G_{\Xi}(p^2) \neq 0$ as $p^2 \rightarrow 0$ we see that the singularity of the propagator is no longer located at $p^2 = 0$, but at $p^2 + p^2 G_{\Xi}(p^2) = 0$. The value of p^2 which satisfies this equation will be our gluon mass.

We note that our new gluon mass depends on g_s^2 . We could also calculate



corrections to this which would depend on higher powers of the strong coupling. If we were able to solve the asymptotic propagators exactly then we would use that form including a massive gluon throughout our calculations; since we are forced to employ a perturbative approach it will only become necessary to include the increasingly higher order corrections as we calculate higher order diagrams. By the same token, when calculating diagrams at lower orders (such as all the examples contained in this thesis) it is not necessary to take the mass of the gluon into account. This does not cause any problems with potential infrared singularities arising from neglecting the gluon mass since these can only occur at higher orders in perturbation theory.

4.6 Infrared finite amplitudes

Now that we know that the gluon will have a dynamically generated mass we can finally see how our approach will result in infrared finite amplitudes. Our powercounting approach earlier showed that problems could potentially arise if we had reduced diagrams which included effective two or three point interactions. We then looked more closely at the form of the two point effective interactions and saw that (at one loop) there was no problem associated with the two point fermion interaction, but that the two point gluon interaction could still potentially introduce infrared divergences. Our discovery that the gluon will have a dynamically generated mass, however, means that this two point interaction will no longer be a problem⁸. In fact, it appears to be no coincidence that a mass is generated in the gluon case where it is necessary for the theory to be finite and not in the fermion case where it

⁸In calculations of a low enough order for us to neglect the gluon mass even two and three point effective vertices are not enough to cause infrared singularities.

is unnecessary. This is due to the fact that the hard vertices which introduce the potentially problematic factors in the reduced diagrams obey the relation $f_s(\Delta) + f_h(\Delta) = 1$ which means that if we consider the sum over diagrams with all possible combinations of soft and hard vertices we must recover a result with no dependence on Δ . Since the powers of p^2/Δ which cause problems when we consider the reduced diagrams (where we have hard vertices) are the same as those which introduce a mass in our calculation of the propagator (where we have soft vertices), it follows that we expect these two situations to coincide in order to recover the case with no Δ dependence⁹. This allows us to be confident that although we have only checked these issues at one loop, we won't run into problems at higher orders; it also suggests that the seeming dependence of this proof of infrared finiteness on our choice of vertex function is actually misleading since any vertex function which did not produce a gluon mass would result in an effective two point gluon interaction which did not alter the powercounting of reduced diagrams.

It is now simple to check that three point effective vertices will also not lead to infrared divergences. We consider specifically the case of a completely soft subdiagram since our earlier analysis distinguished between fermions and bosons; a similar argument can be made for the case including jets if we consider the smaller contribution of fermions to the negative powercounting. From Eq.(4.18) we see that the contribution to μ at each vertex is

$$\frac{3}{2}f_v - 4 \tag{4.80}$$

⁹To recover the case without Δ dependence we must also consider the cases with one hard vertex and one soft vertex. It is, however, unlikely that the relevant powers of p^2/Δ should be present in the hard-hard and hard-soft amplitudes and yet absent from the soft-soft amplitude. Consequently, this is unlikely to present a problem.

where we have disregarded the gluon contribution since they are now massive. It is immediately obvious that an effective three point fermion vertex will make a positive contribution to the powercounting and so will not contribute to infrared divergences. An effective three point vertex with one or more gluons will clearly have an even larger positive contribution. The final check we need to make is that our earlier argument that increasing the value of λ could not reduce the value of μ holds in the case of three point vertices¹⁰. We now have a theory with fermion lines being the only potential source of singularities since our gluon is now massive, and so we now have a contribution of only -1 from each of the I_i soft fermion lines and there is no possibility of soft gluon lines adding negative powercounting. We now update Eq.(4.19) to get

$$\mu = 4L_i - I_i + 2L_j - N_i - N_j \tag{4.81}$$

We follow the reasoning through to find that

$$\mu(S) = 4L_i - I_i = 4 + 4N_i + 3I_i - 4(V_1 + V_2) \tag{4.82}$$

eventually ending up with the updated form of Eq.(4.25):

$$\mu = \sum_v \left(\frac{3}{2}i_v + \frac{1}{2}j_v - 2v_V - 4v_1 \right) + 2 \tag{4.83}$$

It is now apparent that since any three-point mixed vertex must have $i_v = 1$ and $j_v = 2$ we will recover the result of a contribution of $+\frac{1}{2}$ to μ from each of the two vertices required to increase λ by 1. Consequently, we now have a theory which produces infrared finite completely hard amplitudes.

¹⁰It is impossible to have a mixed two point vertex.

4.7 Infrared finite phase space integrals

While the main focus of this thesis is on the calculation of the amplitudes themselves, we can see that for our method to be successful it is also a necessary condition that no infrared singularities appear when we integrate the completely hard amplitudes over the final state phase space. Consequently we shall now take a very brief look at how this occurs.

The simple explanation for this is that the hard splitting functions which are present at every vertex which is connected to an external line (and, of course, at any other vertices too) will be zero whenever an external particle becomes soft or collinear to the particle from which it has been emitted. This will ensure that the regions of the phase space which contain potential infrared singularities are removed from the integral.

To give a very basic demonstration of how this works we shall consider the case of $\gamma \rightarrow q\bar{q}g$ at tree level; one configuration for this process was shown in Figure 2.6. The three particle phase space is proportional to $\int s_{13}s_{23}$ where $s_{ij} = (p_i + p_j)^2$ and p_3 represents the momentum of the particle emitted from one of the external legs. This integral will therefore become divergent if we have terms containing $1/s_{13}$ or $1/s_{23}$. Each of the possible diagrams will contain one of these factors (the configuration in Figure 2.6 has a factor of $1/s_{13}$, a factor of $1/s_{23}$ appears when the gluon is emitted from the other fermion leg), but we can see that it will cancel with the numerator of the relevant hard vertex factor in each case. Consequently, the presence of hard vertices will render the results of the phase space integrals finite.

We shall not consider more complicated cases in any detail here, but the end result is that the numerators of the hard vertex factors will always cancel any

denominators which might potentially introduce infrared divergences. Amplitudes with hard vertices only will therefore be completely infrared finite. Amplitudes which contain some soft vertices may still pick up some infrared divergences from the phase space integration; these will invariably belong to asymptotic states with fewer asymptotic “particles” and the divergences will cancel when combined with the other amplitudes present in that group.

Chapter 5

Example calculations

In order to demonstrate how our new approach will work we shall now look at some example calculations. Although our ultimate aim will be to perform the calculations completely numerically, we shall start by considering analytic calculations in order to gain more insight into the workings of the theory. Also, as we saw in Section 3.6.2, we will need to calculate a selection of diagrams with various combinations of hard and soft vertices; the application of the method to distinct examples will help to illustrate the ways in which these different contributions contribute to the various observables. Consequently we shall start with a simple example: $e^+e^- \rightarrow$ two jets at NLO. We shall then briefly consider how this method would be applied to more complicated examples, where the potential difficulties with our approach will appear and how we can deal with them. In all of our examples we shall apply the asymptotic interaction treatment to QCD interactions only. Consequently, the QED parts of the interactions - such as quark-photon vertices - will not have any vertex splitting functions attached to them.

5.1 $e^+e^- \rightarrow$ two jets at NLO

As in the usual approach, we will calculate diagrams with both real and virtual gluons, although in our case this is not due to the fact that the results for these two configurations are divergent when considered separately, but rather that our consideration of asymptotic rather than free external states will cause us to include various parts of different traditional external states. We shall designate the conventional final states which we will need to consider by $|q_{p_1}\bar{q}_{p_2}\rangle$ and $|q_{p_1}\bar{q}_{p_2}g_{p_3}\rangle$ while we represent the asymptotic final states by $|\{q_{p_1}\bar{q}_{p_2}\}\rangle$ and $|\{q_{p_1}\bar{q}_{p_2}g_{p_3}\}\rangle$. The two particle states consist of a quark and an antiquark with momenta p_1 and p_2 respectively, but as we shall see later the asymptotic two particle state may also contain additional soft or collinear particles (up to one gluon at NLO). The state does not depend on the momentum of this gluon since we are completely inclusive with respect to soft and collinear emissions. The three particle states will both contain a gluon with momentum p_3 in addition to the quark antiquark pair; even though there is no possibility of any extra soft or collinear particles in the asymptotic state at NLO these two states are indeed different as the asymptotic state will not allow the gluon to be soft or collinear to one of the quarks. For the moment we will consider only the QCD part of the amplitude; we shall deal with the initial QED interaction when we perform the phase space calculation.

The general virtual correction diagram for any particular combination of hard

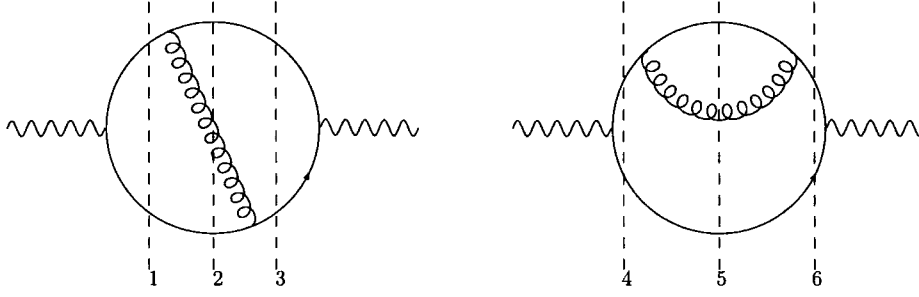


Figure 5.1: Some of the cut diagrams for the vertex correction calculation.

and soft vertices can be written as

$$\begin{aligned} \mathcal{A}_{VC1,ij} = & \int \frac{d^D k}{2\pi^D} \frac{\langle p_1 | (ig_s t^A \gamma^\alpha) i(\not{p}_1 + \not{k}) (ie\gamma^\mu) i(\not{k} - \not{p}_2) (ig_s t^B \gamma^\beta) | p_2 \rangle}{[k^2 + i0^+][(k + p_1)^2 + i0^+][(k - p_2)^2 + i0^+]} \\ & \times \delta_{AB} \left(g_{\alpha\beta} - \xi_X \frac{k_\alpha k_\beta}{k^2} \right) f_i(p_1, k, p_1 + k) f_j(p_2, k, p_2 - k) \quad (5.1) \end{aligned}$$

and corresponds to the right-hand side of cut 1 in Figure 5.1. Here $\langle p_1 |$ and $| p_2 \rangle$ are helicity spinors such as those described in [43].

We will also need to include virtual correction diagrams such as the right-hand side of cut 4 in Figure 5.1 and the similar case where the gluon is attached to the other fermion leg. We can write this diagram as

$$\begin{aligned} \mathcal{A}_{VC2,ij} = & \int \frac{d^D k}{2\pi^D} \frac{\langle p_1 | (ig_s t^A \gamma^\alpha) i(\not{p}_1 + \not{k}) (ig_s t^B \gamma^\beta) i\not{p}_1 (ie\gamma^\mu) | p_2 \rangle}{[k^2 + i0^+][(k + p_1)^2 + i0^+][p_1^2 + i0^+]} \\ & \times \delta_{AB} \left(g_{\alpha\beta} - \xi_X \frac{k_\alpha k_\beta}{k^2} \right) f_i(p_1, k, p_1 + k) f_j(p_1, k, p_1 + k) \quad (5.2) \end{aligned}$$

We now perform these calculations for the specific cases of two hard vertices, two soft vertices and one of the cases with one hard and one soft vertex¹.

Once we have the relevant amplitudes we will need to calculate the different

¹Since the only scales present in the calculation are Δ and $p_1 \cdot p_2$ and the diagram is unchanged under the transformation $p_1 \rightarrow -p_2$, $p_2 \rightarrow -p_1$, both possible configurations for one hard and one soft vertex will yield the same result.

cross sections which appear in Figure 5.1. In order to proceed we will need the following expressions for the two and three-particle phase space [4]

$$\text{PS}^{(2)} = A_0 \int ds_{12} \delta(y_{12} - 1) \frac{1}{4s^2} \quad (5.3)$$

$$\begin{aligned} \text{PS}^{(3)} = & \frac{A_0}{8} \left(\frac{1}{8\pi^2} \left(\frac{4\pi}{s} \right)^\epsilon \frac{1}{\Gamma(1-\epsilon)} \right) \int dy_{13} dy_{23} (y_{13} y_{23} (1 - y_{13} - y_{23}))^{-\epsilon} \\ & \times \theta(1 - y_{13} - y_{23}) \end{aligned} \quad (5.4)$$

where s is the centre of mass energy, we introduce relations for the following invariants

$$s_{ij} = (p_i + p_j)^2, \quad s_{ijk} = (p_i + p_j + p_k)^2, \quad y_{ij} = \frac{s_{ij}}{s} \quad (5.5)$$

and A_0 is given by

$$A_0 = \left(\frac{1}{2\pi} \frac{\Gamma(1-\epsilon)}{\Gamma(2-2\epsilon)} \left(\frac{4\pi}{s} \right)^\epsilon s \right) \quad (5.6)$$

We will also need to include the QED part of the interaction at this point. We can write the whole amplitude in terms of a QED part, L^μ (which will be unchanged for all our amplitudes), and a QCD part, H^σ (which will correspond to the particular QCD amplitude we're calculating), as follows

$$\mathcal{A} = L^\mu \frac{-ig^{\mu\sigma}}{s} H^\sigma = \langle l_2 | ie\gamma^\mu | l_1 \rangle \frac{-ig^{\mu\sigma}}{s} H^\sigma \quad (5.7)$$

where l_1 and l_2 are the momenta of the incoming electron and positron.

The amplitude squared can then be written in the form

$$|\mathcal{A}|^2 = L^{\mu\nu} \frac{1}{s^2} H_{\mu\nu} \quad (5.8)$$

with $L^{\mu\nu}$ given by

$$L^{\mu\nu} = -e^2 \text{tr}(\not{l}_2 \gamma^\mu \not{l}_1 \gamma^\nu) = 4e^2 \left(\frac{s}{2} g^{\mu\nu} - l_1^\mu l_2^\nu - l_1^\nu l_2^\mu \right) \quad (5.9)$$

Since the leptonic part of the calculation will always be the same, we can simplify the rest of the process by working with the average of the leptonic tensor, $\langle L^{\mu\nu} \rangle$. This is given by

$$\langle L^{\mu\nu} \rangle = \frac{4e^2}{3} (s g^{\mu\nu} - (l_1 + l_2)^\mu (l_1 + l_2)^\nu) \quad (5.10)$$

We can then replace the lepton momenta using the relation $l_1 + l_2 = \sum p_i$ which then allows us to calculate our desired cross section from the expression

$$\langle L^{\mu\nu} \rangle H_{\mu\nu} \frac{1}{s^2} \frac{1}{8s} \quad (5.11)$$

where the phase-space integration is now only over the QCD part and the factor $1/(8s)$ comes from considering the average flux.

Writing the virtual correction amplitudes in the form

$$\mathcal{A}_{VC,ij} = -ie \langle p_1 | \gamma^\mu | p_2 \rangle H_{VC,ij} = \mathcal{A}^{(0)} H_{VC,ij} \quad (5.12)$$

where the superscript (0) indicates the power of the strong coupling, g_s , we can then calculate the various NLO cross sections by multiplying by the complex conjugate of the leading order contribution and integrating over the

phase space with the relevant jet function

$$\begin{aligned}\sigma_{VC,ij} &= \frac{-e^2}{8s^3} PS^{(2)} \langle L^{\mu\nu} \rangle \text{tr}(\not{p}_1 \gamma_\mu (-\not{p}_2) \gamma_\nu) H_{VC,ij} J(p_1, p_2) \\ &= -\frac{A_0 e^2}{12s} \int dy_{12} \delta(y_{12} - 1) (2 - 2\epsilon) H_{VC,ij} J(p_1, p_2)\end{aligned}\quad (5.13)$$

In the case where the jet function is 1 this will give us $H_{VC,ij}$ multiplied by the Born cross section.

These calculations are relatively straightforward and, after expanding in $\Delta_s = \Delta/s$, we arrive at the following results, with the designations $VC1$ and $VC2$ corresponding to the topologies of the diagrams containing cuts 1 and 4 in Figure 5.1 respectively:

$$\begin{aligned}\mathcal{A}_{VC1, hh}^{(2)} &= \mathcal{A}^{(0)} C_F c_\epsilon \frac{\alpha}{4\pi} \left(\frac{-s}{\mu^2} \right)^{-\epsilon} \\ &\times \left[\frac{\xi}{\epsilon} - 2 \ln^2 \Delta_s - 4 \ln \Delta_s - 6 + 2\xi + 2(1 + \xi) \ln 2 - \frac{\pi^2}{3} + \mathcal{O}(\Delta_s) \right]\end{aligned}\quad (5.14)$$

$$\begin{aligned}\mathcal{A}_{VC1, hs}^{(2)} &= \mathcal{A}^{(0)} C_F c_\epsilon \frac{\alpha_s}{4\pi} \left(\frac{-s}{\mu^2} \right)^{-\epsilon} \left[-\frac{2(\ln(\Delta_s) + 1)}{\epsilon} \right. \\ &\left. + 3 \ln^2(\Delta_s) - (\xi - 3) \ln(\Delta_s) - (\xi + 1)(1 + \ln(2)) + \frac{\pi^2}{2} + \mathcal{O}(\Delta_s) \right]\end{aligned}\quad (5.15)$$

$$\begin{aligned}\mathcal{A}_{VC1, ss}^{(2)} &= \mathcal{A}^{(0)} C_F c_\epsilon \frac{\alpha_s}{4\pi} \left(\frac{-s}{\mu^2} \right)^{-\epsilon} \\ &\times \left[-\frac{2}{\epsilon^2} + \frac{(4 \ln(\Delta_s) + 1 - \xi)}{\epsilon} - 4 \ln^2(\Delta_s) - 2(1 - \xi) \ln(\Delta_s) - \frac{\pi^2}{2} + \mathcal{O}(\Delta_s) \right]\end{aligned}\quad (5.16)$$

$$\begin{aligned}\mathcal{A}_{VC2, hh}^{(2)} &= \mathcal{A}^{(0)} C_F c_\epsilon \frac{\alpha_s}{4\pi} \left(\frac{-s}{\mu^2} \right)^{-\epsilon} \left[-\frac{\xi}{\epsilon} + (\ln(\Delta_s) - \ln(2))\xi + \frac{3 + \xi}{4} + \mathcal{O}(\Delta_s) \right]\end{aligned}\quad (5.17)$$

$$\mathcal{A}_{VC2,hs}^{(2)} = \mathcal{A}^{(0)} C_F c_\epsilon \frac{\alpha_s}{4\pi} [-\xi + \mathcal{O}(\Delta_s)] \quad (5.18)$$

$$\mathcal{A}_{VC2,ss}^{(2)} = \mathcal{A}^{(0)} C_F c_\epsilon \frac{\alpha_s}{4\pi} \left(\frac{-s}{\mu^2} \right)^{-\epsilon} \left[\frac{\xi}{\epsilon} - (\ln(\Delta_s) - \ln(2)) \xi - \frac{3-7\xi}{4} + \mathcal{O}(\Delta_s) \right] \quad (5.19)$$

where C_F is the colour factor, $c_\epsilon = (4\pi)^\epsilon e^{-\epsilon\gamma_E}$ as before, and the terms $\mathcal{O}(\Delta_s)$ are finite in the limit $\Delta \rightarrow 0$. The full form of these results without any expansion in Δ can be found in Appendix A. In order to arrive at the corresponding cross sections, we must perform the phase space integral; this will result in replacing $\mathcal{A}^{(0)}$ with σ_0 which was defined in Eq.(2.68). We note that the singular parts in the hard-hard amplitudes are due to ultraviolet divergences and could be removed by renormalisation in the usual manner. However, in this particular case, we shall see that the ultraviolet divergences which appear in the two different topologies will cancel when we sum them and so we can choose to ignore them. This will not be possible for all other calculations. If we were performing the calculation numerically we would have to add counterterms to the separate amplitudes in the manner of [11].

The two possible contributions to the real emission diagram are given by

$$\mathcal{A}_{RE1,i}^{(1)} = \frac{\langle p_1 | (ig_s t^A \not{\epsilon}^*(p_3)) i(\not{p}_1 + \not{p}_3) (ie\gamma^\mu) | p_2 \rangle}{[(p_1 + p_3)^2 + i0^+]} f_i(p_1, p_3, p_1 + p_3) \quad (5.20)$$

$$\mathcal{A}_{RE2,i}^{(1)} = - \frac{\langle p_1 | (ie\gamma^\mu) i(\not{p}_2 + \not{p}_3) (ig_s t^A \not{\epsilon}^*(p_3)) | p_2 \rangle}{[(p_2 + p_3)^2 + i0^+]} f_i(p_2, p_3, p_2 + p_3) \quad (5.21)$$

where the label *RE1* refers to emission from the leg with momentum p_1 and *RE2* refers to emission from the leg with momentum p_2 ; they correspond to the two sides of cut 2 in Figure 5.1.

When we construct the possible cross sections there are again two possible topologies: products of amplitudes with emission from the same leg, and

products with emission from different legs. We shall denote the first case by σ_{RE1} and use the case where gluon emission occurs from the p_1 leg, and the second by σ_{RE2} . We find the following results for the two categories of diagram

$$\begin{aligned} \sigma_{RE1,ij} = PS^{(3)} & \frac{8(2-2\epsilon)(y_{12}y_{13} + (2-2\epsilon)y_{23})}{3y_{13}} \\ & \times \frac{1}{8s^3} e^4 g_s^2 s f_i(p_1, p_3, p_1 + p_3) f_j(p_1, p_3, p_1 + p_3) \end{aligned} \quad (5.22)$$

$$\begin{aligned} \sigma_{RE2,ij} = PS^{(3)} & \frac{8(2-2\epsilon)(2y_{12}(y_{12} + y_{13}) - y_{12}y_{13}y_{23} + 2(y_{12} + 2\epsilon y_{13})y_{23})}{3y_{13}y_{23}} \\ & \times \frac{1}{8s^3} e^4 g_s^2 f_i(p_1, p_3, p_1 + p_3) f_j(p_2, p_3, p_2 + p_3) \end{aligned} \quad (5.23)$$

and once we've performed the phase space integrals² and expanded in Δ_s we arrive at the following results

$$\sigma_{RE1,hh} = \sigma_0 C_F c_\epsilon \frac{\alpha_s}{4\pi} \left[2 \ln^2(\Delta_s) + 4 \ln(\Delta_s) + \frac{23}{6} - \frac{\pi^2}{3} + \mathcal{O}(\Delta_s) \right] \quad (5.24)$$

$$\begin{aligned} \sigma_{RE1,hs} = \sigma_0 C_F c_\epsilon \frac{\alpha_s}{4\pi} \left(\frac{s}{\mu^2} \right)^{-\epsilon} & \left[\frac{2(\ln(\Delta_s) + 1)}{\epsilon} \right. \\ & \left. - 3 \ln^2(\Delta_s) - 2 \ln(\Delta_s) + 4 - \frac{2\pi^2}{3} + \mathcal{O}(\Delta_s) \right] \end{aligned} \quad (5.25)$$

²Normally we would be interested in a certain jet definition and so would not integrate the totally hard part over the full phase space; we do this here for the purposes of comparing our answer with the conventional method of calculating the total cross section.

$$\sigma_{RE1,ss} = \sigma_0 C_F c_\epsilon \frac{\alpha_s}{4\pi} \left(\frac{s}{\mu^2}\right)^{-\epsilon} \left[\frac{2}{\epsilon^2} - \frac{4 \log(\Delta_s)}{\epsilon} + 4 \log^2(\Delta_s) + \frac{\pi^2}{2} + \mathcal{O}(\Delta_s) \right] \quad (5.26)$$

$$\sigma_{RE2,hh} = \sigma_0 C_F c_\epsilon \frac{\alpha_s}{4\pi} \left[-\ln(\Delta_s) - \frac{7}{3} + \mathcal{O}(\Delta_s) \right] \quad (5.27)$$

$$\sigma_{RE2,hs} = \sigma_0 C_F c_\epsilon \frac{\alpha_s}{4\pi} [1 + \mathcal{O}(\Delta_s)] \quad (5.28)$$

$$\sigma_{RE2,ss} = \sigma_0 C_F c_\epsilon \frac{\alpha_s}{4\pi} \left(\frac{s}{\mu^2}\right)^{-\epsilon} \left[-\frac{1}{\epsilon} + \ln(\Delta_s) - 2 + \mathcal{O}(\Delta_s) \right] \quad (5.29)$$

5.1.1 Allocating cross sections to the different asymptotic states

At this stage we need to consider how we will allocate the different cross sections which we have calculated to the $|\{q_{p_1} \bar{q}_{p_2}\}\rangle$ and $|\{q_{p_1} \bar{q}_{p_2} g_{p_3}\}\rangle$ final states. It is obvious that the various virtual correction cross sections can never mimic a three jet event and so will clearly belong to the $|\{q_{p_1} \bar{q}_{p_2}\}\rangle$ state. Similarly, the real emission cross section with all hard vertices is part of $|\{q_{p_1} \bar{q}_{p_2} g_{p_3}\}\rangle$ by construction while the real emission cross section with all soft vertices clearly belongs to $|\{q_{p_1} \bar{q}_{p_2}\}\rangle$. The other cross sections will require more thought though since they contain both hard and soft vertices on their external legs. This would seem to suggest that one of the amplitudes making up the cross section belongs in $|\{q_{p_1} \bar{q}_{p_2}\}\rangle$ while the other belongs in $|\{q_{p_1} \bar{q}_{p_2} g_{p_3}\}\rangle$.

On closer inspection this is not the case for $\sigma_{RE1,hs}$ since here the hard vertex prevents the gluon from becoming soft or collinear to p_1 , but does nothing to prevent it becoming collinear to p_2 . This is also consistent with the soft vertex, and so we see that this does fit into $|\{q_{p_1} \bar{q}_{p_2}\}\rangle$. This analysis is

upheld by the presence of an infrared divergence in this cross section which must cancel with other amplitudes in the group, prohibiting it from being a member of $|\{q_{p_1}\bar{q}_{p_2}g_{p_3}\}\rangle$.

If we apply the same analysis to $\sigma_{RE2,hs}$, we see that this case is genuinely ambiguous since the hard vertex prohibits the gluon from becoming soft or collinear to p_1 while the soft vertex requires it. This reasoning would imply that the diagram should be zero, but due to the fact that our vertex functions only tend to their required values in the soft/hard limits there is some overlap; we shall come back to this point a little later on. Since this cross section is finite we could safely place it in either category without disrupting the infrared finite nature of the amplitudes. For the purposes of this example we shall place it in $|\{q_{p_1}\bar{q}_{p_2}\}\rangle$.

5.1.2 The complete result

We now have all the elements we require for the final result for $e^+e^- \rightarrow$ two jets at NLO. To reach the total real and virtual cross section results, $\sigma(\{q_{p_1}, \bar{q}_{p_2}, g_{p_3}\})$ and $\sigma(\{q_{p_1}, \bar{q}_{p_2}\})$ respectively, we add the relevant cross sections with the correct weighting. This weighting corresponds to the number of cut diagrams which share identical topologies; we also include a factor of a half for those diagrams, $\sigma_{VC2,ij}$, which comprise the contributions of $\sqrt{Z_\Xi}$. This is because these diagrams correspond to Σ if we write $Z_\Xi = 1 + \alpha_s \Sigma$. Consequently, when we expand the factors of $\sqrt{Z_\Xi}$ which appear in the calculation, these diagrams appear with a factor of a half as we get the form $1 - \frac{1}{2}\alpha_s \Sigma$. To give an example, we see that $\sigma_{VC1,hs}$ has a weighting factor of four; one factor of two is a result of the fact that this cross section is given by cuts 1 and 3 in Figure 5.1 while the other comes from the two possible

configurations of one hard and one soft vertex. Similarly, we see that $\sigma_{VC2,ss}$ has a weighting factor of two; one factor of two as a result that cuts 4 and 6 contribute, another factor of two for the similar diagrams with the gluon emitted from the other quark leg and the factor of a half as a result of $\sqrt{Z_\Xi}$.

In order to show how this approach will work at the amplitude level, we would also like to write the parts of the real cross section which will end up in the $|\{q_{p_1}, \bar{q}_{p_2}\}\rangle$ final state as amplitudes. The amplitudes and their complex conjugates which make up the virtual terms contain factors of $\ln^n(-s)$ and $[\ln^n(-s)]^*$ respectively³, with $n \in \{1, 2\}$. The real terms contain factors of $\ln(s)$ and $\ln^2(s)$. We rewrite these as $\ln(s) = 1/2(\ln(-s) + \ln^*(-s))$ and $\ln^2(s) = 1/2(\ln^2(-s) + \pi^2) + 1/2(\ln^2(-s) + \pi^2)^*$ and associate the two parts with the amplitude and its complex conjugate respectively. This will only affect the form of the result for $\sigma_{RE1,ss}$ which - once we have replaced σ_0 with $\mathcal{A}^{(0)}$ - now reads

$$\sigma_{RE1,ss} = \mathcal{A}^{(0)} C_F c_\epsilon \frac{\alpha_s}{4\pi} \left(\frac{-s}{\mu^2}\right)^{-\epsilon} \left[\frac{2}{\epsilon^2} - \frac{4 \log(\Delta_s)}{\epsilon} + 4 \log^2(\Delta_s) + \frac{3\pi^2}{2} + \mathcal{O}(\Delta_s) \right] \quad (5.30)$$

A similar substitution can be made for the other real contributions.

Once we now add up all the relevant contributions we get

$$\begin{aligned} \sigma(\{q_{p_1}, \bar{q}_{p_2}, g_{p_3}\}) &= 2\sigma_{RE1,hh} + 2\sigma_{RE2,hh} \\ &= \sigma_0 C_F c_\epsilon \frac{\alpha_s}{4\pi} \left[3 - \frac{2\pi^2}{3} + 2 \ln(\Delta_s)(3 + 2 \ln(\Delta_s)) + \mathcal{O}(\Delta_s) \right] \end{aligned} \quad (5.31)$$

³These appear explicitly in our results when we expand the factors of $(-s)^{-\epsilon}$.

$$\begin{aligned}
\mathcal{A}^{(2)}(\{q_{p_1}, \bar{q}_{p_2}\}) &= 2\mathcal{A}_{VC1,hh}^{(2)} + 2\mathcal{A}_{VC2,hh}^{(2)} + 4\mathcal{A}_{RE1,hs}^{(2)} + 4\mathcal{A}_{RE2,hs}^{(2)} + 4\mathcal{A}_{VC1,hs}^{(2)} \\
&\quad + 4\mathcal{A}_{VC1,hs}^{(2)} + 4\mathcal{A}_{VC2,hs}^{(2)} + 2\mathcal{A}_{RE1,ss}^{(2)} + 2\mathcal{A}_{RE2,ss}^{(2)} + 2\mathcal{A}_{VC1,ss}^{(2)} + 2\mathcal{A}_{VC2,ss}^{(2)} \\
&= \mathcal{A}^{(0)} C_F c_\epsilon \frac{\alpha_s}{4\pi} \left[\frac{2\pi^2}{3} - 2\ln(\Delta_s)(3 + 2\ln(\Delta_s)) + \mathcal{O}(\Delta_s) \right]
\end{aligned} \tag{5.32}$$

where the divergences cancel giving us a finite amplitude. We can now trivially perform the phase space integration to arrive at the cross section

$$\sigma(\{q_{p_1}, \bar{q}_{p_2}\}) = \sigma_0 C_F c_\epsilon \frac{\alpha_s}{4\pi} \left[\frac{2\pi^2}{3} - 2\ln(\Delta_s)(3 + 2\ln(\Delta_s)) + \mathcal{O}(\Delta_s) \right] \tag{5.33}$$

We can see that if we add the two parts of the result together all dependence on Δ cancels and we recover the conventional result given in Eq.2.71. The result is exactly the same if we use the unexpanded versions of the cross sections which are given in Appendix A. This is as we expect since we've included all possible combinations of hard and soft vertices in our calculations and so the total sum is equivalent to the calculation performed with the conventional method. We note also that the expected factors of $\ln(\Delta_s)$ which we predicted in Section 4.4 do appear in our expressions, giving us the return of our soft and collinear singularities if we were to send $\Delta \rightarrow 0$.

We can now investigate how our three jet result compares to the standard three jet result; in order to do this we choose a basic jet definition

$$J = \Theta(y_{12} - y_{cut})\Theta(y_{13} - y_{cut})\Theta(y_{23} - y_{cut}) \tag{5.34}$$

and use this as we perform the phase space integration for the two cases. The results of these integrations can be found in Appendix B. We now plot the results as a function of y_{cut} for different values of Δ_s ; the results are shown

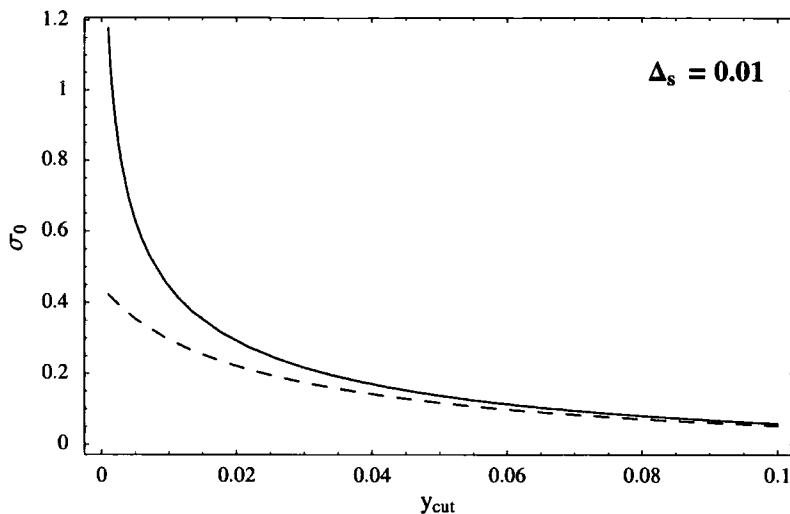


Figure 5.2: A comparison between the results for cross sections formed using the final states $|q_{p_1} \bar{q}_{p_2} g_{p_3}\rangle$ (solid line) and $|\{q_{p_1} \bar{q}_{p_2} g_{p_3}\}\rangle$ (dashed line) for $\Delta_s = 0.01$.

in Figures 5.2 and 5.3.

As we expect, we find that when our value of y_{cut} is significantly larger than our value of Δ_s the two results will give the same answer. As y_{cut} becomes smaller the two results start to separate as the jet definition starts to be able to resolve jets with more accuracy than we include in our resolution parameter, Δ_s . In the case where we have picked a smaller value of Δ_s we note that this divergence takes place at a lower value of y_{cut} . This confirms that our approach will be applicable to various situations providing that we choose a value of Δ_s appropriate to the jet definition we are using. We also note that while the standard three jet result diverges as y_{cut} tends to zero, the asymptotic three jet result will remain finite.

We can carry out the same procedure with the two jet part of the cross section, this time varying Δ_s and arriving at the result shown in Figure 5.4. We note that while we can plot the $|\{q_{p_1} \bar{q}_{p_2}\}\rangle$ and $|\{q_{p_1} \bar{q}_{p_2} g_{p_3}\}\rangle$ contributions separately, we must combine the $|q_{p_1} \bar{q}_{p_2}\rangle$ and $|q_{p_1} \bar{q}_{p_2} g_{p_3}\rangle$ parts in order to

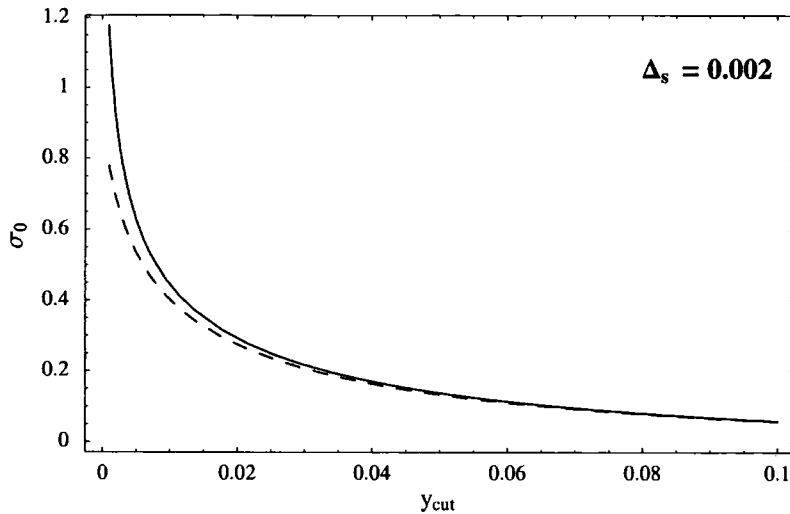


Figure 5.3: A comparison between the results for cross sections formed using the final states $|q_{p_1} \bar{q}_{p_2} g_{p_3}\rangle$ (solid line) and $|\{q_{p_1} \bar{q}_{p_2} g_{p_3}\}\rangle$ (dashed line) for $\Delta_s = 0.002$.

achieve a finite result; we also note that while the two separate asymptotic contributions diverge as $\Delta_s \rightarrow 0$ their sum remains finite. Once again we see that as the value of Δ_s falls beneath that of y_{cut} we start to recover the conventional result.

5.2 Extending our approach

We now want to extend our approach to more complicated examples. However, when we do this we see that there are deficiencies in our split of the Lagrangian into hard and soft parts as they do not cut off sharply, but instead tend to one or zero in their respective limits. This has, in fact, also had an effect on our previous example since it is this aspect of our splitting functions which is responsible for the fact that the contribution to the fermion self-energy diagram in Figure 4.1 with one hard and one soft vertex is not zero, but finite; this is also the cause of our ambiguous contribution to

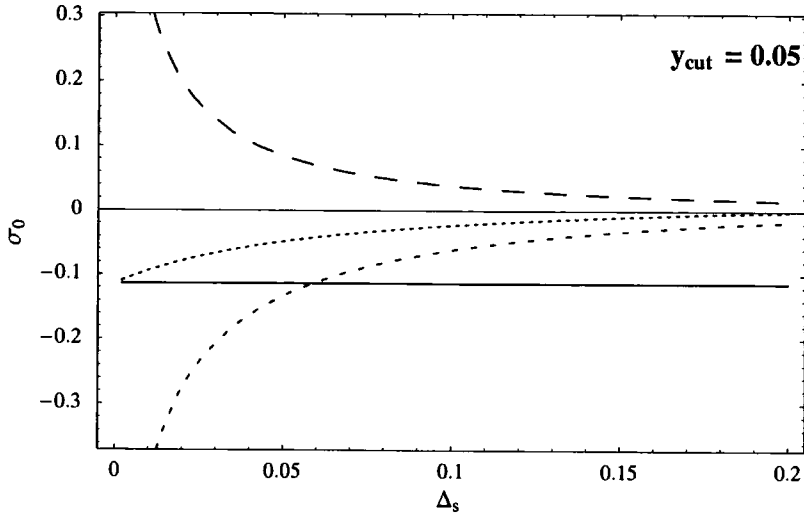


Figure 5.4: A comparison between the results for the $|\{q_{p_1}\bar{q}_{p_2}\}\rangle$ cross section (long dashed line), the two jet part of the $|\{q_{p_1}\bar{q}_{p_2}g_{p_3}\}\rangle$ cross section (short dashed line), their sum (dotted line) and the two jet result obtained from $|q_{p_1}\bar{q}_{p_2}\rangle$ and $|q_{p_1}\bar{q}_{p_2}g_{p_3}\rangle$ (solid line) for $y_{cut} = 0.05$.

the cross section which could be placed in either $|\{q_{p_1}\bar{q}_{p_2}\}\rangle$ or $|\{q_{p_1}\bar{q}_{p_2}g_{p_3}\}\rangle$ in Section 5.1.1. Although this is inconvenient, it does not cause any problems since the unexpected contributions will all not only be finite, but will be suppressed by a factor of Δ_s and so do not affect our division of the amplitudes into two and three jet contributions. In more complicated examples, however, we may come across situations where our choice of splitting functions not only fails to set certain diagrams to zero, but even results in them having divergent parts; this will clearly cause problems with our allocation of amplitudes into the different asymptotic final state groups.

If we consider the form of the numerator of our hard vertex function, which is responsible for setting the amplitude to zero when all the attached lines are on shell, we see that it has dimensions of mass squared and so can effectively only negate the singularity coming from one propagator going on shell. This means that problems can arise in diagrams where a single hard vertex should

set the diagram to zero when one of two or more identical propagators goes on shell. As each hard vertex can only cancel one propagator this will result in finite corrections when one of these propagators goes on shell, but in the case where two or more of them go on shell together we see that cancelling one of them does not remove the infrared singularity completely.

To give a simple example of this we look at cut a in Figure 5.7 with vertices 1 and 3 hard and the rest soft. The hard vertices on one side of the cut should clearly prevent any infrared divergences arising from the phase space integration, but if we look closer we will see that this is not, in fact, the case. Discarding the tensor structure of the diagram and the constant factors we are left with

$$\int dy_{134} dy_{234} dy_{34} \Theta(y_{34}) \Theta(y_{34} + 1 - y_{134} - y_{234}) \Theta(y_{134}y_{234} - y_{34}) \\ \times \left(\frac{1}{y_{134} y_{34}} \frac{y_{34}}{y_{34} + \Delta_s} \frac{y_{34} + y_{134}}{y_{34} + y_{134} + \Delta_s} \right) \left(\frac{1}{y_{134} y_{34}} \frac{\Delta_s}{y_{34} + \Delta_s} \frac{\Delta_s}{y_{34} + y_{134} + \Delta_s} \right) \quad (5.35)$$

We can immediately see that, although one power of $1/y_{34}$ will be cancelled by the numerator of one of the hard vertices, we will still be left with one more such factor and this will result in a singularity when we perform the y_{34} integration.

Consequently there is a certain amount of “mixing” of the infrared singularities between the various amplitudes. In order to address the problems that this will cause when we allocate the various amplitudes to different asymptotic final states we will need to make a more appropriate choice of our splitting functions. In the example above, we see that in order to avoid unintended infrared singularities it would be sufficient for us to have one

more power of y_{34} in the numerator. Consequently, if we were to define new splitting functions f'_h and f'_s through the relation $f'_i(\{p\}; \Delta) = f_i^2(\{p\}; \Delta)$ we would once again achieve the proper distribution of infrared singularities in our example. This approach would not address the inclusion of unwanted finite parts however and, furthermore, we can see that if we were to calculate more and more complex examples we could always find diagrams where the power we chose to raise our original splitting functions to would not be large enough and we would be forced to increase it. This indicates that really we need to find a new form for these functions.

One possible form which avoids all these problems is

$$f_s(p_1, p_2, p_3; \Delta) = \Theta(\Delta - |p_1^2|) \Theta(\Delta - |p_2^2|) \Theta(\Delta - |p_3^2|) \quad (5.36)$$

$$f_h(p_1, p_2, p_3; \Delta) = 1 - \Theta(\Delta - |p_1^2|) \Theta(\Delta - |p_2^2|) \Theta(\Delta - |p_3^2|) \quad (5.37)$$

The obvious drawback to this formulation though is that it is not practical for performing analytic calculations. This does not present any problems for our ultimate aim as there should be no specific difficulty in implementing these in a numerical approach, but it does limit our ability to pursue further investigation analytically.

It is immediately clear that using this division of the Lagrangian highlights the relation between the approach based on our LSZ formula and a simple reallocation of the singularities which we discussed in Section 3.6.3. The new form of the splitting functions sets many of the fermion self energy diagrams with mixed hard and soft vertices to zero. For example, all the diagrams in Figure 5.5 are trivially zero as is any diagram where a hard vertex is connected only to soft vertices. Similarly, an external line radiating other

lines is zero if a soft vertex appears earlier in the chain than a hard vertex.

If we consider Figure 5.6, we have the relation

$$p_{1,m+1} \geq p_{1,m} \quad (5.38)$$

since all the p_i are on shell. If we now suppose that we have the first hard vertex at vertex m then we see that we have the vertex function

$$1 - \Theta(\Delta - |p_{1,m}^2|)\Theta(\Delta - |p_{m+1}^2|)\Theta(\Delta - |p_{1,m+1}^2|) \quad (5.39)$$

Now we have $p_{m+1}^2 = 0$ since it is an external momentum and $p_{1,m}^2 = 0$ since all the previous vertices are soft. This means that we must have $p_{1,m+1}^2 > \Delta$ otherwise the hard vertex function will set the diagram to zero. As a result, the presence of a soft vertex later on in the chain would involve the vertex function

$$\Theta(\Delta - |p_{1,r}^2|)\Theta(\Delta - |p_{r+1}^2|)\Theta(\Delta - |p_{1,r+1}^2|), \quad r > m \quad (5.40)$$

which must be zero due to the relation in Eq.(5.38). It is straightforward to apply this to the diagrams produced by the completely real cuts of a cut diagram where each side of the diagram will correspond to a tree-level Feynman diagram. For each separate Feynman diagram we move along each branch from the outside, noting the form of each vertex we pass. If the first vertex we come to is soft, we combine the two partons to form a parent parton. Similarly, for each additional soft vertex we reach we reduce the parton number by one each time as we continue to combine the original partons into one asymptotic parton. However, once we hit the first hard vertex this process immediately stops (and as we have seen earlier, the presence of any

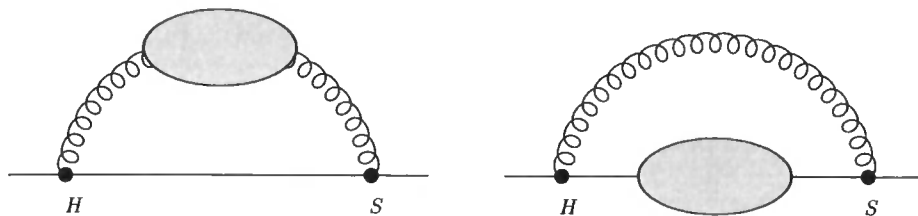


Figure 5.5: Some diagrams which will be zero under the new splitting functions.

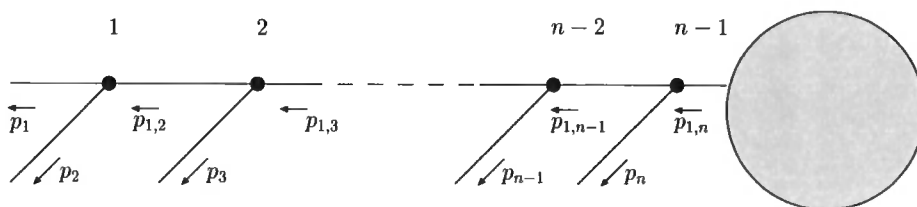


Figure 5.6: Showering from an external leg. Here we have used the notation $p_{a,b} = \sum_{i=a}^b p_i$.

soft vertices after this point will set the diagram to zero).

This collection of all the particles produced by soft vertices along an external branch of a diagram corresponds to a parton shower. The fact that such an object appears naturally in our approach suggests that it may be relatively straightforward to link up with other parton shower generators, possibly performing calculations at higher orders in the powers of α_s associated with the soft vertices than with the hard vertices.

We can, of course, apply this reasoning to as many different branches as exist in the diagram. The reasoning for diagrams with one or more loops is relatively straightforward when considering specific diagrams, but much harder to formulate in a general manner. We shall consider some specific examples in the rest of this chapter.

Consideration of all these developments clearly brings us much closer to the scenario described by the LSZ approach where diagrams are made up of hard

vertices while the propagators and the external states include a collection of soft interactions.

5.2.1 Categorising external states

In order to investigate the relation between conventional external states and asymptotic external states in more detail we shall now consider an example at higher order in perturbation theory. We choose $e^+e^- \rightarrow$ two jets again, but this time at NNLO. Also, in order to reduce the number of diagrams which we will have to consider, we will only consider the contribution proportional to N_F .

This time there will be three different classes of diagram which will eventually contribute to the result: the virtual correction diagrams at NNLO, the real emission diagrams at NLO and $e^+e^- \rightarrow$ four jets at LO as shown by the various cuts in Figure 5.7. Cuts a and d comprise the four jet LO diagrams, cuts b and e comprise the real emission LO and NLO diagrams and cuts c and f comprise the virtual correction LO and NNLO diagrams. We denote the cross sections by $\sigma_{x,ijkl}$ where i, j, k and l denote whether vertices 1, 2, 3 and 4 respectively are hard or soft and x will be replaced by VC , RE or $4J$ to refer to the cuts which result in two, three and four particle final states, with suffixes 1 and 2 denoting the diagram with cuts a, b and c or the diagram with cuts d, e and f respectively in the case where we need to differentiate between them.

We have not included every possible permutation of hard and soft vertices since here (and in the real emission and four jet examples as well) we can

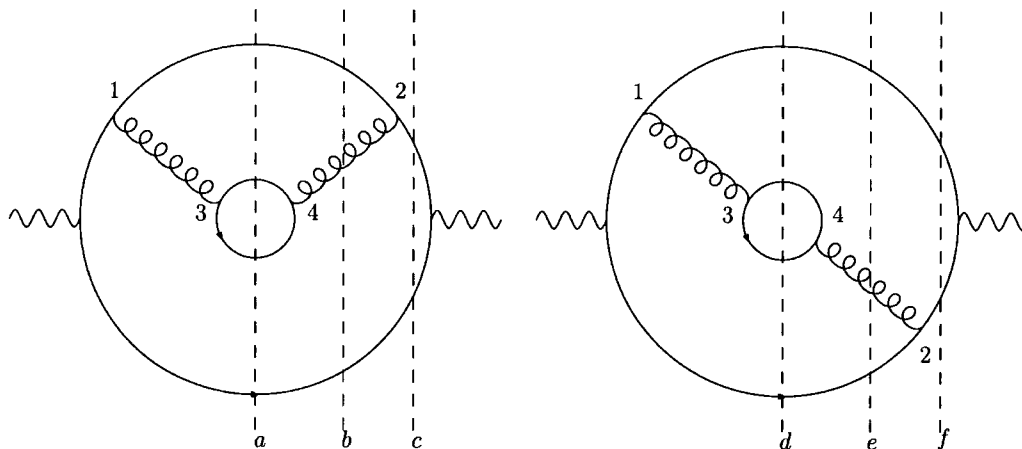


Figure 5.7: Cuts for the N_F contribution at NNLO

use the relations

$$\sigma_{VC,ijkl} = \sigma_{VC,jikl} \quad \text{and} \quad \sigma_{VC,ijkl} = \sigma_{VC,ijlk} \quad (5.41)$$

We must now consider which of these cross sections belong to which groups of asymptotic final states. Once again it is clear that all the virtual correction cross sections belong in the asymptotic two jet group along with the totally soft cross sections for the real emission and four jet cases. Similarly, we can place the totally hard real emission cross section and the totally hard four jet cross section in the asymptotic three and four jet groups respectively. We will now consider the remaining cross sections more carefully.

First we consider the real emission cross sections. Since they differ from the LO case purely in the addition of a fermion loop to the external gluon, and since this loop can do nothing to affect the momentum of the gluon we see that we can discount the nature of the vertices in the fermion loop and apply exactly the same analysis as we did to the leading order case (note that the only possibilities for the vertices in the fermion loop are both hard or both

soft as a mix of hard and soft would set the diagram to zero). Consequently we see that $\sigma_{RE,sskl}$ will belong in the asymptotic two jet group for any k, l . $\sigma_{RE2,hskl}$ will belong in the asymptotic two jet group as well while $\sigma_{RE1,hskl}$ will be zero.

In the four jet case, the situation is rather more complicated. We shall consider the possible halves of the cut diagrams separately at first, classifying them by their asymptotic final state form, and then match them up with other diagrams which fit into the same group. It is possible to have diagrams which, while they may not forbid certain groups of particles to become collinear, are not themselves singular in this limit; they will only give rise to singularities if multiplied by the complex conjugate of a diagram which is singular in this limit. The first half cut diagram may therefore find itself in different asymptotic final states depending on which other half cut diagram it is paired with; an example of this from earlier would be $\sigma_{RE1,hh}$ and $\sigma_{RE1,hs}$, two different possibilities for cut 2 in Figure 5.1. If we take the left hand side of the cut to contain a hard vertex in both cases we see that this vertex will forbid the gluon from becoming collinear to the quark from which it was emitted, but not to the other quark; it must therefore include parts of both $|\{q_{p_1}\bar{q}_{p_2}g_{p_3}\}\rangle$ and $|\{q_{p_1}\bar{q}_{p_2}\}\rangle$ states. In the case of $\sigma_{RE1,hh}$, the other half of the cut diagram prevents the remaining collinear possibility and so projects out the finite $|\{q_{p_1}\bar{q}_{p_2}g_{p_3}\}\rangle$ state. In the case of $\sigma_{RE1,hs}$, the other half of the cut diagram requires the gluon to be collinear and so it projects out the singular $|\{q_{p_1}\bar{q}_{p_2}\}\rangle$ state. As we have seen though, the total contribution to $|\{q_{p_1}\bar{q}_{p_2}\}\rangle$ is finite.

For our analysis here we shall consider the left hand side of cut a in Figure 5.7 and refer to the “original” quarks produced by the initial interaction as

having momenta p_1 and p_2 , while the quark pair produced at vertex 3 have momenta p_3 and p_4 . The cut diagrams with both vertices hard obviously adopt a four jet profile since p_3 and p_4 cannot go collinear.

If vertex 1 is soft and vertex 3 is hard our new splitting functions set the diagram to zero. In the case where we now have vertex 3 soft and vertex 1 hard we have a three jet profile since p_3 and p_4 can now go collinear or one of them can go soft. The hard vertex will prevent p_3 and p_4 both going collinear to p_1 or both going soft and so stops this becoming a two jet event. When both vertices are soft we will clearly have a two jet event, either with p_1, p_3 and p_4 all collinear or with some of them soft. A simple consideration of the restrictions imposed by various combinations of hard and soft vertices will show that $\sigma_{x1,hskl}$, $\sigma_{x,ijhs}$ and $\sigma_{4J1,hj sl}$ will all be set to zero where the designation x can be any one of VC , RE or $4J$.

We can now allocate our cross sections to their separate groups. In the two jet group we have $\sigma_{VC,ijkl}$, $\sigma_{RE,sjkl}$ and $\sigma_{4J,sj sl}$ for any (i, j, k, l) subject to the previously mentioned constraints which would set the diagrams to zero and allowing the possible permutations given in Eq.(5.41). In the three jet group we have $\sigma_{RE,hhhh}$, $\sigma_{RE,hhss}$ and $\sigma_{4J,hhss}$. In the four jet group we have $\sigma_{4J,hhhh}$.

We can now see how our allocation of the various amplitudes to the different asymptotic final state groups will result in infrared finite amplitudes. We know that the sum over all cuts of a cut diagram which corresponds to an infrared safe observable will be infrared finite [44] and if we look at the amplitudes included in each group we see that we can use this fact to investigate the divergences separately within the different groups.

It is not necessary to consider the amplitudes with hard vertices only since

these will be separately finite and therefore the fact that different cuts place them in different groups does not result in any divergences. Since the only diagram which remains in the four jet group is one with hard vertices only, this means that we only need to consider the two and three jet groups.

In the three jet group (other than diagrams with hard vertices only), we only have $\sigma_{RE,hhs}$ and $\sigma_{4J,hhs}$. At first glance this appears to be a problem since we are missing the virtual correction cuts of this amplitude. When we consider this more carefully, however, we see that the cut diagrams included in the two jet section all include the fermion loop contribution to the gluon self energy with soft vertices (as shown in Figure 4.2). When we calculated this with the old splitting functions we discovered that it was finite provided the gluon was off shell. We now note that the hard vertices which make up the other interactions in each of these diagrams will prevent the gluon momenta from going on shell; this tells us that each of these diagrams must be separately finite as we can consider them to be composed of hard vertices only and propagators that are only divergent when they're on shell. This realisation that all the relevant cut diagrams which are excluded from the three jet group are separately finite means that the sum over the cut diagrams in the three jet group must also be finite. We could also consider this from the perspective that this configuration of the soft vertices makes up a divergent subdiagram and the cuts which are included in the group make up the complete set of cuts over this subdiagram; this also implies that the family of cuts which exist in this group should be infrared finite.

This leaves us with only the diagrams which are left in the two jet group. Since this is an infrared safe observable and the four jet and three jet contributions are both finite it follows that the two jet contribution must be finite

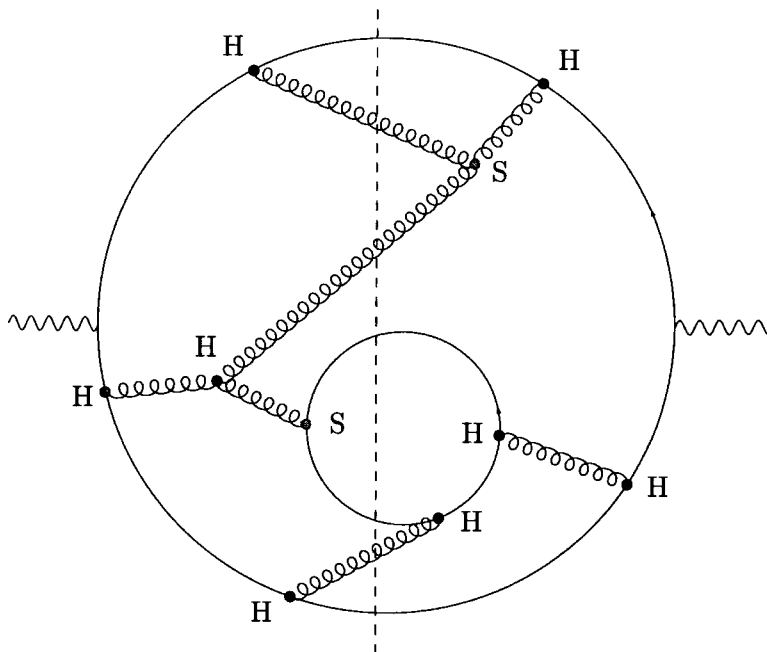


Figure 5.8: Cut diagram with apparently mismatched external states.

too. Thus we see how our division of the amplitudes will result in infrared finite amplitudes.

As our last example of classifying the external states we will look at one very specific example where the two halves of the cut diagram appear to be completely mismatched in order to demonstrate how such apparent contradictions will be reconciled. We choose as our example the diagram shown in Figure 5.8 where the black dots correspond to hard vertices and the grey dots to soft vertices.

If we now consider the naive external states suggested by both sides of the cut, we arrive at the forms shown in Figure 5.9 where we have combined external partons produced by soft vertices into the asymptotic partons present after the last hard vertex in the chain.

We can immediately see that one half appears to have an external state

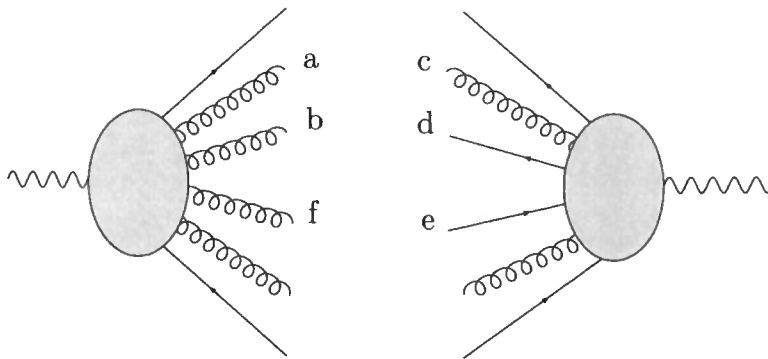


Figure 5.9: The naive external states expected from the cut diagram in Figure 5.8.

$|\{q\bar{q}gggg\}\rangle$, the other appears to have an external state $|\{q\bar{q}q\bar{q}gg\}\rangle$. In order to resolve this conflict we must note, as we did earlier, that the hard vertices only prevent partons from becoming collinear to other partons in such a way that would result in a singularity. This leaves the possibility for them to become collinear with other partons where this situation would not arise.

If we now look closer at the left hand side of the cut we see that the gluons labelled a and b are not connected by a hard vertex and so are not prevented from becoming collinear. Consequently, the soft vertex on the right hand side of the cut will project out this area of the phase space and they will match up with gluon c . Similarly, the quarks labelled d and e on the right hand side of the cut will have the section of the phase space where they are collinear projected out by the soft vertex on the left hand side of the cut and match up with gluon f . Now the external states on both sides of the cut do match up and we can see that the true external state to which this diagram belongs is in fact $|\{q\bar{q}gggg\}\rangle$.

5.2.2 Towards a numerical approach

Now that we have a reasonable understanding of how the asymptotic external states work in practice, the next goal is to implement a numerical approach to our calculations. As we have seen, although our approach does produce separately infrared finite amplitudes, the different parts which make up these amplitudes still contain infrared divergences if calculated separately. Some of the amplitudes will also contain ultraviolet divergences. In order to pursue a numerical approach, both of these sources will have to be removed. This is relatively straightforward in the case of the ultraviolet divergences where we shall use an approach along the lines of the one outlined in [11]. In the case of the infrared singularities however, some of the divergences appear in the amplitude through loop integrals while other divergences appear in the phase space integrals. Consequently we need to find a method of aligning the parameterisation of the loop and phase space integrations so that we can write the sum of all the contributions to the amplitude as one finite integral. We will now give a brief outline of how such a scheme might proceed.

We imagine starting from a completely real cross section (e.g. tree level diagrams on both sides of the cut) with n external particles where we will perform our numerical integration by repeatedly generating the momenta of the external particles. If we now generate a set of on-shell momenta, p_i where i runs from 1 to n , for these particles we can infer the momenta of all the internal lines of the diagram. This allows us to categorise each vertex as either hard or soft. In the case where we have generated a completely hard diagram there will be no divergences and we can simply store the result. If we now imagine that one vertex at the end of a branch is soft (a single soft vertex further along a branch is kinematically impossible) this will clearly give rise

to an infrared singularity and so we will have to consider the relevant extra cut diagrams which will make this finite. From our previous consideration of the external asymptotic states we know that these extra diagrams will have a soft loop in place of the soft vertex with the cut redrawn appropriately either side of it. The precise details of how we determine these extra contributions and the cross section to which they are assigned, particularly for cases with a more complex arrangement of soft vertices, are yet to be addressed.

In general we will end up with an expression of the form

$$\int \{d^3 p_i\} [I_R + I_V + I_{UV}] \quad (5.42)$$

where I_R represents the real contribution, I_V represents the virtual contribution and I_{UV} is the ultraviolet counterterm. In the case mentioned above where all the vertices were hard the only nonzero term would be I_R . In other cases we will have to deal with the fact that the virtual contribution contains a loop momentum which is not constrained to be on-shell; consequently we will require a method of performing the integral over the energy part of this momentum, leaving all the terms in the same form. The implementation of a suitable method for this along with the determination of which virtual contributions to include should then allow the numerical calculation of cross sections.

Chapter 6

Conclusions and outlook

In this thesis we have discussed an approach to producing covariant scattering amplitudes for non-abelian gauge theories which are infrared finite. In Chapter 1 we provided a motivation for investigating infrared finite amplitudes and reviewed the previous research in this area. We saw that a general method for cancelling infrared singularities at NLO existed, but that the more complex form of singularities present in NNLO calculations meant that no general method was available; this indicated that a method for working with infrared finite amplitudes would clearly be of benefit. We saw that two approaches to defining infrared finite amplitudes had been investigated, but that in the case of non-abelian theories no satisfactory methods for performing actual calculations existed.

In Chapter 2 we started our investigation of infrared finite amplitudes by considering the traditional calculational methods in order that we might later modify them in order to avoid the incorrect assumptions described in Chapter 1. We presented the conventional theoretical approach to calculating amplitudes and cross sections, focusing on areas which we would later alter,

Chapter 6: Conclusions and outlook

and demonstrated the application of the traditional method of cancelling infrared divergences through a simple example.

In Chapter 3 we considered how to adapt the conventional approach in order to produce infrared finite amplitudes. We introduced the asymptotic interaction picture as the basis for our calculations. This involved splitting the Lagrangian up into asymptotic and hard parts, subsuming the soft and collinear areas of the interaction Lagrangian into the definition of our asymptotic Lagrangian. This asymptotic Lagrangian was then used to construct our external states, leaving the hard part of the Lagrangian to determine the interactions of the theory. We then saw how this gives rise to an altered LSZ reduction formula which has many similarities to the usual formula, but with the crucial difference that it is now given in terms of asymptotic external states. We saw that the inclusion of an interaction term in our definition of the external states meant that we were unable to solve for them exactly, leading to problems in incorporating this into our theory. Consequently, we looked at the problems caused by the asymptotic external states in more detail and saw that it might be helpful to adopt a more pragmatic view of our approach, considering it as a method of dividing up the traditional calculation differently such that infrared singularities could be cancelled at an amplitude level.

In Chapter 4 we looked more closely at how we split the interaction Lagrangian into hard and soft parts. Since we were unable to determine the exact form of the asymptotic Lagrangian we were forced to introduce the parameter Δ to describe how we chose to make the split. Once we had chosen a form for this split we demonstrated how this would produce infrared finite amplitudes with all hard vertices. In order to show this we had to look at

Chapter 6: Conclusions and outlook

the form of the propagators in more detail, and as a result we saw how the gluon would acquire a dynamically generated mass.

In Chapter 5 we looked at a couple of example calculations in order to illustrate the method and to gain more insight into the categorisation of the asymptotic external states. We saw that our method did indeed produce the correct results for $e^+e^- \rightarrow 2$ jets at NLO and investigated the effect of our choice of the resolution parameter, Δ , on the predictions for different observables. We then saw how our choice of a splitting function which would facilitate analytic calculation would be unsuitable for more complex examples. We defined another possible form of splitting function which would be more suitable for application to numerical calculations and demonstrated how this would be applied to a more complicated example and how this illustrates the connection between the two approaches.

The main aim of future work will be the generalisation of our method in such a way that it can be applied at higher orders. In practice this means extending our understanding of the approach in two separate areas. Firstly, more work is required on understanding the modified LSZ formula and in particular on a more detailed understanding of the asymptotic states. Any complete understanding of the asymptotic states, while highly desirable, seems unlikely. However, a deeper investigation into how the approach derived from the modified LSZ formula and a simple alternative division of the conventional amplitudes relate to each other and how the conventional external states fit into the definition of the asymptotic picture would be an important next step. Although we have seen that it is possible to ascertain which conventional final states belong in which asymptotic final states through careful inspection of the amplitudes, we have no systematic process for categorising

Chapter 6: Conclusions and outlook

them automatically yet; from the investigations into the subject which we have performed so far though it appears probable that we should be able to formulate the ideas which we have developed in such a manner without too much trouble. It would be most desirable to devise a general method for achieving this. This would allow an automated process for grouping the various components of the calculation into their correct finite groups.

Secondly, once we have a more thorough understanding of the method we would like to take the next step to making full use of the infrared finite nature of the calculations. This would involve constructing methods for calculating the various finite groups of amplitudes numerically. In order to implement this we will need to include a system for subtracting the ultraviolet divergences as in [11] although this should not present too many problems. Once such a system is in place we would, of course, need to compare the results obtained against various known calculations in order to confirm that the method does indeed work correctly. As it stands at the moment there are certainly challenges to be overcome before this method could be considered as a possible angle of attack for the infrared problem but the prospects certainly appear to be very promising.

Appendix A

The full result for the vertex correction calculation

In this appendix we present the full result of the vertex correction calculation performed in Section 5. Before performing the expansion in Δ the results are

$$\begin{aligned}
 \sigma_{RE1,hh} = \sigma_0 C_F c_\epsilon \frac{\alpha_s}{24\pi} & \left(-3 \ln(-\Delta_s - 1) \Delta_s (\Delta_s + 1)^2 + 24 \ln(\Delta_s) \right. \\
 & - 24 \ln(\Delta_s + 1) - 9\Delta_s (2\Delta_s + 1) - 6\text{Li}_2 \left(\frac{\Delta_s}{2\Delta_s + 1} \right) (2\Delta_s + 1) (\Delta_s^2 - 2) \\
 + 6\text{Li}_2 \left(\frac{\Delta_s + 1}{2\Delta_s + 1} \right) & (2\Delta_s + 1) (\Delta_s^2 - 2) + 3 \left(-2(2\Delta_s + 1) (\Delta_s^2 - 2) \ln^2(\Delta_s) \right. \\
 + \left. \left(2 \ln(\Delta_s + 1) (2\Delta_s + 1) (\Delta_s^2 - 2) - 2 \ln \left(\frac{\Delta_s + 1}{2\Delta_s + 1} \right) (2\Delta_s + 1) (\Delta_s^2 - 2) \right. \right. \\
 & \left. \left. + \Delta_s (5 - \Delta_s (7\Delta_s + 10)) \right) \ln(\Delta_s) + \ln(-\Delta_s) \Delta_s (\Delta_s + 1)^2 \right. \\
 & \left. + \ln(\Delta_s + 1) \left(2 \ln \left(\frac{\Delta_s}{2\Delta_s + 1} \right) (2\Delta_s + 1) (\Delta_s^2 - 2) \right. \right. \\
 & \left. \left. + \Delta_s (\Delta_s (7\Delta_s + 10) - 5) \right) \right) + 23 \Big) \quad (\text{A.1})
 \end{aligned}$$

$$\sigma_{RE2,hh} = \sigma_0 C_F c_\epsilon \frac{\alpha_s}{12\pi} \left(6\Delta_s^2 - 3\Delta_s - \ln(-\Delta_s) (-6\Delta_s^3 + 9\Delta_s + 3) \right. \\ \left. - \ln(-\Delta_s - 1) (6\Delta_s^3 - 9\Delta_s - 3) - 7 \right) \quad (\text{A.2})$$

$$\mathcal{A}_{VC1,hh}^{(2)} = \mathcal{A}^{(0)} C_F c_\epsilon \left(\frac{-s}{\mu^2} \right)^{-\epsilon} \left(\frac{\alpha_s \xi}{4\pi\epsilon} + \frac{\alpha_s}{24\pi} \left(-12(\Delta_s + 1)^2 \ln^2 \left(\frac{1 + 4\Delta_s + \sqrt{8\Delta_s + 1}}{4\Delta_s} \right) \right. \right. \\ \left. \left. - 6 \frac{-8\Delta_s^2 + 18\Delta_s + (6\Delta_s^2 - 11\Delta_s + 5) \ln(-s) - 8}{\Delta_s - 1} \right. \right. \\ \left. \left. + 12(\xi - 2 \ln(-s) - 2 \ln(\Delta_s) + 2 \ln(2) + 1) - \frac{24}{\Delta_s - 1} (-2\Delta_s^2 + 3\Delta_s) \right. \right. \\ \left. \left. - (2\Delta_s^2 - 3\Delta_s + 1)(\ln(-s) + \Delta_s \ln \left(\frac{\Delta_s + 1}{\Delta_s} \right) + \ln(\Delta_s + 1) - \ln(2) - 2) - 2 \right) \right. \\ \left. \left. + \frac{6}{\Delta_s - 1} (-2\Delta_s + (\Delta_s - 1)(\xi + 2\Delta_s - 3)(-\ln(-s) - \ln(\Delta_s)) \right. \right. \\ \left. \left. + \sqrt{8\Delta_s + 1} \left(\ln(\Delta_s) - 2 \ln(\sqrt{8\Delta_s + 1} + 1) + 3 \ln(2) \right) + \ln(2) \right) \right) \\ \left. \left. - 12(\Delta_s - 1)(3\Delta_s - 1) \left(\ln(\Delta_s) \ln \left(\frac{\Delta_s}{2(\Delta_s - 1)} \right) + \ln \left(\frac{\Delta_s + 1}{\Delta_s} \right) \ln \left(\frac{\Delta_s}{\Delta_s - 1} \right) \right) \right. \right. \\ \left. \left. + \ln(2) \ln(\Delta_s + 1) - Li_2 \left(\frac{1}{1 - \Delta_s} \right) + Li_2 \left(\frac{1 + \Delta_s}{1 - \Delta_s} \right) + \frac{\pi^2}{12} \right) \right) \\ \left. \left. + 6(\Delta_s - 1)(3\Delta_s - 1) \left(-\ln^2 \left(\frac{\Delta_s}{\Delta_s - 1} \right) - 2 \ln \left(\frac{\Delta_s + 1}{\Delta_s} \right) \ln \left(\frac{\Delta_s}{\Delta_s - 1} \right) \right) \right. \right. \\ \left. \left. + \ln^2 \left(\frac{4\Delta_s}{4\Delta_s - 1 - \sqrt{8\Delta_s + 1}} \right) + \ln^2 \left(\frac{4\Delta_s}{4\Delta_s - 1 + \sqrt{8\Delta_s + 1}} \right) + 2 \ln(2) \ln \left(\frac{8\Delta_s}{\Delta_s + 1} \right) \right. \right. \\ \left. \left. - 2 \ln(2) \ln \left(\frac{4\Delta_s + 1 - \sqrt{8\Delta_s + 1}}{\Delta_s} \right) \right) \right) \\ \left. \left. + 2 \ln \left(\frac{4\Delta_s + 1 - \sqrt{8\Delta_s + 1}}{4\Delta_s} \right) \ln \left(\frac{8\Delta_s}{4\Delta_s - 1 + \sqrt{8\Delta_s + 1}} \right) \right) \right. \\ \left. \left. + 2 \ln \left(\frac{4\Delta_s + 1 + \sqrt{8\Delta_s + 1}}{4\Delta_s} \right) \ln \left(\frac{4\Delta_s}{4\Delta_s - 1 - \sqrt{8\Delta_s + 1}} \right) \right) \right) \\ \left. \left. - 2 Li_2 \left(\frac{1 + \Delta_s}{1 - \Delta_s} \right) + 2 Li_2 \left(\frac{-4\Delta_s - 1 + \sqrt{8\Delta_s + 1}}{4\Delta_s - 1 + \sqrt{8\Delta_s + 1}} \right) + \right. \right. \\ \left. \left. 2 Li_2 \left(\frac{4\Delta_s + 1 + \sqrt{8\Delta_s + 1}}{-4\Delta_s + 1 + \sqrt{8\Delta_s + 1}} \right) - 2 \ln^2(2) + \frac{\pi^2}{6} \right) \right) \quad (\text{A.3})$$

Chapter A: The full result for the vertex correction calculation

$$\mathcal{A}_{VC2,hh}^{(2)} = \mathcal{A}^{(0)} C_F c_\epsilon \left(-\frac{\xi \alpha_s}{4\pi\epsilon} + \frac{\alpha_s}{16\pi} (4 \ln(-s)\xi + 4 \ln(\Delta_s)\xi - 4 \ln(2)\xi + \xi + 3) \right) \quad (\text{A.4})$$

$$\begin{aligned} \sigma_{RE1,hs} = & \sigma_0 C_F c_\epsilon \left(\frac{s}{\mu^2} \right)^{-\epsilon} \left(\frac{\alpha_s}{2\pi\epsilon} \left(1 + (\Delta_s + 1) \ln \left(\frac{\Delta_s}{\Delta_s + 1} \right) \right) \right. \\ & + \frac{\alpha_s}{4\pi} \left(\ln \left(\frac{\Delta_s + 1}{\Delta_s} \right) \left(\ln \left(\frac{\Delta_s + 1}{\Delta_s} \right) + 6 \ln \left(\frac{1}{\Delta_s + 1} \right) \right) (\Delta_s + 1) \right. \\ & \quad - 6 \text{Li}_2 \left(\frac{\Delta_s}{\Delta_s + 1} \right) (\Delta_s + 1) + \pi^2 (\Delta_s + 1) \\ & \quad \left. \left. + 2 \ln(s) \left(1 - \ln \left(\frac{\Delta_s + 1}{\Delta_s} \right) (\Delta_s + 1) \right) - 6 \right) \right. \\ & + \frac{\alpha_s}{16\pi} \left(4 (2\Delta_s + 1) (\Delta_s^2 - 2) \ln^2(\Delta_s) + 2 \left((5\Delta_s - 4) (\Delta_s + 1) \right)^2 \right. \\ & - 2 \ln(\Delta_s + 1) (2\Delta_s + 1) (\Delta_s^2 - 2) + 2 \ln \left(\frac{\Delta_s + 1}{2\Delta_s + 1} \right) (2\Delta_s + 1) (\Delta_s^2 - 2) \ln(\Delta_s) \\ & \quad + \Delta_s (10\Delta_s + 3) + 4 \text{Li}_2 \left(\frac{\Delta_s}{2\Delta_s + 1} \right) (2\Delta_s + 1) (\Delta_s^2 - 2) \\ & - 4 \text{Li}_2 \left(\frac{\Delta_s + 1}{2\Delta_s + 1} \right) (2\Delta_s + 1) (\Delta_s^2 - 2) + 2 \ln(\Delta_s + 1) \left((4 - 5\Delta_s) (\Delta_s + 1) \right)^2 \\ & \quad \left. \left. - 2 \ln \left(\frac{\Delta_s}{2\Delta_s + 1} \right) (2\Delta_s + 1) (\Delta_s^2 - 2) \right) - 8 \right) \right) \quad (\text{A.5}) \end{aligned}$$

$$\sigma_{RE2,hs} = \sigma_0 C_F c_\epsilon \frac{\alpha_s}{16\pi} \left(-6\Delta_s^2 + 6(\Delta_s - 1)(\Delta_s + 1) \ln \left(\frac{\Delta_s + 1}{\Delta_s} \right) \Delta_s + 3\Delta_s + 4 \right) \quad (\text{A.6})$$

Chapter A: The full result for the vertex correction calculation

$$\begin{aligned}
\mathcal{A}_{VC1,hs}^{(2)} = & \mathcal{A}^{(0)} C_F c_\epsilon \left(\frac{-s}{\mu^2} \right)^{-\epsilon} \left(-\frac{\alpha_s}{2\pi\epsilon} \left(1 + (\Delta_s + 1) \ln \left(\frac{\Delta_s}{\Delta_s + 1} \right) \right) \right. \\
& + \frac{\alpha_s}{24\pi} \left(6 \ln^2(-s) - 6(\xi - 2 \ln(\Delta_s) + 2 \ln(2) - 3) \ln(-s) + 6 \ln^2 \left(\frac{\Delta_s}{2} \right) \right. \\
& \quad \left. + 12(\Delta_s + 1)^2 \ln^2 \left(\frac{4\Delta_s + 1 + \sqrt{8\Delta_s + 1}}{4\Delta_s} \right) - 6\xi \right. \\
& + 12 \frac{(3 - 2\Delta_s)(\Delta_s + (2\Delta_s^2 - 3\Delta_s + 1) \ln(-s))}{\Delta_s - 1} - 12 \ln \left(\frac{\Delta_s}{2} \right) - 6\xi \ln(\Delta_s) + 30 \ln(\Delta_s) \\
& \quad - \frac{6}{\Delta_s - 1} (-2\Delta_s + (\Delta_s - 1)(\xi + 2\Delta_s - 3)(-\ln(-s) - \ln(\Delta_s)) \\
& \quad \left. + \sqrt{8\Delta_s + 1}(\ln(\Delta_s) - 2 \ln(\sqrt{8\Delta_s + 1} + 1) + 3 \ln(2)) + \ln(2)) \right) \\
& - \frac{24}{\Delta_s - 1} (2\Delta_s^2 - 3\Delta_s + 2) + 36\Delta_s(\ln(-s/2) + \Delta_s \ln \left(\frac{\Delta_s + 1}{\Delta_s} \right) + \ln(\Delta_s + 1) - 2) \\
& \quad - (-6 \ln^2(-s) + 12(\Delta_s \ln(\Delta_s) + \ln(2) + 2) \ln(-s) + \pi^2(2\Delta_s + 1) \\
& + 6\Delta_s(\ln \left(\frac{\Delta_s}{4} \right) - 4) \ln(\Delta_s) + 12(\Delta_s + 1)(-\ln(-s) - \ln \left(\frac{\Delta_s + 1}{\Delta_s} \right) + \ln(2) + 2) \ln(\Delta_s + 1) \\
& + 12(\Delta_s + 1) Li_2(-\Delta_s) - 6(8 + \ln^2(2) + 4 \ln(2))) + 24(\Delta_s - 1)\Delta_s(\ln(\Delta_s) \ln \left(\frac{\Delta_s}{2(\Delta_s - 1)} \right) \\
& + \ln \left(\frac{\Delta_s + 1}{\Delta_s} \right) \ln \left(\frac{\Delta_s}{\Delta_s - 1} \right) + \ln(2) \ln(\Delta_s + 1) - Li_2 \left(\frac{1}{1 - \Delta_s} \right) + Li_2 \left(\frac{1 + \Delta_s}{1 - \Delta_s} \right) + \frac{\pi^2}{12} \\
& \quad - 6(\Delta_s - 1)(3\Delta_s + 1)(-\ln^2 \left(\frac{\Delta_s}{\Delta_s - 1} \right) - 2 \ln \left(\frac{\Delta_s + 1}{\Delta_s} \right) \ln \left(\frac{\Delta_s}{\Delta_s - 1} \right) \\
& + \ln^2 \left(\frac{4\Delta_s}{4\Delta_s - 1 - \sqrt{8\Delta_s + 1}} \right) + \ln^2 \left(\frac{4\Delta_s}{4\Delta_s - 1 + \sqrt{8\Delta_s + 1}} \right) + 2 \ln(2) \ln \left(\frac{8\Delta_s}{\Delta_s + 1} \right) \\
& \quad - 2 \ln(2) \ln \left(\frac{4\Delta_s + 1 - \sqrt{8\Delta_s + 1}}{\Delta_s} \right) \\
& \quad + 2 \ln \left(\frac{4\Delta_s + 1 - \sqrt{8\Delta_s + 1}}{4\Delta_s} \right) \ln \left(\frac{8\Delta_s}{4\Delta_s - 1 + \sqrt{8\Delta_s + 1}} \right) \\
& \quad + 2 \ln \left(\frac{4\Delta_s + 1 + \sqrt{8\Delta_s + 1}}{4\Delta_s} \right) \ln \left(\frac{4\Delta_s}{4\Delta_s - 1 - \sqrt{8\Delta_s + 1}} \right) \\
& \quad - 2 Li_2 \left(\frac{1 + \Delta_s}{1 - \Delta_s} \right) + 2 Li_2 \left(\frac{-4\Delta_s - 1 + \sqrt{8\Delta_s + 1}}{4\Delta_s - 1 + \sqrt{8\Delta_s + 1}} \right) + \\
& \left. 2 Li_2 \left(\frac{4\Delta_s + 1 + \sqrt{8\Delta_s + 1}}{-4\Delta_s + 1 + \sqrt{8\Delta_s + 1}} \right) - 2 \ln^2(2) + \frac{\pi^2}{6} + 6\xi \ln(2) - 30 \ln(2) + \pi^2 - 6 \right) \Bigg)
\end{aligned}$$

(A.7)

Chapter A: The full result for the vertex correction calculation

$$\mathcal{A}_{VC2,hs}^{(2)} = -\mathcal{A}^{(0)} C_F c_\epsilon \frac{\xi \alpha_s}{4\pi} \quad (\text{A.8})$$

$$\begin{aligned} \sigma_{RE1,ss} = & \sigma_0 C_F c_\epsilon \left(\frac{s}{\mu^2} \right)^{-\epsilon} \left(\frac{\alpha_s}{2\pi\epsilon^2} - \frac{\alpha_s}{2\pi\epsilon} \left(\ln(s) - 2(\Delta_s + 1) \ln \left(\frac{\Delta_s + 1}{\Delta_s} \right) \right) \right) \\ & + \frac{\alpha_s}{24\pi} \left(-72 \text{Li}_2 \left(\frac{\Delta_s}{\Delta_s + 1} \right) (\Delta_s + 1) + \pi^2 (12\Delta_s + 5) + 6 \left(\ln^2(s) \right. \right. \\ & - 4 \ln \left(1 + \frac{1}{\Delta_s} \right) (\Delta_s + 1) \ln(s) + 2 \ln \left(1 + \frac{1}{\Delta_s} \right) \left(\ln \left(1 + \frac{1}{\Delta_s} \right) \right. \\ & \left. \left. + 6 \ln \left(\frac{1}{\Delta_s + 1} \right) \right) (\Delta_s + 1) \right) - 6 \left((2\Delta_s + 1) (\Delta_s^2 - 2) \ln^2(\Delta_s) \right. \\ & \left. + \left(2(\Delta_s + 1) \Delta_s^2 - \ln(\Delta_s + 1) (2\Delta_s + 1) (\Delta_s^2 - 2) \right. \right. \\ & \left. \left. + \ln \left(\frac{\Delta_s + 1}{2\Delta_s + 1} \right) (2\Delta_s + 1) (\Delta_s^2 - 2) \right) \ln(\Delta_s) + 2\Delta_s^2 \right. \\ & \left. + \text{Li}_2 \left(\frac{\Delta_s}{2\Delta_s + 1} \right) (2\Delta_s + 1) (\Delta_s^2 - 2) - \text{Li}_2 \left(\frac{\Delta_s + 1}{2\Delta_s + 1} \right) (2\Delta_s + 1) (\Delta_s^2 - 2) \right. \\ & \left. \left. + \ln(\Delta_s + 1) \left(-2(\Delta_s + 1) \Delta_s^2 - \ln \left(\frac{\Delta_s}{2\Delta_s + 1} \right) (2\Delta_s + 1) (\Delta_s^2 - 2) \right) \right) \right) \right) \quad (\text{A.9}) \end{aligned}$$

$$\begin{aligned} \sigma_{RE2,ss} = & \sigma_0 C_F c_\epsilon \left(\frac{s}{\mu^2} \right)^{-\epsilon} \left(-\frac{\alpha_s}{4\pi\epsilon} + \frac{\alpha_s}{8\pi} \left(2 \ln(s) - 5 + 2\Delta_s^2 - \Delta_s \right. \right. \\ & \left. \left. - 2 \ln \left(\frac{\Delta_s + 1}{\Delta_s} \right) (\Delta_s^3 + 1) + 1 \right) \right) \quad (\text{A.10}) \end{aligned}$$

Chapter A: The full result for the vertex correction calculation

$$\begin{aligned}
\mathcal{A}_{VC1,ss}^{(2)} = & \mathcal{A}^{(0)} C_F c_\epsilon \left(\frac{-s}{\mu^2} \right)^{-\epsilon} \left(-\frac{\alpha_s}{2\pi\epsilon^2} - \frac{\alpha_s}{4\pi\epsilon} \left(\xi - 2\ln(-s) + 4(\Delta_s + 1) \ln \left(\frac{\Delta_s + 1}{\Delta_s} \right) \right. \right. \\
& - 1) - \frac{\alpha_s}{24\pi} \left(-12 \ln^2 \left(\frac{\sqrt{8\Delta_s + 1} + 1}{4\Delta_s} + 1 \right) (\Delta_s + 1)^2 - \left(12 \ln \left(\frac{\Delta_s}{2(\Delta_s - 1)} \right) \ln(\Delta_s) \right. \right. \\
& + 12 \ln \left(\frac{\Delta_s + 1}{\Delta_s} \right) \ln \left(\frac{\Delta_s}{\Delta_s - 1} \right) + 12 \ln(2) \ln(\Delta_s + 1) - 12 \text{Li}_2 \left(\frac{1}{1 - \Delta_s} \right) \\
& + 12 \text{Li}_2 \left(\frac{\Delta_s + 1}{1 - \Delta_s} \right) + \pi^2) (\Delta_s - 1) (\Delta_s + 1) - 2 \left(6 \ln^2(-s) - 6(\xi - 2 \ln(\Delta_s) \right. \\
& + \ln(4) - 1) \ln(-s) + 6 \ln^2 \left(\frac{\Delta_s}{2} \right) - 12 \ln \left(\frac{\Delta_s}{2} \right) - 6\xi \ln(\Delta_s) + 18 \ln(\Delta_s) \\
& + \xi \ln(64) - 18 \ln(2) + \pi^2) + \left(-6 \ln^2 \left(\frac{\Delta_s}{\Delta_s - 1} \right) - 12 \ln \left(1 + \frac{1}{\Delta_s} \right) \ln \left(\frac{\Delta_s}{\Delta_s - 1} \right) \right. \\
& + 6 \ln^2 \left(\frac{4\Delta_s}{4\Delta_s - \sqrt{8\Delta_s + 1} - 1} \right) + 6 \ln^2 \left(\frac{4\Delta_s}{4\Delta_s + \sqrt{8\Delta_s + 1} - 1} \right) \\
& + 12 \ln(2) \ln(8\Delta_s) - 12 \ln(2) \ln(\Delta_s + 1) - 12 \ln(2) \ln \left(\frac{4\Delta_s - \sqrt{8\Delta_s + 1} + 1}{\Delta_s} \right) \\
& + 12 \ln \left(\frac{4\Delta_s - \sqrt{8\Delta_s + 1} + 1}{4\Delta_s} \right) \ln \left(\frac{8\Delta_s}{4\Delta_s + \sqrt{8\Delta_s + 1} - 1} \right) \\
& + 12 \ln \left(\frac{4\Delta_s}{4\Delta_s - \sqrt{8\Delta_s + 1} - 1} \right) \ln \left(\frac{4\Delta_s + \sqrt{8\Delta_s + 1} + 1}{4\Delta_s} \right) - 12 \text{Li}_2 \left(\frac{\Delta_s + 1}{1 - \Delta_s} \right) \\
& + 12 \text{Li}_2 \left(\frac{-4\Delta_s + \sqrt{8\Delta_s + 1} - 1}{4\Delta_s + \sqrt{8\Delta_s + 1} - 1} \right) + 12 \text{Li}_2 \left(\frac{4\Delta_s + \sqrt{8\Delta_s + 1} + 1}{-4\Delta_s + \sqrt{8\Delta_s + 1} + 1} \right) - 12 \ln^2(2) \\
& + \pi^2) (\Delta_s - 1) (3\Delta_s + 1) + \frac{6}{\Delta_s - 1} \left(-2\Delta_s - 2(\Delta_s - 1)(\xi + 2\Delta_s - 3) \right. \\
& + (\Delta_s - 1)(\xi + 2\Delta_s - 3)(-\ln(-s) - \ln(\Delta_s) + (\ln(\Delta_s) \\
& - 2 \ln(\sqrt{8\Delta_s + 1} + 1)) \sqrt{8\Delta_s + 1} + \ln(8) \sqrt{8\Delta_s + 1} + \ln(2) + 2) \\
& - \frac{2}{\Delta_s - 1} \left(12(-\ln(-s) - \ln(\Delta_s + 1) + \ln(\Delta_s) \Delta_s - \ln(\Delta_s + 1) \Delta_s + \ln(2) \right. \\
& + 2) (\Delta_s^2 - 1) - 12(2\Delta_s^2 - 3\Delta_s + 2) - (1 - \Delta_s) \left(-6 \ln^2(-s) + 12 \left(\ln(\Delta_s) \Delta_s \right. \right. \\
& + \ln(2) + 2) \ln(-s) + 6 \left(\ln \left(\frac{\Delta_s}{4} \right) - 4 \right) \ln(\Delta_s) \Delta_s + 12(-\ln(-s) - \ln \left(1 + \frac{1}{\Delta_s} \right) \\
& + \ln(2) + 2) \ln(\Delta_s + 1) (\Delta_s + 1) + 12 \text{Li}_2(-\Delta_s) (\Delta_s + 1) + \pi^2 (2\Delta_s + 1) - 6(8 + \ln^2(2) \\
& \left. \left. \left. + \ln(16)) \right) \right) - 6 \ln^2(-s) - 12(\Delta_s - 1) \ln(-s) + \pi^2 - 12 \frac{\Delta_s}{\Delta_s - 1} \right) \right) \quad (\text{A.11})
\end{aligned}$$

Chapter A: The full result for the vertex correction calculation

$$\mathcal{A}_{VC2,ss}^{(2)} = \mathcal{A}^{(0)} C_F c_\epsilon \left(\frac{-s}{\mu^2} \right)^{-\epsilon} \left(\frac{\xi \alpha_s}{4\pi\epsilon} + \frac{\alpha_s}{16\pi} \left(-4 \ln(-s)\xi - 4 \ln(\Delta_s)\xi \right. \right. \\ \left. \left. + \ln(16)\xi + 7\xi - 3 \right) \right) \quad (\text{A.12})$$

$$\sigma(\{q_{p_1}, \bar{q}_{p_2}, g_{p_3}\}) = \sigma_0 C_F c_\epsilon \frac{\alpha_s}{4\pi} \left(-4 \ln^2(\Delta_s) \Delta_s^3 - 2 \ln(\Delta_s) \Delta_s^3 \right. \\ + 4 \ln(\Delta_s) \ln(\Delta_s + 1) \Delta_s^3 + 2 \ln(\Delta_s + 1) \Delta_s^3 + 4 \ln(\Delta_s + 1) \ln\left(\frac{\Delta_s}{2\Delta_s + 1}\right) \Delta_s^3 \\ - 2 \ln^2(\Delta_s) \Delta_s^2 - 8 \ln(\Delta_s) \Delta_s^2 + 2 \ln(\Delta_s) \ln(\Delta_s + 1) \Delta_s^2 + 7 \ln(\Delta_s + 1) \Delta_s^2 \\ + 2 \ln(\Delta_s + 1) \ln\left(\frac{\Delta_s}{2\Delta_s + 1}\right) \Delta_s^2 - 2\Delta_s^2 + 8 \ln^2(\Delta_s) \Delta_s \\ - 8 \ln(\Delta_s) \ln(\Delta_s + 1) \Delta_s - 2 \ln(\Delta_s + 1) \Delta_s - 8 \ln(\Delta_s + 1) \ln\left(\frac{\Delta_s}{2\Delta_s + 1}\right) \Delta_s \\ - 5\Delta_s + 4 \ln^2(\Delta_s) + \ln(\Delta_s + 1) (\Delta_s + 1)^2 + 6 \ln(\Delta_s) - 4 \ln(\Delta_s) \ln(\Delta_s + 1) \\ - 7 \ln(\Delta_s + 1) - 4 \ln(\Delta_s + 1) \ln\left(\frac{\Delta_s}{2\Delta_s + 1}\right) \\ - 2 \ln(\Delta_s) \ln\left(\frac{\Delta_s + 1}{2\Delta_s + 1}\right) (2\Delta_s + 1) (\Delta_s^2 - 2) + 3 \\ \left. - 2\text{Li}_2\left(\frac{\Delta_s}{2\Delta_s + 1}\right) (2\Delta_s + 1) (\Delta_s^2 - 2) + 2\text{Li}_2\left(\frac{\Delta_s + 1}{2\Delta_s + 1}\right) (2\Delta_s + 1) (\Delta_s^2 - 2) \right) \quad (\text{A.13})$$

Chapter A: The full result for the vertex correction calculation

$$\begin{aligned}
\sigma(\{q_{p_1}, \bar{q}_{p_2}\}) &= \sigma_0 C_F c_\epsilon \frac{\alpha_s}{4\pi} \left(4 \ln^2(\Delta_s) \Delta_s^3 + 2 \ln(\Delta_s) \Delta_s^3 - 4 \ln(\Delta_s) \ln(\Delta_s + 1) \Delta_s^3 \right. \\
&- 2 \ln(\Delta_s + 1) \Delta_s^3 - 4 \ln(\Delta_s + 1) \ln\left(\frac{\Delta_s}{2\Delta_s + 1}\right) \Delta_s^3 + 4 \ln(\Delta_s) \ln\left(\frac{\Delta_s + 1}{2\Delta_s + 1}\right) \Delta_s^3 \\
&+ 2 \ln^2(\Delta_s) \Delta_s^2 + 8 \ln(\Delta_s) \Delta_s^2 - 2 \ln(\Delta_s) \ln(\Delta_s + 1) \Delta_s^2 - 8 \ln(\Delta_s + 1) \Delta_s^2 \\
&- 2 \ln(\Delta_s + 1) \ln\left(\frac{\Delta_s}{2\Delta_s + 1}\right) \Delta_s^2 + 2 \ln(\Delta_s) \ln\left(\frac{\Delta_s + 1}{2\Delta_s + 1}\right) \Delta_s^2 + 2 \Delta_s^2 - 8 \ln^2(\Delta_s) \Delta_s \\
&\quad + 8 \ln(\Delta_s + 1) \ln\left(\frac{\Delta_s}{2\Delta_s + 1}\right) \Delta_s - 8 \ln(\Delta_s) \ln\left(\frac{1}{2\Delta_s + 1}\right) \Delta_s \\
&\quad + 5 \Delta_s - 4 \ln^2(\Delta_s) - 6 \ln(\Delta_s) + 4 \ln(\Delta_s) \ln(\Delta_s + 1) + 6 \ln(\Delta_s + 1) \\
&\quad \quad + 4 \ln(\Delta_s + 1) \ln\left(\frac{\Delta_s}{2\Delta_s + 1}\right) - 4 \ln(\Delta_s) \ln\left(\frac{\Delta_s + 1}{2\Delta_s + 1}\right) \\
&\quad \left. + 2 \left(\text{Li}_2\left(\frac{\Delta_s}{2\Delta_s + 1}\right) - \text{Li}_2\left(\frac{\Delta_s + 1}{2\Delta_s + 1}\right) \right) (2\Delta_s^3 + \Delta_s^2 - 4\Delta_s - 2) \right) \quad (\text{A.14})
\end{aligned}$$

Appendix B

Cross sections for a basic jet definition

In this appendix we present the cross sections for $|q_{p_1}\bar{q}_{p_2}g_{p_3}\rangle$ and $|\{q_{p_1}\bar{q}_{p_2}g_{p_3}\}\rangle$ which were used to create the graphs in Figures 5.2 and 5.3.

$$\begin{aligned} \sigma(q_{p_1}\bar{q}_{p_2}g_{p_3}) = & \frac{1}{40\pi} \left(-3y_{\text{cut}}(3y_{\text{cut}} + 4) - (y_{\text{cut}} - 1)(y_{\text{cut}} + 3) \ln(-y_{\text{cut}}) \right. \\ & \left. - \ln(1 - 2y_{\text{cut}}) \left((y_{\text{cut}} - 10)y_{\text{cut}} + 4 \ln\left(\frac{1}{1 - y_{\text{cut}}}\right) + 4 \ln(y_{\text{cut}}) + 3 \right) \right) \\ & + \ln(y_{\text{cut}}) \left((y_{\text{cut}} - 10)y_{\text{cut}} - 4 \ln(1 - y_{\text{cut}}) + 4 \ln(y_{\text{cut}}) + 3 \right) + y_{\text{cut}}(y_{\text{cut}} + 2) \ln(2y_{\text{cut}} - 1) \\ & - 3 \ln(2y_{\text{cut}} - 1) - 4\text{Li}_2\left(2 + \frac{1}{y_{\text{cut}} - 1}\right) + 4\text{Li}_2\left(\frac{y_{\text{cut}}}{1 - y_{\text{cut}}}\right) + 5 \end{aligned} \quad (\text{B.1})$$

$$\begin{aligned}
 \sigma(\{q_{p_1} \bar{q}_{p_2} g_{p_3}\}) &= \frac{1}{40\pi(\Delta_s + y_{\text{cut}})} \left(2 \left(\text{Li}_2 \left(\frac{-2y_{\text{cut}} + \Delta_s + 1}{-y_{\text{cut}} + 2\Delta_s + 1} \right) \right. \right. \\
 &\quad \left. \left. - \text{Li}_2 \left(\frac{y_{\text{cut}} + \Delta_s}{-y_{\text{cut}} + 2\Delta_s + 1} \right) \right) (y_{\text{cut}} + \Delta_s) (2\Delta_s + 1) (\Delta_s^2 - 2) \right. \\
 &\quad \left. - (3y_{\text{cut}} - 1) (3y_{\text{cut}}^2 - (3\Delta_s^2 + \Delta_s - 5) y_{\text{cut}} - \Delta_s (\Delta_s + 3) (2\Delta_s - 1)) \right. \\
 &\quad \left. - 2(y_{\text{cut}} + \Delta_s) \left(\ln(y_{\text{cut}} + \Delta_s) ((\Delta_s + 4) \Delta_s^2 + \ln(y_{\text{cut}} + \Delta_s) (2\Delta_s + 1) (\Delta_s^2 - 2)) \right. \right. \\
 &\quad \left. \left. + \ln \left(\frac{-2y_{\text{cut}} + \Delta_s + 1}{-y_{\text{cut}} + 2\Delta_s + 1} \right) (2\Delta_s + 1) (\Delta_s^2 - 2) + y_{\text{cut}} (6 - \Delta_s (3\Delta_s + 4)) - 3 \right) \right. \\
 &\quad \left. + \ln(-2y_{\text{cut}} + \Delta_s + 1) \left(-(\Delta_s + 4) \Delta_s^2 - \ln(y_{\text{cut}} + \Delta_s) (2\Delta_s + 1) (\Delta_s^2 - 2) \right. \right. \\
 &\quad \left. \left. - \ln \left(\frac{y_{\text{cut}} + \Delta_s}{-y_{\text{cut}} + 2\Delta_s + 1} \right) (2\Delta_s + 1) (\Delta_s^2 - 2) + y_{\text{cut}} (\Delta_s (3\Delta_s + 4) - 6) + 3 \right) \right) \right)
 \end{aligned} \tag{B.2}$$

Bibliography

- [1] R. K. Ellis, W. J. Stirling, and B. R. Webber, *QCD and Collider Physics*. CUP, 1996.
- [2] T. Muta, *Foundations of Quantum Chromodynamics*. World Scientific, 2000.
- [3] F. Bloch and A. Nordsieck, “Note on the radiation field of the electron,” *Phys. Rev.* **52** (1937) 54–59.
- [4] R. K. Ellis, D. A. Ross, and A. E. Terrano, “The perturbative calculation of jet structure in $e^+ e^-$ annihilation,” *Nucl. Phys.* **B178** (1981) 421.
- [5] W. T. Giele and E. W. N. Glover, “Higher order corrections to jet cross-sections in $e^+ e^-$ annihilation,” *Phys. Rev.* **D46** (1992) 1980–2010.
- [6] S. Frixione, Z. Kunszt, and A. Signer, “Three-jet cross sections to next-to-leading order,” *Nucl. Phys.* **B467** (1996) 399–442hep-ph/9512328.

- [7] S. Catani and M. H. Seymour, "A general algorithm for calculating jet cross sections in NLO QCD," Nucl. Phys. **B485** (1997) 291–419hep-ph/9605323.
- [8] S. D. Ellis, Z. Kunszt, and D. E. Soper, "Two jet production in hadron collisions at order α_s^3 in QCD," Phys. Rev. Lett. **69** (1992) 1496–1499.
- [9] S. D. Ellis, Z. Kunszt, and D. E. Soper, "Jets at hadron colliders at order α_s^3 : A Look inside," Phys. Rev. Lett. **69** (1992) 3615–3618hep-ph/9208249.
- [10] Z. Kunszt and D. E. Soper, "Calculation of jet cross-sections in hadron collisions at order α_s^3 ," Phys. Rev. **D46** (1992) 192–221.
- [11] Z. Nagy and D. E. Soper, "General subtraction method for numerical calculation of one-loop QCD matrix elements," JHEP **09** (2003) 055hep-ph/0308127.
- [12] T. Gehrmann and E. Remiddi, "Progress on two-loop non-propagator integrals," hep-ph/0101147.
- [13] P. Mastrolia and E. Remiddi, "Analytic evaluation of Feynman graph integrals," Nucl. Phys. Proc. Suppl. **116** (2003) 412–416hep-ph/0211210.
- [14] V. A. Smirnov, "Evaluating multiloop Feynman integrals by Mellin-Barnes representation," Nucl. Phys. Proc. Suppl. **135** (2004) 252–256hep-ph/0406052.
- [15] T. Gehrmann, "QCD: Theoretical developments," Int. J. Mod. Phys. **A19** (2004) 851–863hep-ph/0310178.

- [16] E. W. N. Glover, "Progress in NNLO calculations for scattering processes," Nucl. Phys. Proc. Suppl. **116** (2003) 3–7hep-ph/0211412.
- [17] Z. Bern, "Recent progress in perturbative quantum field theory. ((U)) ((W)), " Nucl. Phys. Proc. Suppl. **117** (2003) 260–279hep-ph/0212406.
- [18] P. P. Kulish and L. D. Faddeev, "Asymptotic conditions and infrared divergences in quantum electrodynamics," Theor. Math. Phys. **4** (1970) 745.
- [19] M. Greco, F. Palumbo, G. Pancheri-Srivastava, and Y. Srivastava, "Coherent state approach to the infrared behavior of nonabelian gauge theories," Phys. Lett. **B77** (1978) 282.
- [20] D. R. Butler and C. A. Nelson, "Nonabelian structure of Yang-Mills theory and infrared finite asymptotic states," Phys. Rev. **D18** (1978) 1196.
- [21] C. A. Nelson, "Origin of cancellation of infrared divergences in coherent state approach: forward process $q q \rightarrow q q$ gluon," Nucl. Phys. **B181** (1981) 141.
- [22] C. A. Nelson, "Avoidance of counter example to nonabelian Bloch-Nordsieck conjecture by using coherent state approach," Nucl. Phys. **B186** (1981) 187.
- [23] M. Ciafaloni, "The QCD coherent state from asymptotic dynamics," Phys. Lett. **B150** (1985) 379.
- [24] S. Catani, M. Ciafaloni, and G. Marchesini, "Asymptotic coherent states and color screening," Phys. Lett. **B168** (1986) 284.

- [25] S. Catani, M. Ciafaloni, and G. Marchesini, “Noncancelling infrared divergences in QCD coherent state,” *Nucl. Phys.* **B264** (1986) 588–620.
- [26] S. Catani and M. Ciafaloni, “Generalized coherent state for soft gluon emission,” *Nucl. Phys.* **B249** (1985) 301.
- [27] J. Frenkel, J. G. M. Gatheral, and J. C. Taylor, “Asymptotic states and infrared divergences in nonabelian theories,” *Nucl. Phys.* **B194** (1982) 172.
- [28] V. Chung, “Infrared Divergence in Quantum Electrodynamics,” *Phys. Rev.* **140** (1965) B1110.
- [29] D. Zwanziger, “Reduction formulas for charged particles and coherent states in quantum electrodynamics,” *Phys. Rev.* **D7** (1973) 1082–1099.
- [30] D. Zwanziger, “Scattering theory for Quantum Electrodynamics. 1. Infrared renormalization and asymptotic fields,” *Phys. Rev.* **D11** (1975) 3481.
- [31] H. F. Contopanagos and M. B. Einhorn, “Theory of the asymptotic S matrix for massless particles,” *Phys. Rev.* **D45** (1992) 1291–1321.
- [32] M. Lavelle and D. McMullan, “Constituent quarks from QCD,” *Phys. Rept.* **279** (1997) 1–65hep-ph/9509344.
- [33] E. Bagan, M. Lavelle, and D. McMullan, “Charges from dressed matter: Physics and renormalisation,” *Annals Phys.* **282** (2000) 503–540hep-ph/9909262.
- [34] D. A. Forde and A. Signer, “Infrared-finite amplitudes for massless gauge theories,” *Nucl. Phys.* **B684** (2004) 125–161hep-ph/0311059.

- [35] M. E. Peskin and D. V. Schroeder, *An Introduction To Quantum Field Theory*. Perseus Books, 1995.
- [36] J. D. Bjorken and S. D. Drell, *Relativistic Quantum Fields*. McGraw-Hill, 1965.
- [37] C. Itzykson and J. Zuber, *Quantum Field Theory*. McGraw-Hill, 1980.
- [38] T. Kinoshita, "Mass singularities of Feynman amplitudes," *J. Math. Phys.* **3** (1962) 650–677.
- [39] T. D. Lee and M. Nauenberg, "Degenerate systems and mass singularities," *Phys. Rev.* **133** (1964) B1549–B1562.
- [40] G. Sterman, "Mass divergences in annihilation processes. 1. Origin and nature of divergences in cut vacuum polarization diagrams," *Phys. Rev.* **D17** (1978) 2773.
- [41] S. B. Libby and G. Sterman, "Mass divergences in two particle inelastic scattering," *Phys. Rev.* **D18** (1978) 4737.
- [42] G. Sterman, *An Introduction to Quantum Field Theory*. CUP, 1993.
- [43] P. De Causmaecker, R. Gastmans, W. Troost, and T. T. Wu, "Multiple bremsstrahlung in gauge theories at high-energies. 1. General formalism for quantum electrodynamics," *Nucl. Phys.* **B206** (1982) 53.
- [44] G. 't Hooft and M. J. G. Veltman, "Diagrammar,". In *Louvain 1973, Particle Interactions At Very High Energies, Part B*, New York 1973, 177-322 and CERN Geneva - CERN 73-9 (73,REC.OCT) 114p.

